692
9-16-81

(2)

Lb. 3081

DOE/ET/28384-T1

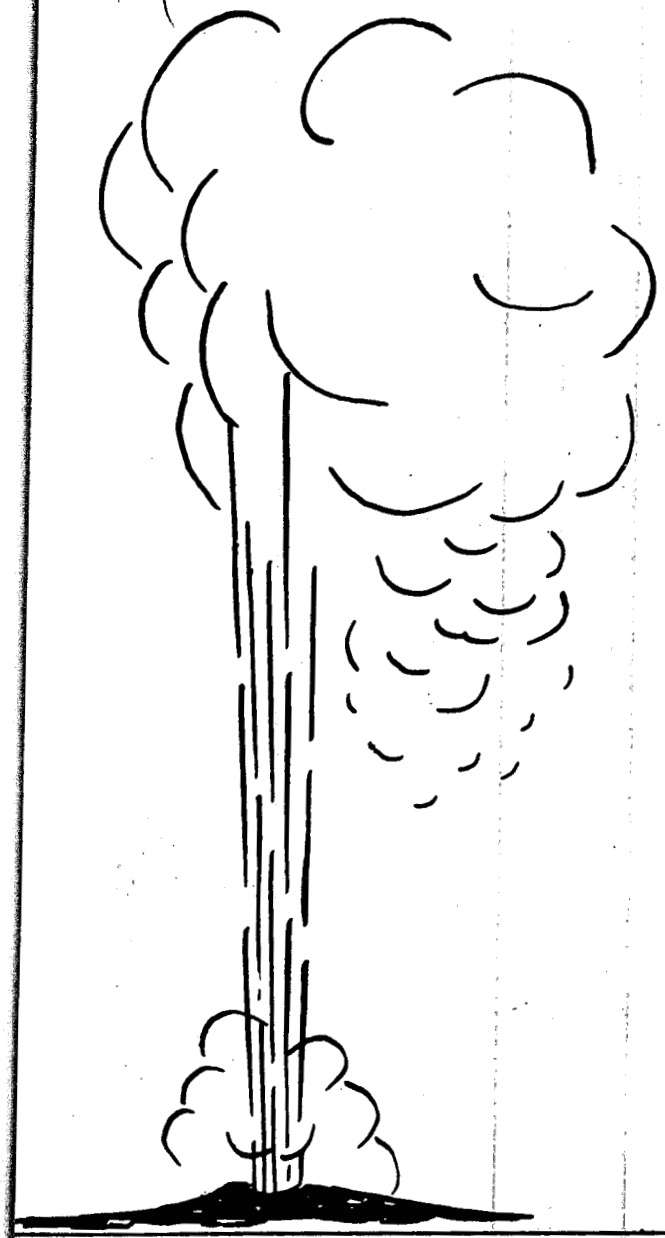

FORMATION EVALUATION IN LIQUID DOMINATED GEOTHERMAL RESERVOIRS

By
Iraj Ershaghi
Elmer E. Dougherty
Lyman L. Handy

April 1981

Work Performed Under Contract No. AT03-76ET28384

University of Southern California
Los Angeles, California

U. S. DEPARTMENT OF ENERGY
Geothermal Energy

DISCLAIMER

DISCLAIMER

Available from the National Technical Information Service, U. S. Department of Commerce, Springfield, Virginia 22161.

Price: Printed Copy A06
Microfiche A01

DOE/ET/28384-T1
Distribution Category UC-66b

FORMATION EVALUATION IN LIQUID DOMINATED GEOTHERMAL RESERVOIRS

By

IRAJ ERSHAGHI
ELMER E. DOUGHERTY
LYMAN L. HANDY

APRIL 1981

WORK PERFORMED UNDER CONTRACT NO. EY-76-S-03-0113 FOR GEOTHERMAL DIVISION OF THE U.S. DEPT. OF ENERGY

DEPARTMENT OF PETROLEUM ENGINEERING
UNIVERSITY OF SOUTHERN CALIFORNIA

TABLE OF CONTENTS

ABSTRACT

The Department of Petroleum Engineering at the University of Southern California was awarded a contract by the Geothermal Division of the U.S. Department of Energy to conduct studies relative to some formation evaluation aspects of geothermal reservoirs. The particular reservoirs considered were the liquid dominated type with a lithology of the sedimentary nature.

Specific problems of interest in the research proposal included the resistivity behavior of brines and rocks at elevated temperatures and studies on the feasibility of using the well log resistivity data to obtain estimates of reservoir permeability. During the course of study a few additional areas were investigated through the extension of the original proposal.

Several papers summarizing the results of these studies were presented at various technical meetings for rapid dissemination of the results to potential users. These papers together with a summary of data most recently generated are included in this final report.

A brief review of the research findings preceeds the technical papers.

INTRODUCTION

The engineering management for the development of geothermal reservoirs requires reliable measurements of reservoir rock and fluid properties combined with methods for interpreting and using such data. This combination will assist in predicting reservoir and well performance under various operating conditions. The technology used for these purposes in oil and gas reservoirs must be extended to account for the effects of high temperatures and geochemical activities encountered in geothermal systems.

The nature of fluids in geothermal reservoirs (being mostly water in liquid or vapor form) creates opportunities in the development of new formation evaluation techniques with no parallel in oil and gas exploration.

Because of extremely high temperatures and complex lithological units encountered in geothermal systems, many disciplines in science and engineering must contribute to the development of both the tools, measurement methods, and the interpretation techniques.

Over the last several years many researchers have been engaged in high-temperature tool research.[1] Calibration data relative to complex lithologies are now being prepared.[2] In the absence of such capabilities certain geothermal systems with similar geological characteristics to oil and gas reservoirs may be studied with existing tools and interpretation techniques.

The main focus of this study was the geothermal reservoirs of the sedimentary nature containing liquid brine. Reservoirs of this type have

been identified in various parts of the world such as the ones in Imperial Valley, California, and the Cerro Prieto field in Mexico.[3]

Interpretation of electric logs in such systems requires accurate data on the resistivity behavior of brine and rocks at elevated temperatures. A major portion of our effort under this research contract was devoted to the development of correlations for brine resistivity with temperature and concentrations. Furthermore, we studied the electrical resistivity behavior of porous and permeable rocks at elevated temperatures.

Since liquid dominated systems contain mostly a one phase fluid (liquid water) certain new concepts in subsurface geophysical surveys may be examined which may have no application in petroleum exploration. One idea scrutinized in this study was the use of dual-resistivity data in establishing a depth profile of formation permeability.

During the course of research covering the above topics, the need for some additional work was established. This included development of brine viscosity data at elevated temperatures, effect of dissolved gases on brine resistivity, design of a modified API filter test apparatus, and modeling of filter cake buildup during drilling.

A brief review of each aspect of study will preceed the published text of the results.

REFERENCES

1. Dennis, B.R., "Borehole Survey Instrumentation Development for Geothermal Application," Paper D, Trans. SPWLA (1980).

2. Mathews, M., " Calibration Models for Fractured Igneous Rock Environments," Paper L, Trans. SPWLA (1980).

3. Brook, C.A., Morines, R.H., Mabey, D.R., Swanson, J.R., Guffanti, M. and Muffler, L.J.P., "Hydrothermal Convection Systems with Reservoir Temperature $\geq$ 90°C," U.S. Geological Survey Circular 790 (1979) p.33.

BRINE RESISTIVITY AT ELEVATED TEMPERATURE

As a part of the research contracts and according to an agreement with the U.S. Geological Survey measurements of brine resistivity and rock resistivity were made using the high-pressure, high-temperature equipment at the U.S.G.S. Center in Denver. Dr. Gary Olhoeft, a research scientist at the center collaborated in this study. The study was conducted by a doctoral candidate (H. Ucok) under the supervision of Drs. I. Ershaghi, L. L. Handy, and E. L. Dougherty.

A paper encompassing the significant results of the study was prepared and presented at the 1979 International Meeting of the Society of Petroleum Engineers on Oilfield and Geothermal Chemistry held in Houston, Texas (January 22-24, 1979). The same paper was also presented at the 1979 California Regional Meeting of SPE which was held in Ventura (April 1979). The paper was later published in the April 1980 issue of the Journal of Petroleum Technology.

In summary, this study resulted in the development of new correlations for estimation of brine resistivity at temperatures up to 375^{o}C. Furthermore, the study showed that existing correlations available for petroleum reservoirs may not be extrapolated to elevated temperature.

In addition to a mathematical correlation for generating data using a computerized approach, modified multipliers were developed for rapid field application.

Electrical Resistivity of Geothermal Brines

Hikmet Ucok,* SPE, U. of Southern California
Iraj Ershaghi, SPE, U. of Southern California
Gary R. Olhoeft, USGS

Introduction

The electrical resistivity of dilute aqueous salt solutions has been studied for a number of years,[1] but very few data exist on concentrations above 0.1 molar.[2,3] Normal groundwaters commonly are near 0.1 molar,[4] while most geothermal and oilfield fluids are at least several molar[5,6] (Table 1). Thus, the interpretation of electrical measurements in geothermal areas[7] at present is based mainly on extrapolation of lower temperature and lower concentration data.[8] Such extrapolation may introduce serious errors into the interpretation of geothermal reservoir characteristics determined from electrical measurements.[9]

This paper presents new experimental data and an improved descriptive model of the electrical properties of brines as a function of temperature from 22 to 375°C and concentration from roughly 3 to 26 wt% while under 31 MPa hydrostatic pressure. Data and models are given for brines composed of the chlorides of sodium, calcium, and potassium, and their mixtures. Comparison of the older log interpretation formulas[10] to the new models illustrates an order of magnitude improvement in accuracy with an overall fit to within ±2%.

Resistivity Dependence Upon Temperature

Some researchers have postulated that the electrical resistivity of fluid saturated rocks follows the temperature dependence of the saturating fluid in the absence of conducting minerals or significant surface conduction along altered pore walls.[11-13] This assumption resulted from the success of a simple empirical formula relating the resistivity of a rock to the resistivity of the fluid filling the pores of the rock[14]:

$$\rho_r = F\rho_w,$$

where

ρ_r = resistivity of clay-free, nonshale material that is 100% saturated,
ρ_w = resistivity of saturating solution, and
F = formation resistivity factor.

A number of investigators have derived formulas that add the temperature of the saturating fluids.[15,16]

Experimental observations have shown that some rocks obey these formulas while others do not.[17-19] Part of the problem is the inadequate knowledge of the resistivity dependence on temperature for the solution that fills the rock pores.

We have found empirically that the best fit of the resistivity data to temperature is

$$\rho_w = b_0 + b_1 T^{-1} + b_2 T + b_3 T^2 + b_4 T^3,$$

where T is temperature and coefficients b are found empirically.

*Now with Union Oil Co. of California.

0149-2136/80/0004-7878$00.25

Improved correlations for estimation of electrical resistivities of brines are presented. These correlations are based on laboratory-measured data obtained using aqueous solutions of chlorides of sodium, calcium, and potassium. The concentration range from 3 to 26 wt% and the temperature range from 22 to 375° were studied.

TABLE 1 – EXAMPLES OF TYPICAL WATER CHEMISTRIES IN WEIGHT PERCENT

Ion	Normal Groundwater	Seawater	Salton Sea Brine	East Mesa Brine	Cerro Prieto Brine
Na^+	0.061	1.5	5.04	0.7	0.6
K^+	0.061	0.038	1.75	0.089	0.17
Ca^{++}	0.0037	0.04	2.8	0.077	0.034
Cl^-	0.0082	1.9	15.5	1.4	1.1
Mg^{++}	0.00024	0.135	0.0054	0.0016	0.0016
SO_4^{--}	0.1	0.27	–	0.02	–
$(HCO_3)^-$	0.0429	0.014	0.01	0.03	0.0011
Total dissolved solids	0.198	3.45	25.8	2.5	2.0
Molarity	0.03	0.56	3.6	0.36	0.3
T, °C			340	138	290
Reference	6	6	5	26	26

Resistivity Dependence on Concentration

The concentration dependence of the electrical resistivity of aqueous solutions has been studied extensively and is represented best by the formula

$$\rho_w = 10/(\Lambda c),$$

where Λ is the equivalent conductivity according to[20]

$$\Lambda = B_0 - B_1 c^{1/2} + B_2 c \ln c + \text{higher-order terms},$$

where c is the molar concentration and coefficients B depend on the solution chemistry.[21] Further discussion appears in nearly any text on electrochemistry.[21]

Experimental

Measurement of electrical resistivity of concentrated salt solutions at elevated temperatures is very difficult due to the corrosive nature of the solution chemistries. A special sample holder (Figs. 1 and 2) and pressure vessel assembly were manufactured from mullite ceramic, platinum, Inconel™, stainless steel, and Teflon® components. The salt solution contacted only mullite and platinum. A four-electrode configuration at a measurement frequency of 1 kHz was chosen to eliminate electrode polarization problems. Measurements at frequencies from 0.1 to 10 kHz were performed to confirm the lack of polarization at the electrodes. Two electrode measurements were found to have polarization errors of one order of magnitude.

Cumulative experimental errors due to thermal expansion, errors in determining cell constants, instrument errors, and so forth did not exceed ±1% in the final resistivity determination. The temperature of the solution was measured with a Type S, Pt-10%Rh thermocouple in the solution with an accuracy of ±1°C. The system was pressurized hydrostatically with argon gas through a series of snubbers and pressure regulators as illustrated in Fig. 3. Pressure was measured and monitored with two strain-gauge pressure transducers and one manual Bourdon tube gauge. The electrical resistance of the sample cell was measured with an HP 4262A automatic digital LCR meter. A computer was used to control the environmental parameters and perform the electrical measurements as schematically illustrated in Fig. 3.

Each experiment began with cleaning in distilled water and assembly of the sample cell and pressure vessel. A Teflon calibration cell of precisely known geometry was used with standard potassium chloride solutions[22] to calibrate the pressure vessel sample cell.

Salt solutions were prepared from reagent grade crystals (anhydrous $CaCl_2$), which were measured gravimetrically into 150 000 Ω·m water. Resultant

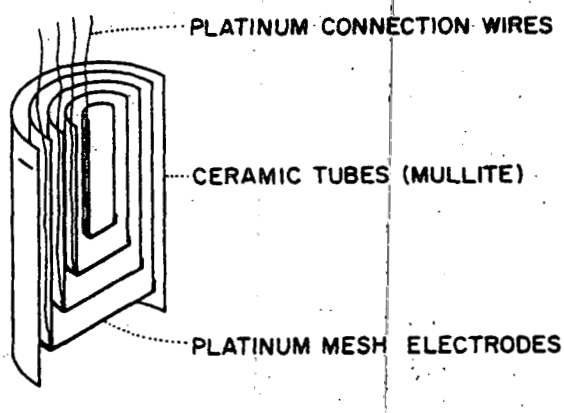

Fig. 1 – Resistivity sample cell made from mullite ceramic with four platinum.

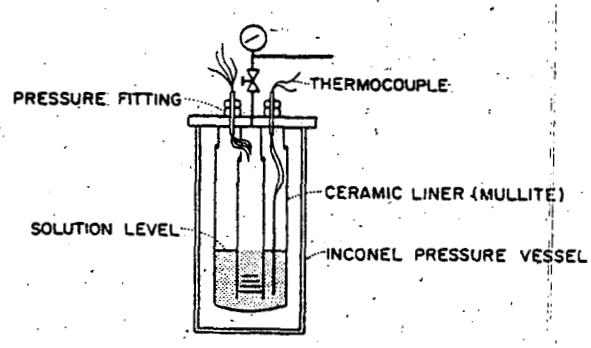

Fig. 2 – Pressure vessel arrangement.

room-temperature (22°C) resistivities were checked against reference table values.[22]

All measurements reported here were performed at hydrostatic pressures of 30 MPa, since the resistivities of the studied solutions were found to be independent of pressure in agreement with earlier studies.[1] Pressure dependence becomes significant only well above the critical region or as the solution nears and passes below its vapor pressure.

Results

Isobaric resistivities of NaCl, KCl, and $CaCl_2$ solutions vs. temperature at several salt concentrations are shown in Figs. 4, 5, and 6. In general, the electrical resistivity decreases with increasing temperature and salt concentration. However, as the critical temperature of the solutions is approached at the higher temperatures studied, the resistivity reaches a minimum and then begins to increase with increasing temperature. Tables 2 and 3 give the numerical values of data points for KCl and $CaCl_2$ solutions.

Quist and Marshall[1] have given the best explanation for the behavior of the physical properties of aqueous salt solutions. The electrical resistivity is controlled by a variety of parameters including viscosity, density, and the dielectric permittivity of the solution. As temperature or concentration increases, these properties of water begin to change very rapidly. The rapid decrease of viscosity with increasing temperature results in a rapid increase in ionic mobilities with a resultant decrease in electrical resistivity. Above roughly 300°C as the critical point is approached, the rate of decrease in viscosity with increasing temperature diminishes and the change in ionic mobility becomes less. As the temperature continues to increase, the changes in density overtake the effects of viscosity. The decreasing density results in a lowering of the dielectric permittivity and in the number of ions per unit volume. This results in the increased association among ion pairs and an increase in the electrical resistivity. Thus, when the increase in ionic mobility is offset by the decrease in permittivity and in ionic concentration, the electrical resistivity reaches a minimum with respect to temperature. As the concentration of the salt solution increases significantly above 0.1 molar, the minimum in the resistivity shifts to higher temperatures due to the effects of the increasing salt concentration upon the critical properties of water.

The solid lines in Figs. 4, 5, and 6 are formula fits to the data points by three-dimensional regression analysis.[23] The coefficient matrices and computer program to generate the resistivity at a given temperature and concentration is given in the Appendix.

Fig. 7 illustrates a comparison of the experimental data with the formula from three-dimensional regression and with Arps' approximation.[16] Both formulas are in reasonable agreement with the data up to about 200°C. Beyond 200°C, Arps' approximation encounters serious difficulties.

Figs. 8, 9, and 10 illustrate the concentration dependence of NaCl, KCl, and $CaCl_2$ at three temperatures. Note that the curves of resistivity vs.

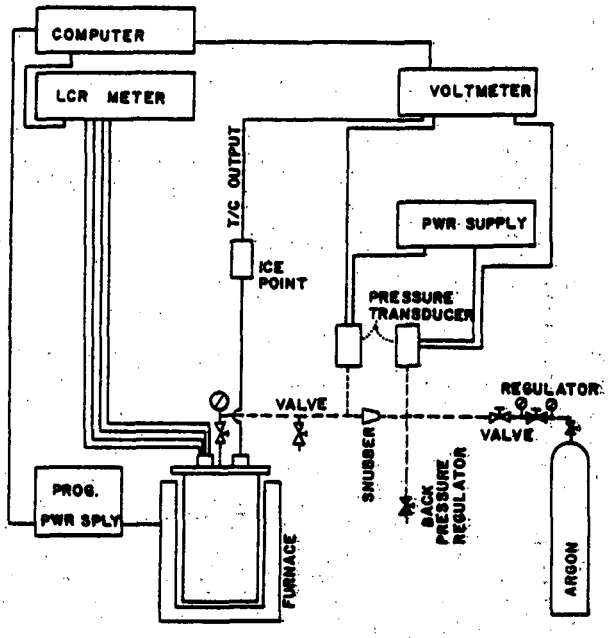

Fig. 3 – Experimental equipment and plumbing.

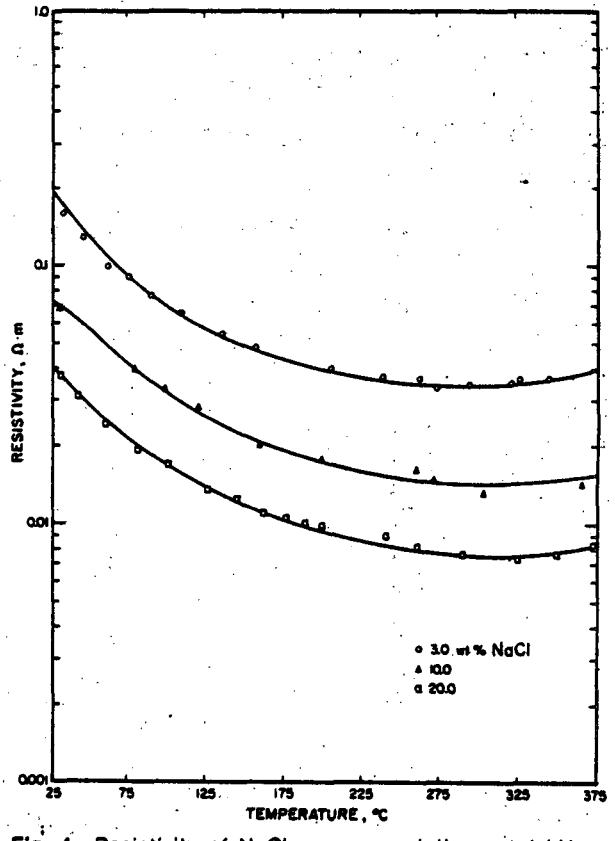

Fig. 4 – Resistivity of NaCl aqueous solutions at 1 kHz under 30 MPa hydrostatic pressure. Solid lines are formula fitted by three-dimensional regression analysis.

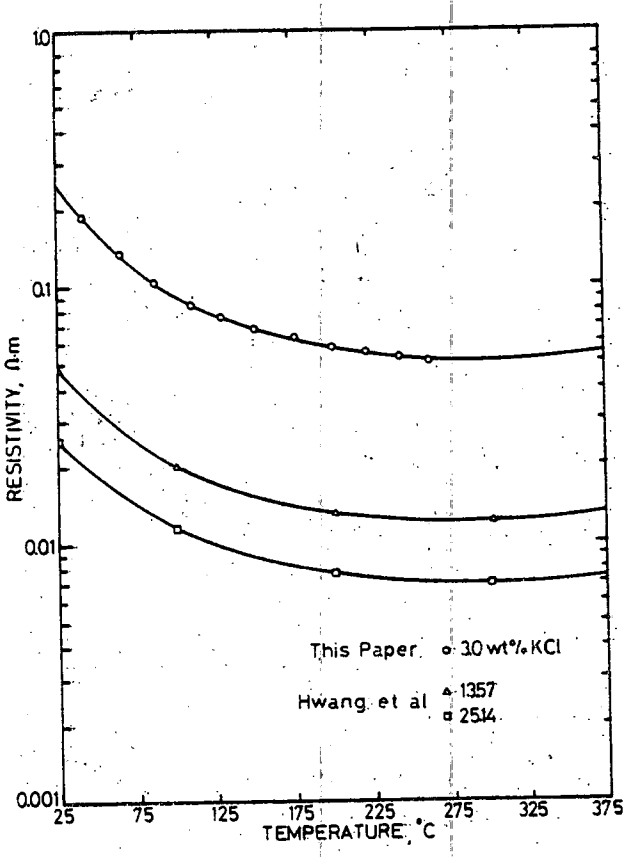

Fig. 5 – Resistivity of KCl solutions as for Fig. 4.

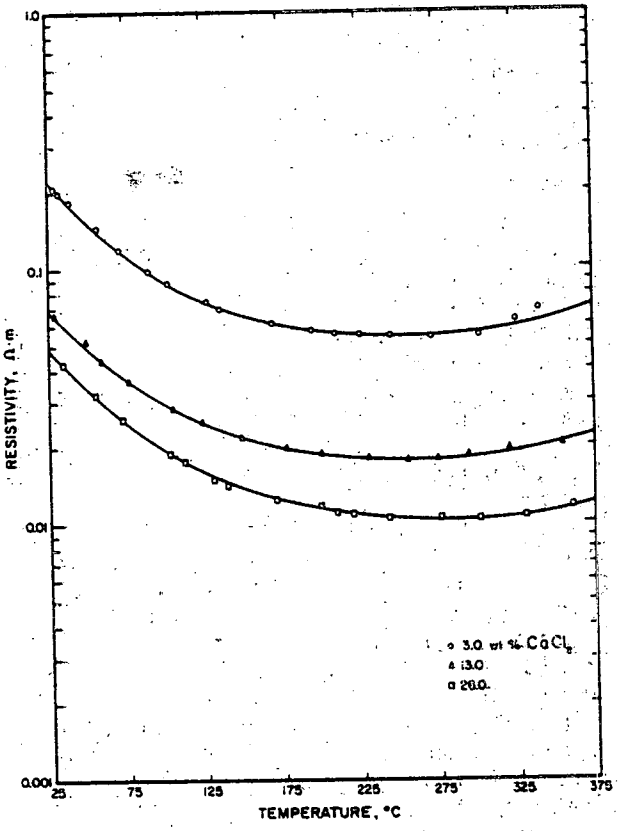

Fig. 6 – Resistivity of $CaCl_2$ solutions as for Fig. 4.

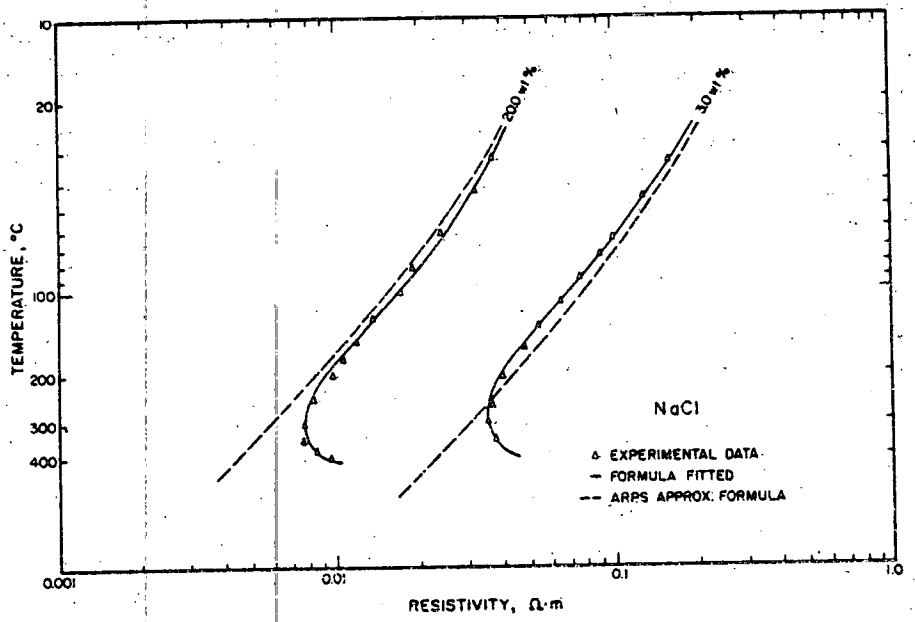

Fig. 7 – Resistivity of NaCl solutions showing fit of Arps' approximation and the proposed new formula to the data.

concentration cross over each other. These crossovers are a direct result of the differences in the salt solution viscosities vs. temperature and concentration. These crossovers also illustrate the need for great caution when reducing a solution of mixed salts to an equivalent solution of NaCl.

Commonly, this is performed by the use of multipliers that convert a given ionic concentration of salt to an equivalent weight-percent amount of NaCl:[24,25]

$$K_K \cdot K^+ + K_{Cl} \cdot Cl^- = \text{measured equivalent NaCl concentration},$$

$$K_{Ca} \cdot Ca^{++} + K_{Cl} \cdot Cl^- = \text{measured equivalent NaCl concentration},$$

where the K's are multipliers and it is assumed that $K_{Na} = K_{Cl} = 1$. The K_K and K_{Ca} multipliers then are determined empirically (usually from electrical resistivity measurements). Desai and Moore[25] report that the multipliers are fairly constant and independent of temperature up to 71°C with errors less than 5% for concentrations below 1 wt%. As illustrated in Figs. 11 and 12, we have found this no longer to be the case at higher temperatures and concentrations. The data points corresponding to Figs. 11, 12, and 14 are given in Tables 4, 5, and 6.

To illustrate the errors involved in the extrapolation of lower temperature and lower concentration data to higher values, a mixed salt of 3 wt% total salt concentration composed of 1.5 wt% NaCl, 0.75 wt% KCl, and 0.75 wt% $CaCl_2$ was measured. Fig. 13 illustrates the results with a 3 wt% NaCl solution for comparison. Table 7 gives the resulting measured resistivities compared with values calculated by our three-dimensional regression formula and values using Desai and Moore's

TABLE 2—RESISTIVITY VARIATION OF KCl SALT SOLUTIONS WITH TEMPERATURE

	Measured		Calculated	
Concentration (wt%)	Temperature (°C)	Resistivity (Ω·m)	Temperature (°C)	Resistivity (Ω·m)
3.0	22	0.228	25	0.252
	42	0.139	50	0.161
	66	0.137	75	0.117
	83	0.105	100	0.0935
	111	0.087	125	0.0769
	131	0.077	150	0.0660
	152	0.069	175	0.0625
	177	0.063	200	0.0579
	201	0.058	225	0.0549
	222	0.055	250	0.0525
	242	0.0535	275	0.0512
	262	0.0503	300	0.0500
			325	0.0512
			350	0.0525
			375	0.0549
			400	0.0580
13.57	25	0.0484	25	0.0484
(Ref. 2)	50	—	50	0.0340
	75	—	75	0.0252
	100	0.0204	100	0.0203
	125	—	125	0.0174
	150	—	150	0.0154
	175	—	175	0.0141
	200	0.0132	200	0.0132
	225	—	225	0.0128
	250	—	250	0.0122
	275	—	275	0.0121
	300	0.0120	300	0.0120
	325	—	325	0.0122
	350	—	350	0.0125
	375	—	375	0.0131
	400	0.0137	400	0.0136
25.14	25	0.0256	25	0.0253
(Ref. 2)	50	—	50	0.0185
	75	—	75	0.0142
	100	0.0117	100	0.0117
	125	—	125	0.0101
	150	—	150	0.0089
	175	—	175	0.0082
	200	0.0076	200	0.0077
	225	—	225	0.0073
	250	—	250	0.0071
	275	—	275	0.0069
	300	0.00694	300	0.0069
	325	—	325	0.0069
	350	—	350	0.0071
	375	—	375	0.0073
	400	0.0076	400	0.0077

TABLE 3—RESISTIVITY VARIATION OF $CaCl_2$ SALT SOLUTIONS WITH TEMPERATURE

	Measured		Calculated	
Concentration (wt%)	Temperature (°C)	Resistivity (Ω·m)	Temperature (°C)	Resistivity (Ω·m)
3.0	22	0.227	25	0.219
	31	0.209	50	0.169
	41	0.185	75	0.117
	57	0.145	100	0.0897
	72	0.119	125	0.0745
	90	0.098	150	0.0654
	103	0.088	175	0.0597
	127	0.074	200	0.0563
	136	0.070	225	0.0544
	171	0.0608	250	0.0538
	195	0.0568	275	0.0544
	211	0.0550	300	0.0561
	225	0.0544	325	0.0593
	245	0.0542	350	0.0642
	272	0.0530	375	0.0717
	303	0.0537	400	0.0835
	325	0.0620		
	339	0.0580		
13.0	22	0.0702	25	0.0683
	50	0.0520	50	0.0520
	59	0.0462	75	0.0374
	77	0.0368	100	0.0294
	105	0.0268	125	0.0247
	124	0.0250	150	0.0218
	151	0.0219	175	0.0199
	177	0.0197	200	0.0189
	209	0.0185	225	0.0181
	230	0.0178	250	0.0178
	255	0.0176	275	0.0178
	274	0.0180	300	0.0182
	294	0.0185	325	0.0190
	320	0.0195	350	0.0203
	354	0.0201	375	0.0224
			400	0.0254
26.0	22	0.0484	25	0.0498
	36	0.0424	50	0.0338
	55	0.0319	75	0.0240
	73	0.0255	100	0.0182
	103	0.0193	125	0.0159
	112	0.0174	150	0.0137
	131	0.0148	175	0.0123
	140	0.0141	200	0.0114
	171	0.0124	225	0.0108
	200	0.0117	250	0.0104
	210	0.0110	275	0.0103
	221	0.0108	300	0.0104
	241	0.0105	325	0.0109
	277	0.0103	350	0.0112
	302	0.0103	375	0.0121
	331	0.0108	400	0.0135
	361	0.0116		
	389	0.0119		
	393	0.0120		
	405	0.0133		

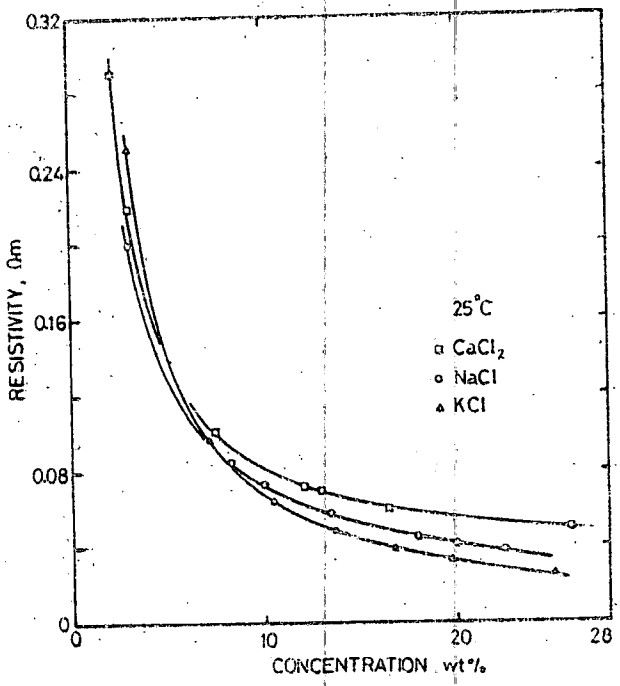

Fig. 8 – Resistivity variations of NaCl, KCl, and $CaCl_2$ solutions with concentration at 1 kHz under 30 MPa hydrostatic pressure at 25°C.

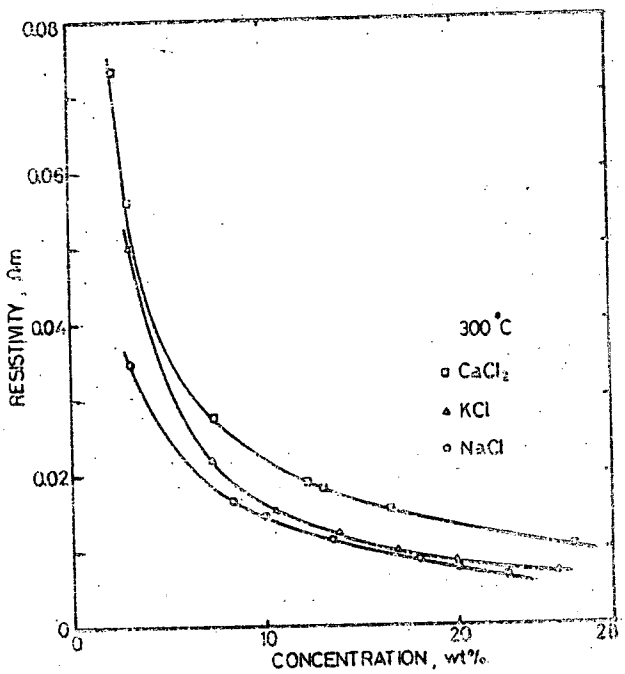

Fig. 10 – Resistivity variations at 300°C as for Fig. 8.

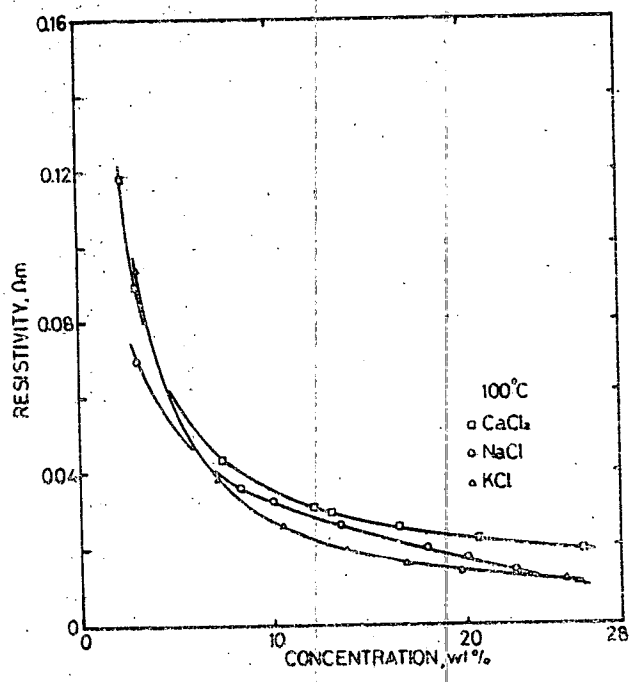

Fig. 9 – Resistivity variations at 100°C as for Fig. 8.

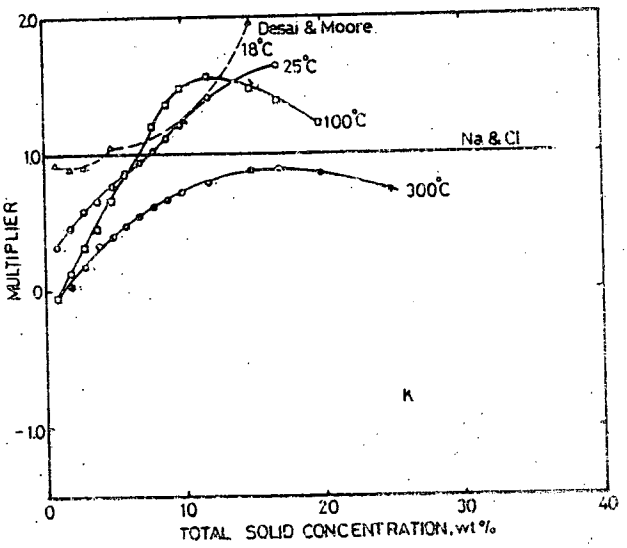

Fig. 11 – NaCl equivalent multipliers for K^+ ion vs. total solid concentration at several temperatures.

multipliers in Arps' equation. Our newer formula is one order of magnitude better.

Conclusions

The use of low temperature and low concentration data to extrapolate electrical resistivities to high salt concentrations at geothermal temperatures must be treated with extreme caution. Errors as high or higher than 25% in the estimation of electrical resistivity may result. Further, different salts have widely varying temperature and concentration dependencies in the normal geothermal range, which greatly complicates the reduction of a mixed salt solution to an equivalent NaCl solution.

A new set of measurements to 375°C and 25 wt% salt concentration has been fitted by three-dimensional regression analysis to an accuracy of ±2% to model the electrical resistivities of aqueous solutions of the chlorides of sodium, potassium, and calcium. New temperature and concentration-dependent NaCl equivalent multipliers have been generated for potassium and calcium. For convenience, Fig. 14 gives the formula-generated curves for the electrical resistivity of NaCl aqueous solutions as a function of temperature and concentration. This graph should replace existing graphs for high-temperature applications in liquid-dominated geothermal systems.

Nomenclature

A = equivalent conductance, $\Omega^{-1}cm^2eq^{-1}$
b = resistivity temperature coefficient
B = resistivity concentration coefficient
c = concentration, molar

TABLE 4 – NaCl EQUIVALENT MULTIPLIERS FOR POTASSIUM ION (K^+)

Temperature		Total Solid Concentration		
(°C)	(°F)	(wt%)	(ppm)	Multipliers
25	77	1.0	10,000	0.331
		2.0	20,000	0.474
		3.0	30,000	0.592
		4.0	40,000	0.665
		5.0	50,000	0.770
		6.0	60,000	0.873
		7.0	70,000	0.945
		8.0	80,000	1.036
		9.0	90,000	1.127
		10.0	100,000	1.210
		12.0	120,000	1.420
		15.0	150,000	1.560
		17.0	170,000	1.64
100	212	1.0	10,000	−0.052
		2.0	20,000	0.140
		3.0	30,000	0.331
		4.0	40,000	0.474
		5.0	50,000	0.675
		6.0	60,000	0.873
		8.0	80,000	1.215
		9.0	90,000	1.360
		10.0	100,000	1.497
		12.0	120,000	1.574
		15.0	150,000	1.480
		17.0	170,000	1.380
		20.0	200,000	1.220
300	572	1.0	10,000	−0.052
		2.0	20,000	0.044
		3.0	30,000	0.203
		4.0	40,000	0.350
		5.0	50,000	0.426
		6.0	60,000	0.490
		7.0	70,000	0.563
		8.0	80,000	0.630
		9.0	90,000	0.680
		10.0	100,000	0.732
		12.0	120,000	0.785
		15.0	150,000	0.898
		17.0	170,000	0.899
		20.0	200,000	0.866
		25.0	250,000	0.740

TABLE 5 – NaCl EQUIVALENT MULTIPLIERS FOR THE CALCIUM ION (Ca^{++})

Temperature		Total Solid Concentration		
(°C)	(°F)	(wt%)	(ppm)	Multipliers
25	77	1.0	10,000	0.723
		3.0	30,000	0.723
		5.0	50,000	0.680
		7.0	70,000	0.644
		9.0	90,000	0.637
		10.0	100,000	0.634
		12.0	120,000	0.587
		15.0	150,000	0.446
		17.0	170,000	0.397
		20.0	200,000	0.280
		25.0	250,000	0.0255
100	212	1.0	10,000	−0.247
		3.0	30,000	0.160
		5.0	50,000	0.324
		7.0	70,000	0.505
		9.0	90,000	0.576
		10.0	100,000	0.612
		12.0	120,000	0.630
		15.0	150,000	0.631
		17.0	170,000	0.576
		20.0	200,000	0.446
		25.0	250,000	0.225
200	392	1.0	10,000	−0.385
		3.0	30,000	−0.154
		5.0	50,000	−0.025
		7.0	70,000	0.0107
		9.0	90,000	0.0766
		10.0	100,000	0.114
		12.0	120,000	0.123
		15.0	150,000	0.169
		17.0	170,000	0.153
		20.0	200,000	0.169
		25.0	250,000	0.037
300	572	1.0	10,000	−0.524
		3.0	30,000	−0.385
		5.0	50,000	−0.274
		7.0	70,000	−0.227
		9.0	90,000	−0.231
		10.0	100,000	−0.244
		12.0	120,000	−0.247
		15.0	150,000	−0.237
		17.0	170,000	−0.238
		20.0	200,000	−0.210
		25.0	250,000	−0.152

TABLE 6 – RESISTIVITY VARIATION OF NaCl SALT SOLUTIONS WITH TEMPERATURE

Concentration (wt%)	Measured Temperature (°C)	Measured Resistivity (Ω·m)	Calculated Temperature (°C)	Calculated Resistivity (Ω·m)
3.0	22	0.22	25	0.200
	33	0.16	50	0.129
	46	0.13	75	0.090
	62	0.10	100	0.0693
	75	0.090	125	0.0569
	90	0.076	150	0.0488
	109	0.0647	175	0.0434
	135	0.0544	200	0.0397
	157	0.0485	225	0.0371
	205	0.0401	250	0.0355
	239	0.0374	275	0.0347
	262	0.0367	300	0.0346
	273	0.0340	325	0.0354
	294	0.0351	350	0.0371
	320	0.0356	375	0.0402
	325	0.0365	400	0.0455
	344	0.0374		
10.0	21	0.077	25	0.0730
	31	0.0681	50	0.0582
	80	0.0390	75	0.0418
	99	0.0329	100	0.0320
	121	0.0282	125	0.0260
	160	0.0200	150	0.0220
	200	0.0177	175	0.0193
	260	0.0163	200	0.0174
	271	0.0149	225	0.0161
	303	0.0130	250	0.0151
	367	0.0143	275	0.0146
	381	0.0146	300	0.0143
	401	0.0170	325	0.0144
			350	0.0148
			375	0.0157
			400	0.0172
20.0	22	0.0434	25	0.0422
	32	0.0370	50	0.0284
	43	0.0320	75	0.0213
	61	0.0239	100	0.0169
	82	0.0188	125	0.0139
	102	0.0174	150	0.0119
	126	0.0136	175	0.0104
	141	0.0125	200	0.0093
	163	0.0113	225	0.0086
	176	0.0107	250	0.0081
	189	0.0102	275	0.0077
	201	0.0099	300	0.0076
	241	0.0090	325	0.0076
	263	0.0082	350	0.0079
	290	0.0077	375	0.0084
	326	0.0073	400	0.0094
	351	0.0076		
	375	0.0082		
	391	0.0089		
	400	0.0095		

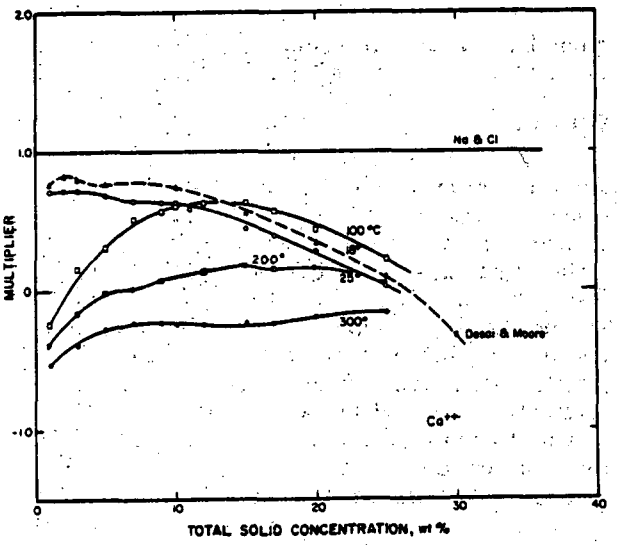

Fig. 12 – Multipliers for Ca^{++} ion as for Fig. 11.

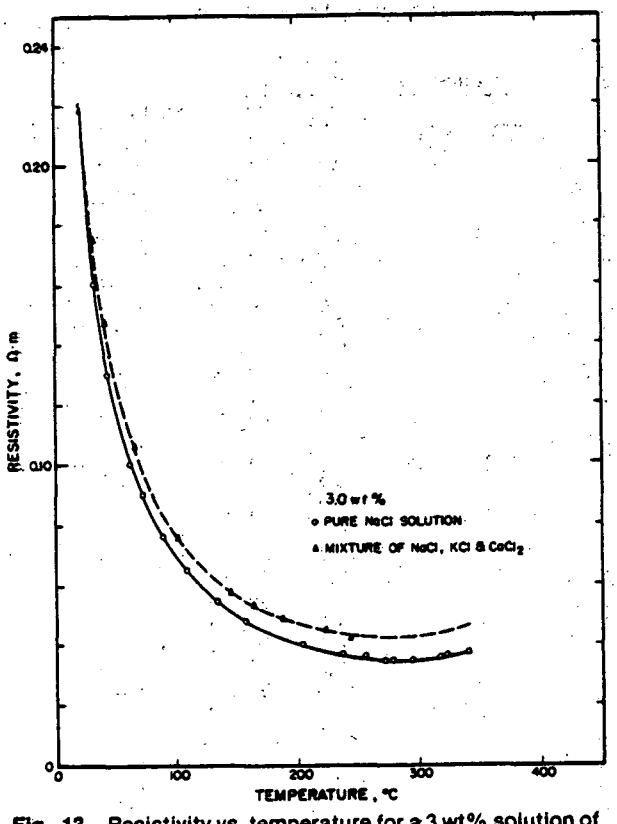

Fig. 13 – Resistivity vs. temperature for a 3 wt% solution of 2:1:1 NaCl:KCl:$CaCl_2$.

TABLE 7 – COMPARISON OF MEASURED RESISTIVITIES WITH VARIOUS DERIVED PARAMETERS
(Chemical composition of solution: TS 3 wt%, 0.5 gal wt% Na^+, 0.3933 K^+, 0.2711 Ca^{++}, 1.7462 Cl^-)

Temperature (°C)	Measured Resistivity (Ω·m)	Desai and Moore's Method: Multipliers (K^+)	Desai and Moore's Method: Multipliers (Ca^{++})	Desai and Moore's Method: Equivalent NaCl (wt%)	Desai and Moore's Method: Estimated Resistivity (Ω·m)	This Study: Multipliers (K^+)	This Study: Multipliers (Ca^{++})	This Study: Equivalent NaCl (wt%)	This Study: Estimated Resistivity (Ω·m)
25	0.22	0.917	0.806	2.92	0.21	0.592	0.723	2.77*	0.22
100	0.078	0.917	0.806	2.92	0.070	0.331	0.160	2.51	0.0765
300	0.043	0.917	0.806	2.92	0.0345	0.203	– 0.385	2.31	0.043

*Example calculation: equivalent NaCl = 0.594 × 1 + 1.7462 × 1 + 0.3933 × 0.592 + 0.2711 × 0.723 = 2.77 wt%.

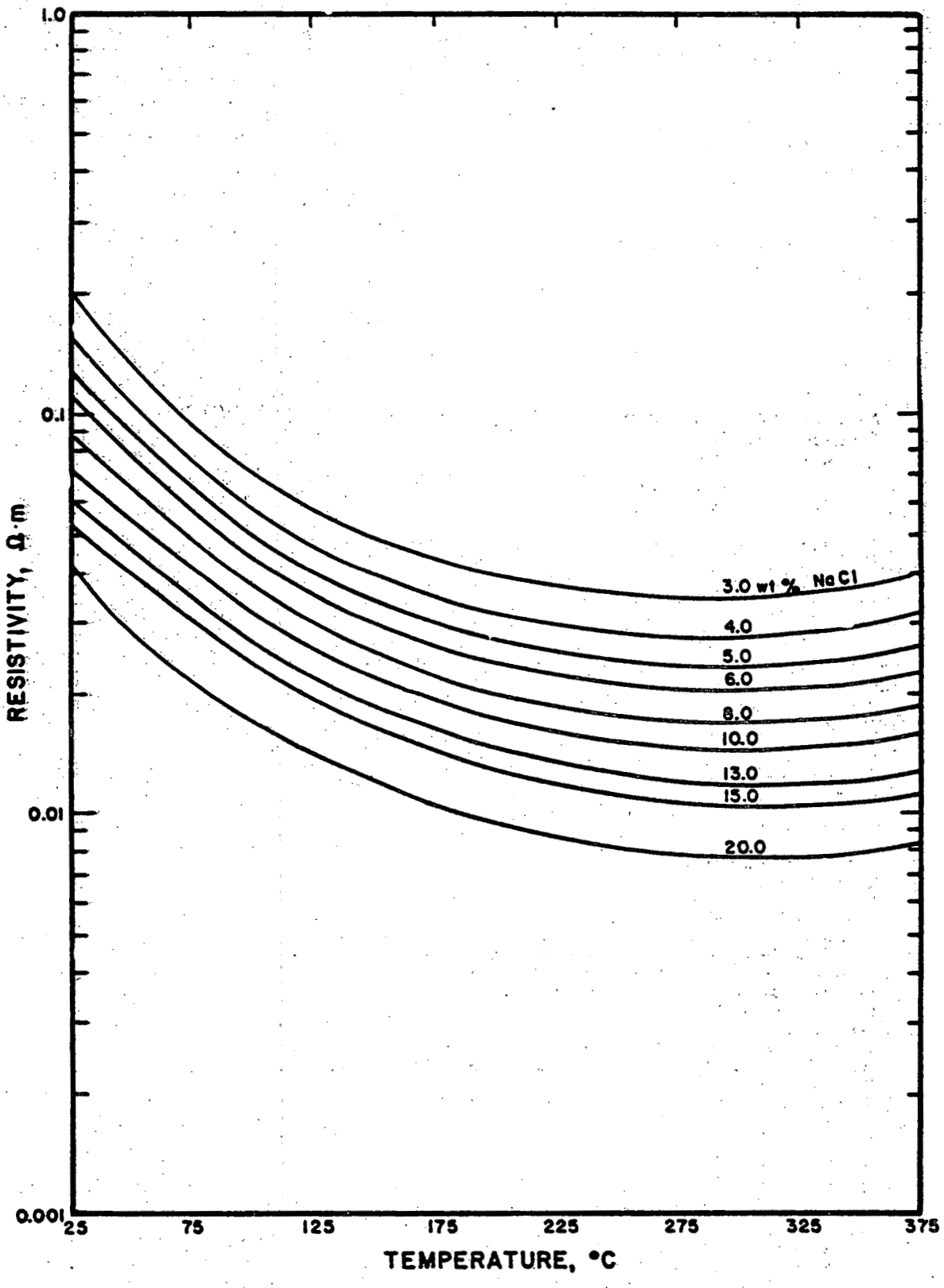

Fig. 14 – Resistivity of NaCl solution vs. temperature and concentration calculated from the regression analysis formula.

TABLE 8 – COEFFICIENT MATRICES FOR B FOR THE THREE-DIMENSIONAL REGRESSION ANALYSIS OF THE DATA IN THE TEXT

$CaCl_2$:		-34.62	24.64	-3.907
		780.3	-492.3	64.59
	$B=$	1.050	-0.5922	0.06735
		-0.002459	0.001461	-1.216×10^{-4}
		9.986×10^{-7}	-7.109×10^{-7}	-4.731×10^{-9}
KCl:		5.783	-6.607	1.665
		-59.23	149.7	-31.21
	$B=$	0.2051	0.1084	-0.03418
		1.815×10^{-4}	-7.037×10^{-4}	1.539×10^{-4}
		-1.094×10^{-6}	1.080×10^{-6}	-1.945×10^{-7}
NaCl:		3.470	-6.650	2.633
		-59.21	198.1	-64.80
	$B=$	0.4551	-0.2058	0.005799
		-9.346×10^{-5}	7.368×10^{-5}	6.741×10^{-5}
		-1.766×10^{-6}	8.768×10^{-7}	-2.136×10^{-7}

F = formation factor
K = equivalent NaCl multiplier
T = temperature, °C
ρ_r = resistivity of clay-free, nonshale material that is 100% solution saturated, $\Omega\cdot m$
ρ_w = solution resistivity, $\Omega\cdot m$

Acknowledgments

This investigation was supported jointly by the U.S. DOE Div. of Geothermal Energy and the USGS Geothermal Program. Trade or manufacturer's names are used for descriptive purposes only and do not imply recommendation or endorsement by the U.S. government.

References

1. Quist, A.S. and Marshall, W.L.: "Electrical Conductances of Aqueous Sodium Chloride Solutions From 0 to 800° and at Pressures to 4000 Bars," *J. Phys. Chem.* (Feb. 1968) 72, 684-702.
2. Hwang, J.U., Ludemann, H.D., and Hartman, D.: "Die elektrische leitfähigkeit konzentrierter wassriger alkalihalogenidlosungen bei hohen drucken und temperaturen," *High Temperature and High Pressure* (1970) 2, 651-659.
3. Wooten, M.J.: "The Conductance of Electrolyte Solutions," *Electrochemistry*, G.J. Hills (sr. reptr.), Specialist Periodical Report, The Chemical Society, London (1973) 3, 20-40.
4. Hem, J.D.: *Study and Interpretation of the Chemical Characteristics of Natural Water*, second edition, USGS water supply paper 1473 (1970).
5. Muffler, L.J.P. and White, D.E.: "Active Metamorphism of Upper Cenozoic Sediments in the Salton Sea Geothermal Field and the Salton Trough Southeastern California," *Bull.*, GSA (1969) 80, 157-182.
6. Roedder, E.: "Composition of Fluid Inclusions," *Data of Geochemistry*, sixth edition, M. Fleischer (ed.), USGS Prof. Paper 440-JJ (1972).
7. Ward, S.H.: "Summary Report: Electrical Methods in Geothermal Exploration," Workshop on Electrical Methods in Geothermal Exploration, Snowbird, UT, USGS Contract No. 14-08-0001-G-359, U. of Utah (1977) 1-10.
8. Ward, S.H. *et al.*: "A Summary of the Geology, Geochemistry, and Geophysics of the Roosevelt Hot Springs Geothermal Area, Utah," *Geophysics* (1978) 43, 1515-1542.
9. Ershaghi, I., Dougherty, E.L., Ucok, H., and Ghassemi, F.: "Problems in Estimation of Salinity Profiles in Liquid Dominated Geothermal Systems," *Proc.*, Geothermal Resources Council Annual Meeting, Hilo, HI (1978) 181-183.
10. *Log Interpretation Charts*, Schlumberger-Doll Research Center, Schlumberger Technology Corp., Ridgefield, CT (1968).
11. Brace, W.F.: "Resistivity of Saturated Crustal Rocks to 40 km Based on Laboratory Studies," *The Structure and Physical Properties of the Earth's Crust*, J.G. Heacock (ed.) 243-256; Monograph 14, AGU, Washington, DC (1971).
12. Hermance, J.F., Nur, A., and Bjornsson, S.: "Electrical Properties of Basalt: Relation of Laboratory to In-Situ Measurements," *J. Geophys. Res.* (1972) 77, 1424-1429.
13. Jackson, P.D., Taylor-Smith, D., and Stanford, P.N.: "Resistivity-Porosity-Particle Shape Relationships for Marine Sands," *Geophysics* (1978) 43, 1250-1268.
14. Archie, G.E.: "The Electrical Resistivity Log as an Aid in Determining Reservoir Characteristics," *Trans.*, AIME (1942) 146, 54-67.
15. Dakhov, V.N.: "Geophysical Well Logging," *Quart. Colo. Sch. of Mines* (1962) 57, 85-127 (translation by G.V. Keller).
16. Arps, J.J.: "The Effect of Temperature on the Density and Electrical Resistivity of Sodium Chloride Solutions," *Trans.*, AIME (1953) 198, 327-330.
17. Hyndman, R.D. and Drury, M.J.: "The Physical Properties of Oceanic Basement Rocks From Deep Drilling on the Mid-Atlantic Ridge," *J. Geophys. Res.* (1976) 81, 4042-4052.
18. Olhoeft, G.R.: "Electrical Properties of Water Saturated Basalt: Preliminary Results to 506K (233°C)," USGS Open File Report D-77-688 (1977).
19. Olhoeft, G.R. and Ucok, H.: "Electrical Resistivity of Water Saturated Basalt," *EOS*, AGU (1977) 50, 1235.
20. Fuoss, R.M. and Ksia, K.L.: "Association of 1:1 Salts in Water," *Proc.*, Natl. Acad. Sci. (1967) 57, 1550-1557.
21. Bockris, J.O.M. and Reddy, A.K.N.: *Modern Electrochemistry*, Plenum Press, New York City (1970) 1, 2.
22. Jones, G. and Bradshaw, B.C.: "Specific Conductance of Standard Potassium Chloride Solutions in $Ohm^{-1}\ cm^{-1}$," *J. Am. Chem. Soc.* (1933) 55, 1780-1800.
23. Olhoeft, G.R.: "Algorithm and BASIC Program for Ordinary Least Squares Regression in Two and Three Dimensions," USGS Open File Report 78-876 (1978).
24. Dunlop, H.F. and Hawthorne, R.R.: "The Calculation of Water Resistivities From Chemical Analyses," *Trans.*, AIME (1951) 192, 373-376.
25. Desai, K.P. and Moore, E.J.: "Equivalent NaCl Determination From Ionic Concentrations," *The Log Analyst* (May-June 1969) 12-21.
26. Wahl, E.F.: *Geothermal Energy Utilization*, John Wiley & Sons, New York City, (1977) 26-80.

APPENDIX

Using the coefficients for B that are listed in Table 8, the following short BASIC program will generate electrical resistivity in ohm·meter at a given temperature in °C and salt concentration (molar).

```
10 DIM B(3,5), O(1,1), C(1,3), T(5,1), D(1,5)
20 FOR I = 1 to 5
30 INPUT B(1,I), B(2,I), B(3,I)
40 NEXT I
50 DISP "Enter molar concentration and Celsius
   temp"
60 INPUT C,T
70 C(1,1) = C
80 C(1,2) = C*SQR(C)
90 C(1,3) = C*C*LOG(C)
100 T(1,1) = 1
110 T(2,1) = 1/T
120 T(3,1) = T
130 T(4,1) = T*T
140 T(5,1) = T*T*T
150 MAT D = C*B
160 MAT O = D*T
```

```
170 PRINT T,C,1/O(1,1)
180 END
```

Line 10 sets up the matrix dimensions.
Lines 20 through 40 enter the B matrix coefficients from Table 3 for the appropriate salt.
Lines 50 through 60 enter the desired concentration and temperature.
Lines 70 through 140 compute the concentration and temperature matrices.
Lines 150 through 160 compute the electrical conductivity (due to the form of the concentration dependence)
Line 170 prints out the temperature (°C), molar concentration, and electrical resistivity (ohm-meter).

To compute the molar concentration of the solution, multiply the solution concentration in weight percent by the density of the solution, multiply that product by 10, and divide by the molecular weight of the solute. Refer to any standard chemistry textbook.

SI Metric Conversion Factors

ft	×	3.048*	E−01	= m
ft-lbf	×	1.355 818	E+00	= J
degree F		(°F−32)/1.8		= °C
in.	×	2.54*	E+00	= cm
psi	×	6.894 757	E−03	= MPa

*Conversion factor is exact.

JPT

Original manuscript received in Society of Petroleum Engineers office Dec. 21, 1978. Paper accepted for publication July 20, 1979. Revised manuscript received Jan. 16, 1980. Paper (SPE 7878) first presented at the SPE 1979 International Symposium on Oilfield and Geothermal Chemistry, held in Houston, Jan. 22-24, 1979.

GAS SOLUBILITY EFFECT

Studies of production data from various geothermal reservoirs have shown the presence of gases such as CO_2, N_2, and CH_4 in the producing intervals. The presence of such gases as a separate phase may influence the resistivity behavior of rocks. The exact influence of such gases in the dissolved form on formation water resistivity have not been discussed in the literature.

Experimental data were generated on gas solubility effect and it is shown within the pressure range studied here (2500 psia) that dissolved carbon dioxide has the greatest influence at low salt concentrations. No significant effect for other gases were observed under the conditions of these experiments. A paper summarizing the results was presented at the 1979 Annual Meeting of the Geothermal Resources Council in Reno, Nevada (September 1979).

EFFECT OF GAS SOLUBILITY ON ELECTRICAL CONDUCTIVITY OF GEOTHERMAL BRINES

F. Ghassemi and I. Ershaghi

University of Southern California

ABSTRACT

Electrical conductivity of geothermal brines, measured by electric logs may be influenced by the presence of soluble gases. This study presents laboratory data measured at room temperature and at pressures up to 2500 psi. The gases studied included carbon dioxide, methane, and nitrogen.

By and large, carbon dioxide has the greatest influence and mainly at low salt concentrations. For the case of dissolved methane and nitrogen no significant change in the electrical conductivity of the brine is detected.

INTRODUCTION

Many field reports on produced brine from geothermal systems indicate the presence of gases such as carbon dioxide, methane, nitrogen, hydrogen sulfide, and ammonia. The solubility of above gases in water as a function of pressure and temperature has been reported in the literature. Culberson and McKetta[1] studied the solubility of methane in water and showed that the methane solubility in normal geothermal brines (hydrostatic pressures and temperatures from 300°F to 600°F) is very minimal (0.0004 g CH_4/100 g H_2O). For geopressured systems, however, somewhat higher solubilities may be expected. As shown by Stewart and Munjal[2] carbon dioxide has a much higher solubility in water.

During the well log interpretations of liquid dominated geothermal reservoirs, one of the parameters of interest is the estimation of formation water resistivity profile. The salinity profile may be used for subsurface correlation.

The production of gases with geothermal brines is an indication that the gas is either in solution or in the form of free gas saturation. Free gas saturation may reflect itself in the form of high R_{wa}'s (apparent water resistivity) computed from electric logs. Upon the availability of certain combinations of logs (such as Density and Neutron log) the presence of free gas may be verified. The influence of soluble gas on the estimation of brine salinity needs to be investigated.

METHOD OF STUDY

An apparatus was constructed for reconstituting samples of brine and gas at room temperature and pressures ranging from atmospheric to 2500 psi. A schematic diagram of the system is shown in Fig. 1. The essential elements included the test chamber, an accumulator for pressurizing the system and various gas tanks.

The test chamber had two connections; the top, which was used for introducing the brine and the gases into the system, and the bottom, which was used for the conductivity cell. The test chamber was designed for rotation on its support allowing for shaking and mixing the samples of a given brine and the gas under study.

Different conductivity cells were tested and in the final design a prefabricated conductivity cell made by Yellow Spring Instrument Company (YSI 3410) containing platinum-Iridium alloy electrodes was used. Resistivity data were recorded using HP-4800A impedance meter at a frequency of 1 KHz.

The base water used was commercially available distilled water with an average resistivity of 2000 ohm-m at room temperature. Synthetic NaCl solutions were made ranging in concentrations from 100 to 1000 ppm.

EXPERIMENTAL PROCEDURE

The details of the test chamber and various connections are shown in Fig. 2. The test chamber was filled with 600-700

cc of brine leaving about 250 to 150 cc of space for the gas under study. The test chamber was then connected to a given gas tank. The mixture was pressurized using the brine in the accumulator driven by a high pressure nitrogen gas. The pressurization was done in several incremental steps. The test chamber was shaken continuously to ensure complete agitation of the brine and to achieve the maximum solubility of the gas in the brine.

EXPERIMENTAL RESULTS

Brine resistivity data for various gases are shown in Fig. 3-4. At low salt concentrations, the apparent resistivity of brine decreases with pressure for carbon dioxide and reaches to an equilibrium at around 800 psi. (This corresponds to liquifaction pressure for carbon dioxide at room temperature).

For nitrogen and methane, there seems to be a slight reduction in apparent brine resistivity but the effect, in comparison with carbon dioxide, is insignificant. For higher brine concentrations, as shown in Fig. 4, very little effect is noticeable, if any.

The data for carbon dioxide measured at 75-80°F (below the critical point) show the role of the gaseous CO_2 as well as liquid CO_2 in lowering the electrical resistivity of brine. Measurement of PH on the final solution indicated a reduction of PH to a level of 4.5 from the original value of 8. It is believed that because of the formation of carbonic acid, a parallel conductor model may be assumed for representation of the system. The proposed model consists of a strong branch due to the original ionic concentration of the solution and a weak branch because of the ionization of the carbonic acid. The contribution of the weak branch to the overall conductivity becomes significant at low brine concentration or at high pressures.

For methane and nitrogen no such model may be assumed. The small reduction in brine resistivity at high pressures may be because of slight volume reduction of the original brine due to its compressibility.

In geothermal brines temperatures above the critical temperature of carbon dioxide, cause the carbon dioxide to stay in vapor phase. The solubility of CO_2 in brine at a given pressure and temperature may be determined from the data given by Ellis and Golding.[3]

Since the low temperature data of this paper suggests no appreciable effect on the conductivity of high salinity water because of carbon dioxide solubility, it may safely be stated that for geothermal brines with salinities above 1000 ppm and temperatures above 300°F the contribution of CO_2 may be neglected. This is further substantiated by considering the "salting out effect" (lowering of gas solubility at high brine concentration) and the increase in the electrical conductance of the original brine with temperature (as shown by Ucok et al.[4]).

ACKNOWLEDGEMENT

This study was supported as a part of a contract with the geothermal division of the U.S. Department of Energy.

REFERENCES

1. Culberson, O. L. and McKetta, J. J., "Phase Equilibrium in Hydrocarbon-Water System. III - The Solubility of Methane in Water at Pressure to 10,000 psia." Trans. AIME (1951), p. 223-226.
2. Stewart, P. B. and Munjal, P., "Solubility of Carbon Dioxide in Pure Water, Synthetic Sea Water, and Synthetic Sea Water Concentrates at -5° to 25°C and 10 to 45 atm Pressure," Jour. of Chemical and Engr. Data Vol. 15, No. 1 (1970) p. 67.
3. Ellis, A. J. and Golding, R. M., "The Solubility of Carbon Dioxide Above 100°C in Water and in Sodium Chloride Solutions," American Journal of Science Vol. 261 (Jan. 1963), p. 47-60.
4. Ucok, H., Ershaghi, I., and Olhoeft, G. R., "Electrical Resistivity of Geothermal Brines," SPE 7878 paper presented at SPE Calif. Regional Meeting, Ventura, Ca. (April 1979).

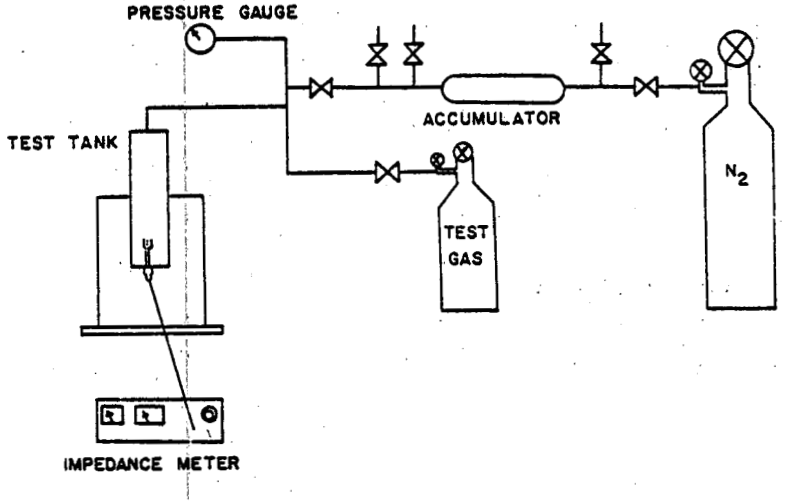

Fig. 1 Schematic diagram of the experimental apparatus.

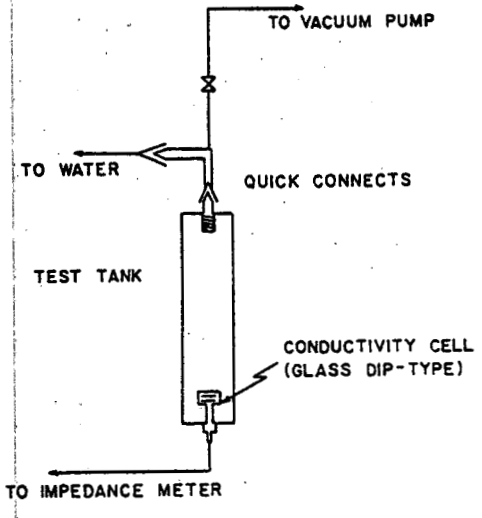

Fig. 2 Details of the test chamber.

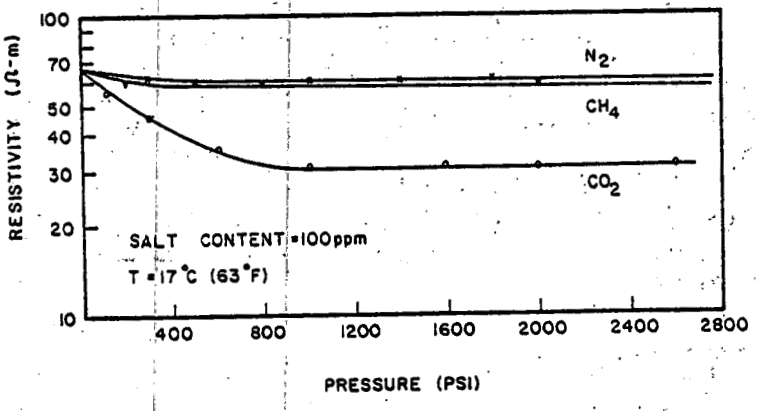

Fig. 3 Effect of dissolved gases at low brine concentrates.

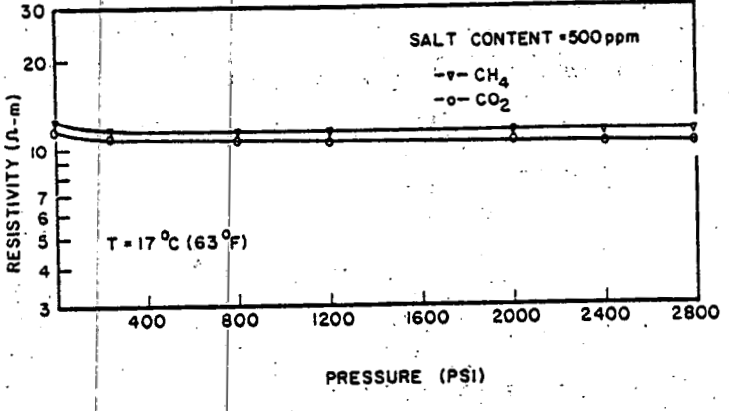

Fig. 4 Effect of dissolved gases at high brine concentrates.

RESERVOIR ROCK RESISTIVITY AT ELEVATED TEMPERATURES

Rock samples studied in this phase included Berea sandstone, Boise sandstone, Cerro Prieto cores, and Hawaiian basalt. The previous studies reported on temperature effect were contradictory and limited to temperature below the levels expected in geothermal reservoirs.

In this study, resistivity behavior of the above rocks saturated with brine were studied up to a temperature of 350°C. Various experimental difficulties had to be overcome and the details of the final design of the experimental set up was reported in Dr. Ucok's Ph.D. Dissertation in file with the University Microfilms International, Ann Arbor, Michigan. A paper summarizing the results was presented at the 1979 Stanford Geothermal Workshop and is included here. Another talk on the subject was presented at the 49th Annual SEG Meeting in New Orleans (November 1979). A more extensive paper on this aspect is being prepared for publication in Geophysics.

In summary, the study showed the significant role of surface conduction as a function of temperature.

Presented at the 1980 Stanford Geothermal Workshop

RESISTIVITY OF BRINE SATURATED ROCK SAMPLES AT ELEVATED TEMPERATURES

Hikmet Ucok, Iraj Ershaghi, USC,
Gary R. Olhoeft, U.S. Geological Survey
and L.L. Handy, USC

Electrical resistivities of rock samples saturated with NaCl solution have been measured at 1 KHz and under 31 MPa hydrostatic pressures and at temperatures up to 350°C. The samples included Berea sandstone, Boise sandstone, cores from the Cerro Prieto geothermal field, Mexico, and Hawaiian basalt.

The measurements were aimed at studying the effect of mineralogy and thermal alteration of rock on the contribution of surface electrical conduction to the overall conductivity. The mineralogical composition of the samples were determined by X-ray diffraction analysis.

The details of the experimental setup have been reported elsewhere and will not be repeated here.[1] Since the overall behavior of saturated rock samples is influenced by the saturating fluid, data from a previous study[2] on the electrical resistivity of brines as a function of temperature are included here.

All samples indicated a typical behavior as shown in Figure 1. In general, the resistivity of the samples decrease sharply between 25°C to 200°C. The rate of decrease slows down considerably beyond this temperature and then a slight increase in resistivity is noticeable above 300°C.

The general behavior of the saturated rock samples shown above is very similar to the behavior of the saturating fluid as shown in Figure 2. In addition to the brine, however, there are other factors controlling the temperature dependence of rock. These include formation resistivity factor, surface conductance, mineralogy, etc.

As shown in Figure 3, formation resistivity factor decreases with temperature up to 150°C - 175°C and then stabilizes at higher temperature. The rate of decrease is a function of surface conduction of the rock sample. The observed decrease in formation resistivity factor is explained by the effect of temperature on the conductance of the ionic double layer. The specific surface conductance of constant charge density surfaces changes only if the average mobility of ions changes with temperature.

Experiments with Berea sandstone samples indicate that the relative contribution of surface conductance to the overall conductivity is dependent upon the solution concentration. This is evident from the comparison of Figure 4 and Figure 5.

As shown in Figure 6 the relative formation resistivity factor of samples with surface conductance vary with temperature. The samples with a high content of clay minerals show a higher decrease in the relative formation resistivity factor. Increasing the solution concentration affects this considerably. For example, the Cerro Prieto sample No. 5 shows a 16% decrease in formation resistivity factor at about 150°C when the pore fluid concentration is 0.5 wt%. The change is reduced to 10% when the pore fluid concentration is 3 wt%.

For a sample of Berea sandstone ignited up to 550°C for four hours, a plot of solution resistivity versus sample resistivity is shown in Figure 7. All data points up to a temperature of 175°C fall on a straight line and deviate from it at higher temperatures. As shown in Figure 8, the formation resistivity factor appears to be constant and independent of temperature up to 175°C and then increases with temperature. Although the pore fluid concentration is 0.5 wt%, no appreciable surface conductance is observed. This is explained by the thermal alteration of the cation exchange capacity of clay materials because of ignition. This is in agreement with the data presented by Kern, et al.[3] but is in contradiction with those of Sanyal.[4]

The observed increase in formation resistivity factor at temperatures higher than 175°C may be attributed to physical changes in pore construction because of thermal expansion. Based on the work published by Maxwell and Verral[5] and Maxwell[6] some degree of reduction in the porosity with temperature is expected. The magnitude of such reduction is, however, not enough to support the hypothesis that the reduction of porosity is fully responsible for the observed increase in formation resistivity factor.

The other contributing factor is the porosity exponent. The composite effect of both the porosity reduction and an increase in porosity exponent is a more reasonable explanation of the observed behavior of the formation resistivity factor.

From the experiment on the ignited Berea sample and another Berea sample unexposed to high temperature, we were able to compute the effect of surface conduction on formation resistivity factor and as a function of temperature, Fig. 9.

In general, above a temperature of 150°C, the structural change in the rock may offset the true effect of surface conduction on the formation resistivity factor.

References

1. Ucok, H., Temperature Dependence of the Electrical Resistivity of Aqueous Salt Solutions and Solution Saturated Porous Rocks, Ph.D. Dissertation, University of Southern California, 1979.

2. Ucok, H., Ershaghi, I. and Olhoeft, G.R., "Electrical Resistivity of Geothermal Brines," Proc. SPE International Symp. on Oilfield and Geothermal Chemistry, Houston, Texas (1979), pp. 163-172.

3. Kern, J.W., Hoyer, W.A. and Spann, M.M., "High Temperature Electrical Conductivity of Shaly Sand," Trans. Eighteenth Annual Symp. of Soc. Prof. Well Log Analysts, Houston, Texas (1977).

4. Sanyal, S.K., The Effect of Temperature on Electrical Resistivity and Capillary Pressure Behavior of Porous Media, Ph.D. Dissertation, Stanford University, 1972.

5. Maxwell, J.C. and Verral, P., "Low Porosity May Limit Oil and Deep Sands," World Oil (1954) 138, pp. 106-113.

6. Maxwell, J.C., "Experiments on Compaction and Cementation of Sand," pp. 105-132, Rock Deformation, D. Griggs and J. Handin, Editors, Mem. 79, Geol. Soc. America, 1960.

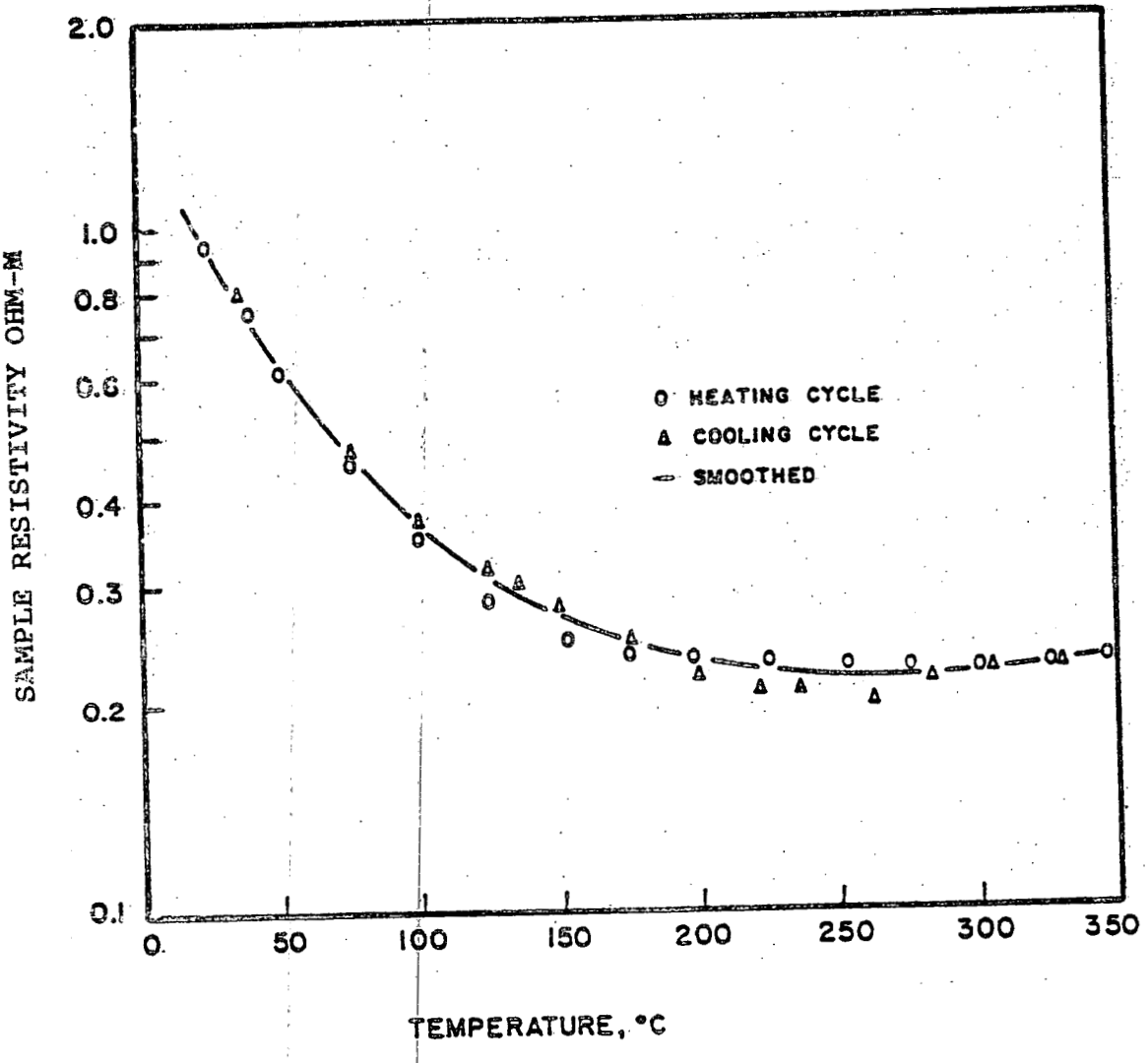

Fig. 1- Typical Resistivity Behavior With Temperature

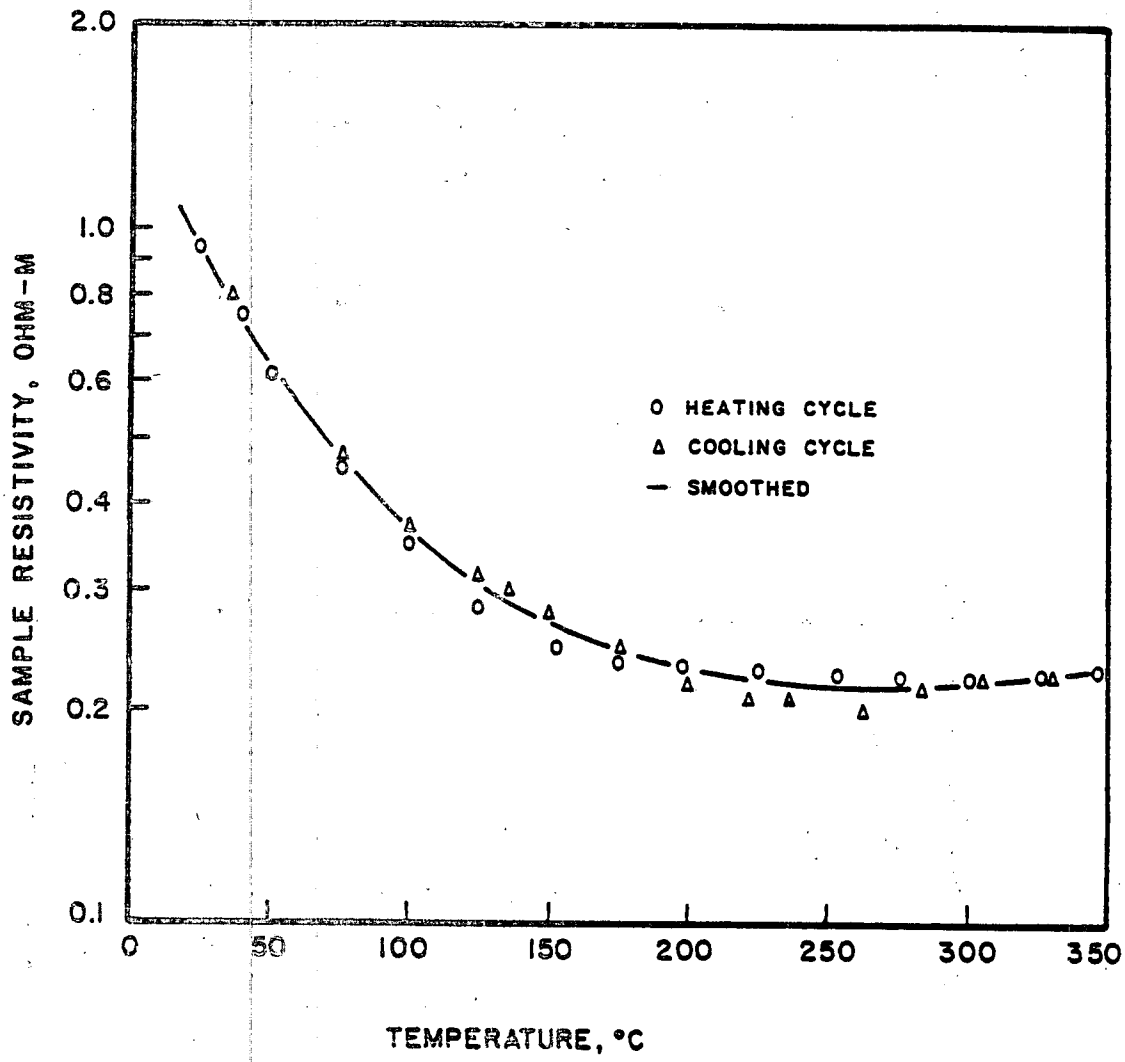
2.0
1.0
0.8
0.6
0.4
0.3
0.2
0.1
SAMPLE RESISTIVITY, OHM-M
0
50
100
150
200
250
300
350
TEMPERATURE, °C
O HEATING CYCLE
Δ COOLING CYCLE
— SMOOTHED

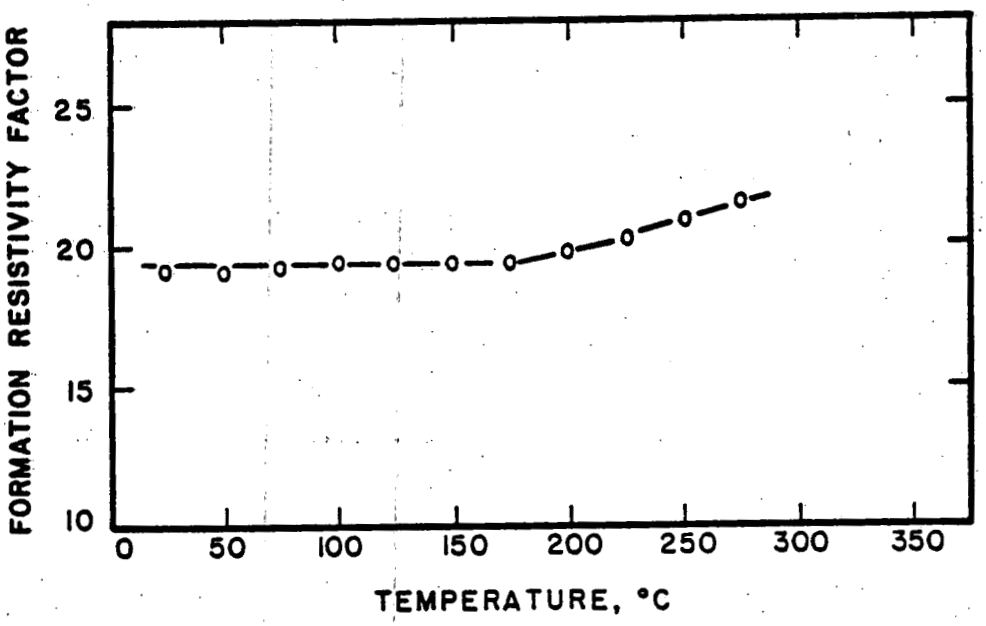

Fig. 8- Formation Resistivity Factor vs. Temperature for the Ignited Core.

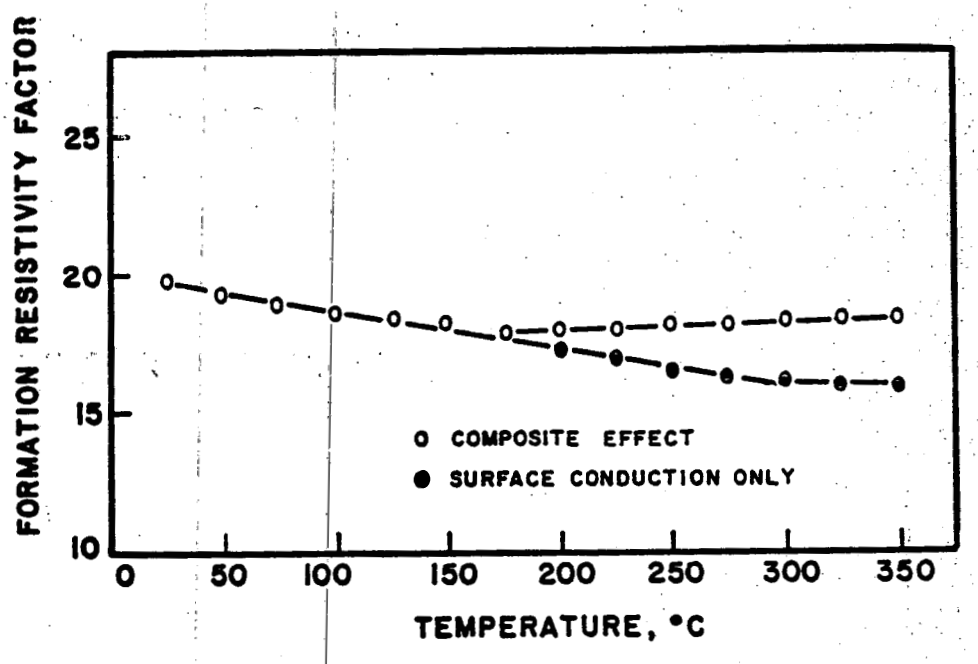

Fig. 9- Effect of Surface Conduction on Formation Resistivity Factor.

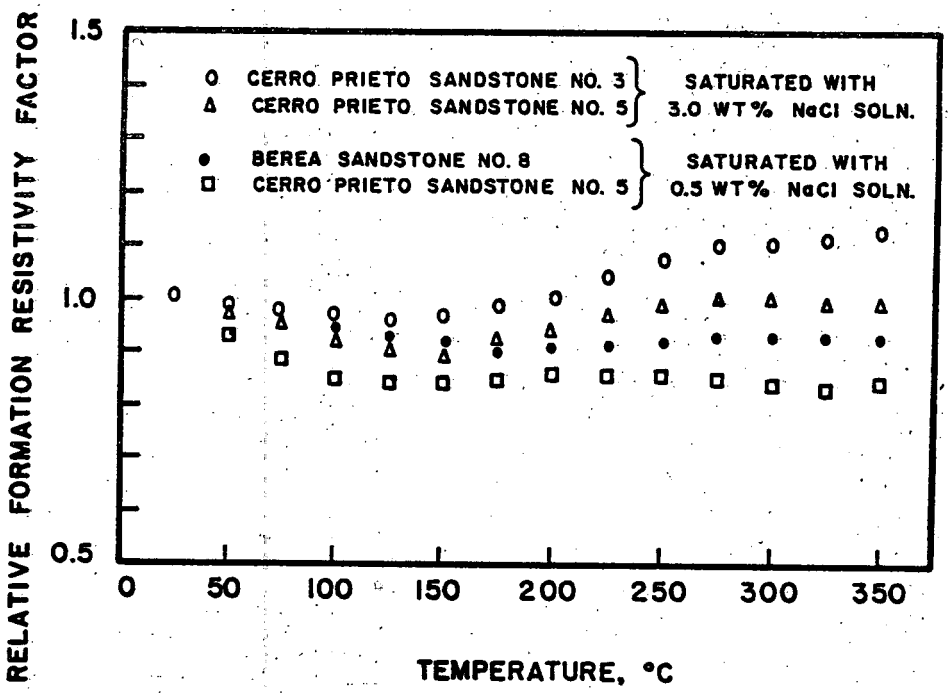

Fig. 6- Effect of Temperature on Relative Formation Resistivity Factor.

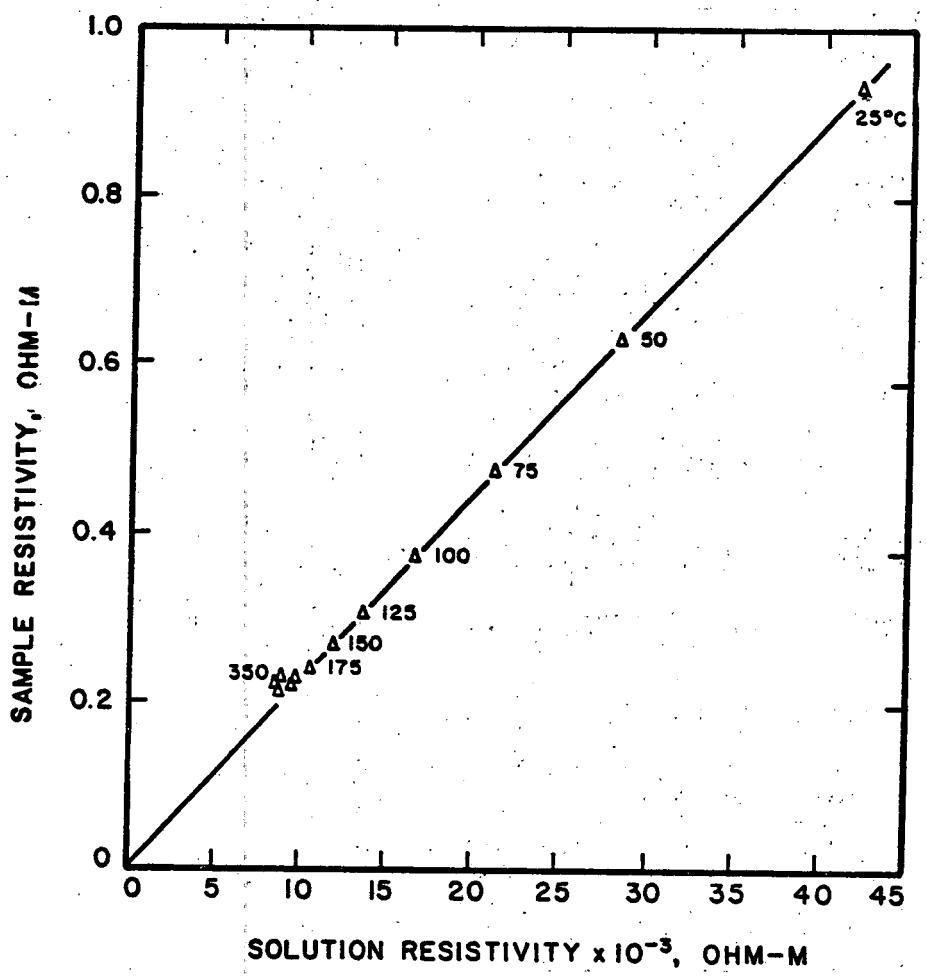

Fig. 7- Sample Resistivity vs. Solution Resistivity for the Ignited Berea Core

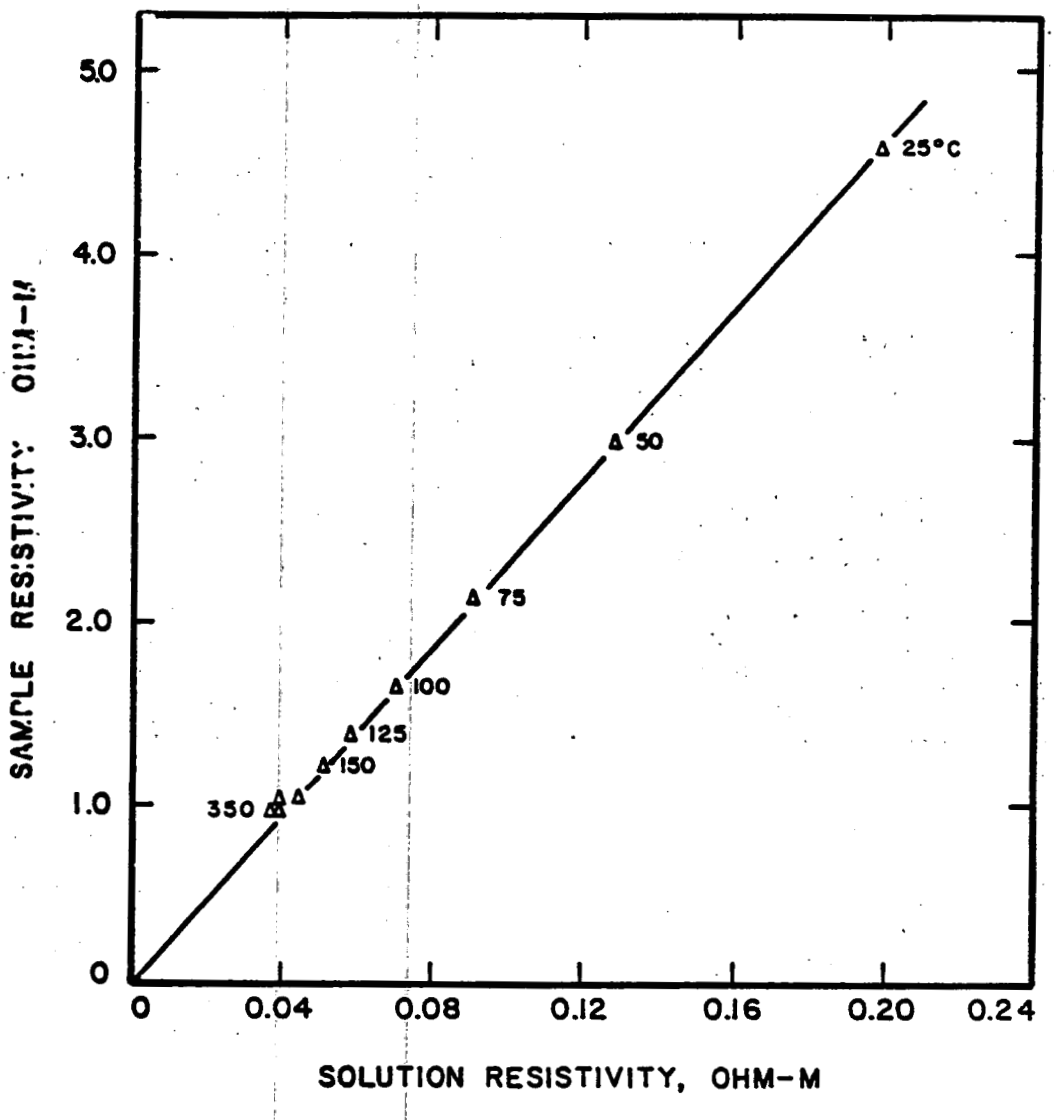

Fig. 5- Behavior of Berea Core Resistivity with Temperature at High Brine Concentration.

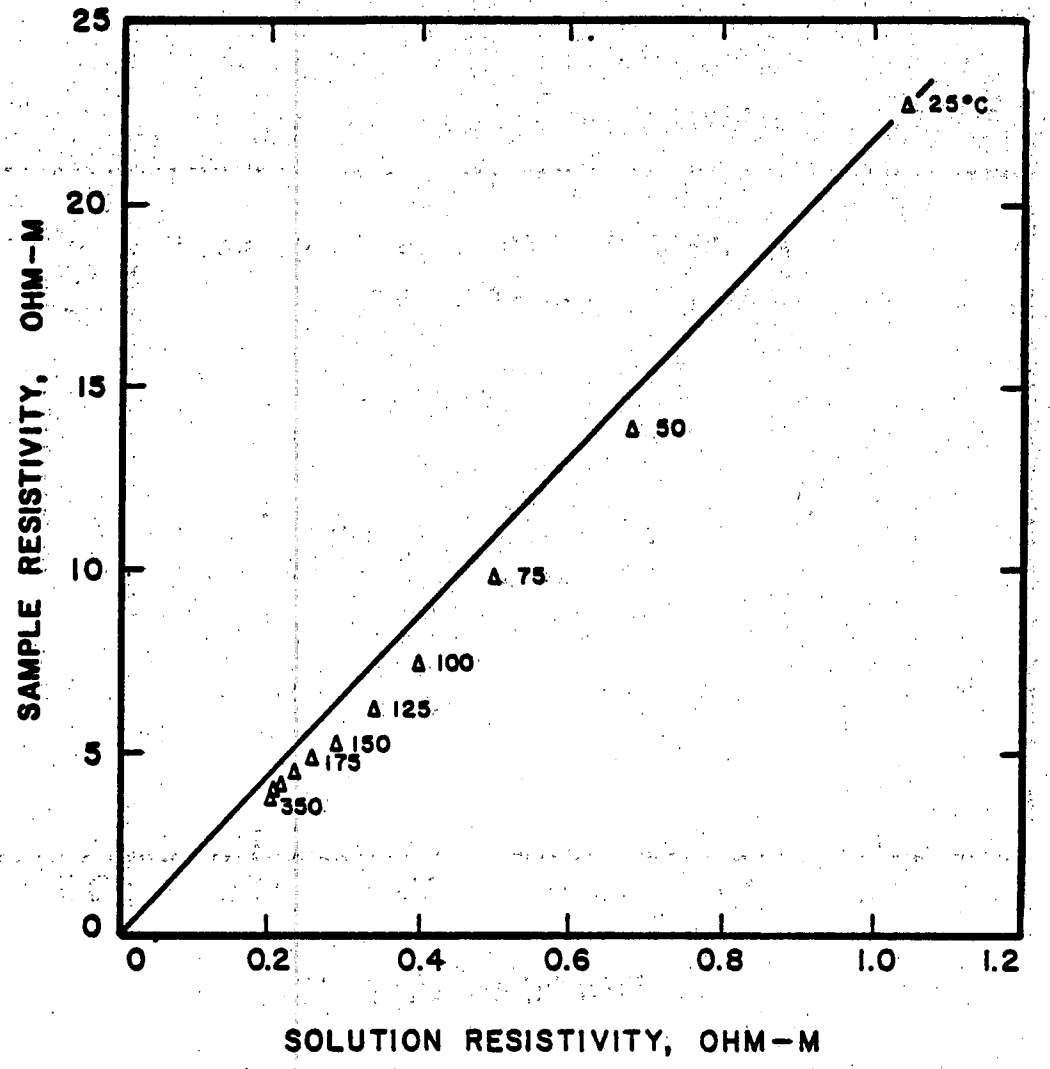

Fig. 4- Behavior of Berea Core Resistivity With Temperature at Low Brine Concentration.

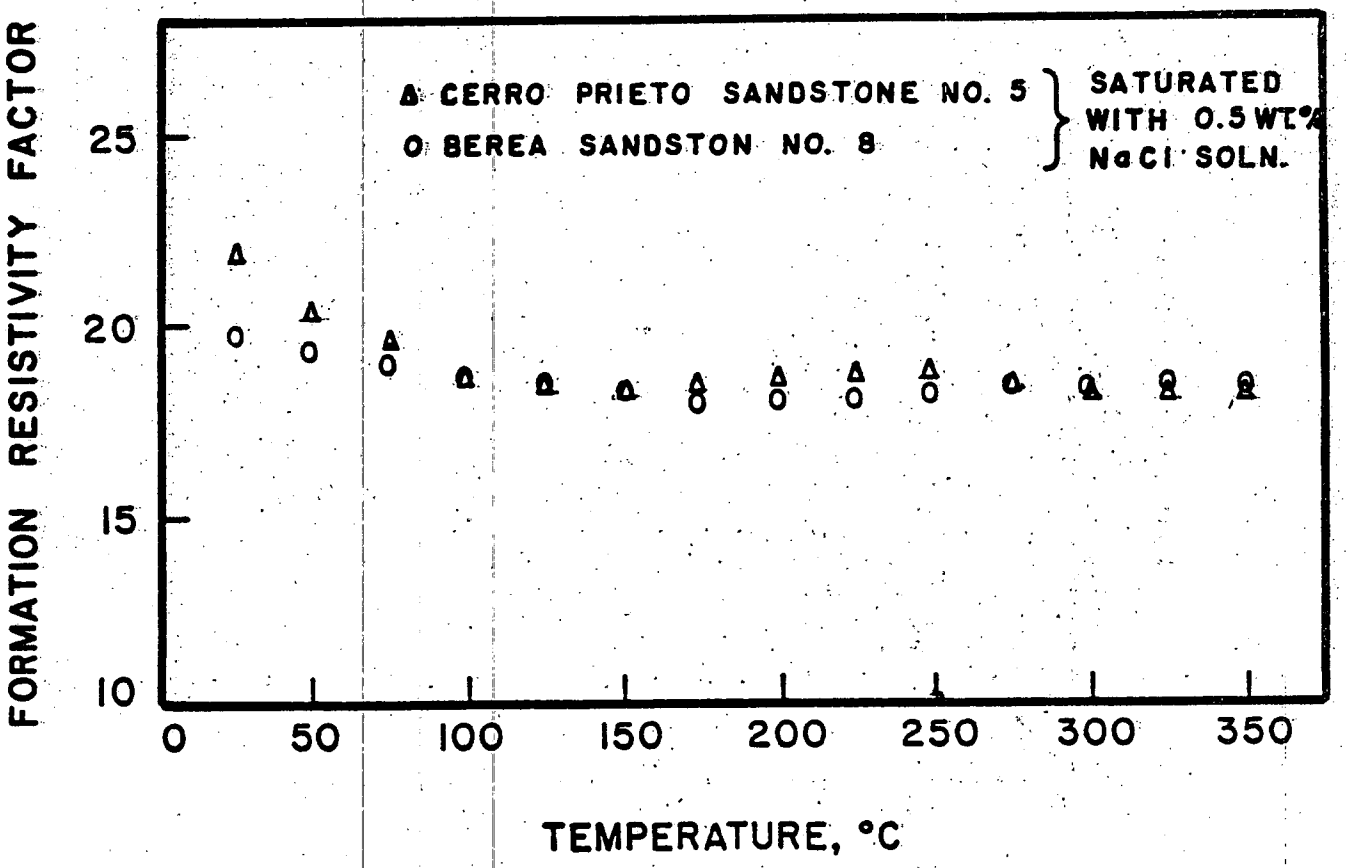

Fig.3-Effect of Temperature on Formation Resistivity Factor.

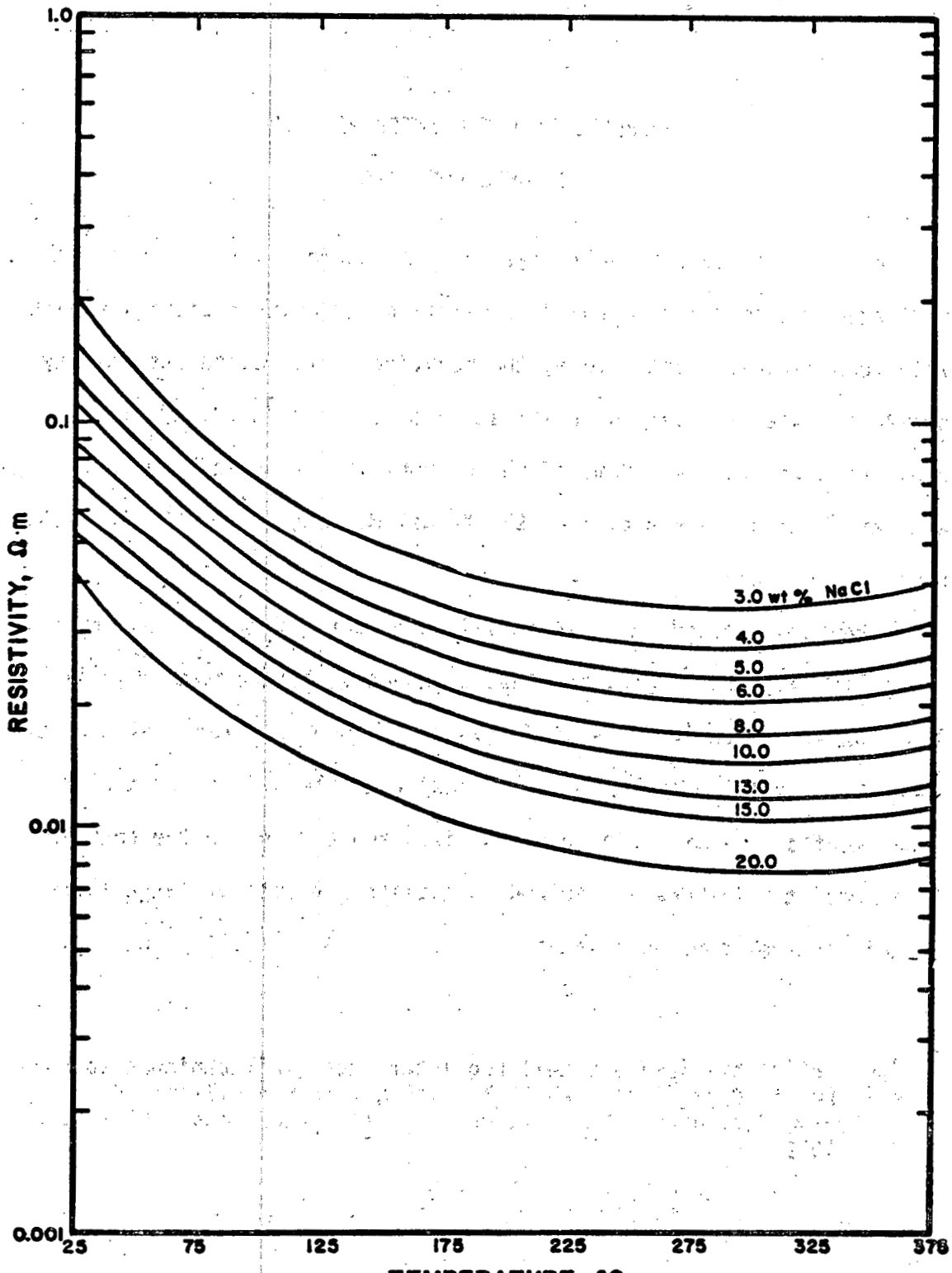

Fig. 2- Resistivity of NaCl Solution as a Function of Temperature (Ref. 2)

PROBLEMS IN FIELD INTERPRETATION OF WELL LOG DATA

A review of certain well logs from the Cerro Prieto field in Mexico indicated the need for improved correlation for brine resistivity data with temperature. Furthermore, the behavior of formation resistivity showed the need for careful examination of clay conductivity effect at elevated temperatures. Some of these problems were briefly discussed in a paper which was given at the 1977 Annual Meeting of the GRC in Hilo, Hawaii.

The study showed inconsistencies in computed formation water resistivity obtained from 3 different approaches; spontaneous potential log, R_{XO} data, and R_t data. Some factors responsible were pointed out in a later study supported by a contract with the GLIP program of the Department of Energy.* The results discussed earlier on the rock and fluid resistivity behavior helped to explain the role of temperature effects in the above observations.

* "Application of Oil-Field Well Log Interpretation Techniques to the Cerro Prieto Geothermal Field," I. Ershaghi, L.B. Phillips, E.L. Dougherty, L.L. Handy. Los Alamos Scientific Lab. Report LA-8130-MS (Oct. 1979).

PROBLEMS IN ESTIMATION OF SALINITY PROFILE IN LIQUID-DOMINATED GEOTHERMAL SYSTEMS

I. Ershaghi, E. L. Dougherty, H. Ucok, and F. Ghassemi

DEPARTMENT OF PETROLEUM ENGINEERING
UNIVERSITY OF SOUTHERN CALIFORNIA

ABSTRACT

Estimation of salinity profile in producing geothermal wells is of great importance in subsurface mapping and in designing the well completion. Well logs have traditionally been used to estimate R_w and, hence salinity, in sedimentary type oil field reservoirs. Geothermal reservoirs introduce complexities which can lead to errors in interpretation of well log data using existing oil field correlations. This paper presents a review of certain aspects of the problem with examples from the Cerro Prieto field in Mexico.

INTRODUCTION

Geothermal systems often consist of massive rock bodies comprising several sub-reservoirs. Depending on the type and the source of the recharge, the percolation path, and the physiochemical state of each reservoir, the chemical composition as well as the total dissolved solid concentration of liquid water often varies among the sub-reservoirs. Commingling of production, as is common in producing wells, yields a mixture of water from these sub-reservoirs. Thus, in most instances well logs provide the only practical means of detecting salinity differences between producing zones. In oil and gas reservoirs observed salinity lows and highs are used to help detect overpressured zones.

In oil and gas reservoirs salinity measurement is somewhat simpler than in a geothermal system. Petroleum reservoirs are generally sedimentary rocks at temperatures below 300°F, and in normally pressured systems the salinity of the water in sands and shales will be related. Geothermal reservoirs, however, are usually found in fractured igneous and metamorphic rocks at temperatures higher than 300°F. Although sedimentary type geothermal reservoirs exist, it is frequently found that because of igneous intrusion, contact metamorphism and hydrothermal alteration, the permeable layers (sandstone-limestone) are in a brittle and fractured state and the non-permeable zones(shale) have considerably different petrophysical properties than surrounding beds or similar layers located at shallower depths. Also, percolation of the recharge water through the permeable section may result in the salinity in such zones being considerably different than that in the thermally altered inaccessible shale layers.

The purpose of this study was to apply some of the interpretative techniques developed for petroleum reservoirs to a typical sedimentary-type geothermal system and estimate the salinity profile. Furthermore, it was our objective to identify shortcomings of existing techniques in handling the geothermal reservoir environment.

Reservoir Description

Geophysical logs recorded in the Cerro Prieto geothermal field in Mexico were used in this study. The field is located in the northwestern part of Mexico within the Mexicali geothermal province. The field is composed of deltaic and non-deltaic sediments. The geology of the area is described by Paredes[1] and Mercado[2].

Methodology

Formation water resistivity, R_w, is an indicator of the total dissolved concentration. Estimation of R_w, however, will not lead to identification of the type and nature of dissolved solids. Three methods are primarily used in the petroleum industry to estimate R_w; these are chemical analysis of formation water, analysis of the SP curve, and the interpretation of formation resistivity logs.

As mentioned earlier, commingling of production from several zones often precludes use of the chemical analysis method for geothermal wells. Even if individual zones were tested separately unless the water samples are maintained in pressurized and thermally insulated containers, the thermodynamic changes that the produced water may undergo during its trip from bottomhole to the surface may result in totally unrepresentative dissolved solid concentrations.

The next logical approach is the use of well log data. Before discussing the merits or drawbacks of log-derived values of R_w, let us point out that verifying the quality and accuracy of well logs depends upon proper calibration and making repeat runs. Furthermore, accurate records of the drilling mud type and properties are also needed.

The magnitude of the SP is determined by:

$$SP = -K \log \frac{a_w}{a_{mf}} \quad (1)$$

where a_w and a_{mf} are the activities of the formation water and mud filtrate, respectively, and K is a function of formation temperature. For brines with salinities below 60,000 ppm the activities may be replaced by resistivities.

$$SP = -K \log \frac{R_{mf}}{R_w} \quad * \quad (2)$$

Thus, if a knowledge of R_{mf} at formation temperature is available, from the reading of SP deflection, R_w may be easily estimated. Unfortunately the presence of shale in reservoir rock tends to reduce the observed potential and the value of R_w computed is too high. Also if formation water is relatively fresh, the presence of ions other than Na^+ and Cl^- sometimes lead to SP's that are too large resulting in low values for R_w. The major uncertainties surrounding the use of the SP in geothermal systems are the correct estimation of temperature and the validity of the existing SP correlation at elevated temperatures.

For a brine saturated system an estimate of R_w is obtained from a deep investigating resistivity tool (such as a deep induction log), using the following relationship:

$$R_w = \frac{R_t}{F} \quad (3)$$

where R_t is the formation true resistivity and F is the formation resistivity factor. Ideally, the above equation may lead to a very reliable estimate for R_w since no need for accurate estimation of reservoir temperature is apparent. But a careful analysis of the equation indicates some inherent problems not to be overlooked. Log analysts obtain formation resistivity factor from an estimation of formation porosity, such as:

$$F = \frac{a}{\phi^m} \quad (4)$$

where ϕ is porosity and a and m are constants. Correlations of this nature are all based on the assumption that F is independent of the type of the fluid. This assumption may be valid in petroleum reservoirs. But for geothermal reservoirs where considerable interaction between rock and fluid at elevated temperature are expected further refinements of the correlation appears to be needed.

Based on work currently underway in our laboratories, preliminary results indicate that the temperature may have a significant effect on the $F - \phi$ relationship. The problem is compounded when one superimposes the electrical conductivity effect of dispersed or laminated shale.

In addition, the above equation assumes that the formation is completely saturated with water ($S_w = 100\%$). This may not be a realistic assumption even in a liquid-dominated geothermal system. The presence of dissolved gases such as CO_2, N_2, H_2S and even CH_4 in produced geothermal fluid strongly suggest the possibility of a free gas saturation in the formation. Although the gas saturation may be below or at the critical level (immobile gas), its effect on the overall formation electrical conductivity may be significant. Use of equation (3) in such cases will obviously lead to estimates of R_w which are too high.

Cross plots of $R_t - \phi$ have also been used in oil field practice. The method is based on plotting log R_t vs log ϕ and estimating m from the slope and a R_w from the intercept. Determining R_w requires a knowledge of the constant, a.

Another approach may be the use of flushed zone data. The following equation may be used to estimate R_w without a need for F.

$$R_w = \left(\frac{R_t}{R_{xo}}\right) R_{mf} \quad (5)$$

where R_{xo} is the resistivity of the flushed zone obtained from a shallow investigating tool. Here, the assumption is that the saturation conditions in the flushed and uninvaded zones are identical (both may contain an immobile gas phase).

In all of the above formulations, no parameter indicating the shale content enters into the equations. Several methods for computing water saturation in shaly sands have been proposed. As shown by Fertl and Hammack[3], all of the shaly sand formulas become insensitive to the shale content as water saturation approaches 100%. Therefore, in the Preliminary Study no attempts were made to utilize the existing formulas.

Results of the Study

A few selected wells in the Cerro Prieto which had yielded good quality logs were analyzed in this study. Table 1 shows a typical trend of the recorded well log data. The Saraband porosities indicate a reduction of effective pore space with depth which may be because of compaction. An apparent increase in R_t with depth is somewhat unexpected. Ordinarily one expects a lowering of R_w with depth both because of increasing TDS and higher temperatures. But a similar increasing trend in the spontaneous potential with depth suggests the possibility that the shale contribution to the overall conductivity of the formation diminishes as higher temperatures are encountered.

Table 2 shows some typical computations applying the methods discussed in this paper to four wells in the field. In general for shallow depths (where Saraband log still shows the shale effect to be existent), the R_w from SP and from eqn.(5) are very similar. R_w's from eqn(3) are, however, lower. For deeper sands where temperatures are higher the results from eqns.(5) and (3) become closer while the R_w's from SP are lower. This may be due partly to our extrapolation of the

* Actually, the equation is more correctly expressed in terms of "equivalent" resistivities which are correlated with actual resistivities.

existing SP equation to elevated temperatures where other thermal effects may need to be considered.

The R_t - ϕ plot approach so far has been inconclusive. This may be attributed mainly to variation in R_w with depth.

Conclusions

Preliminary studies conducted on well logs for a typical liquid dominated system indicate the need for careful study and understanding of temperature effects on the existing oil field petrophysical correlations before their applications to elevated temperatures. Indications are that the hydrothermal alteration of shale with depth significantly affect the R_w's computed from different methods discussed in this paper.

REFERENCES

1. Paredes, E., "Preliminary Report on the Structural Geology of the Cerro Prieto Geothermal Field." Paper presented at 2nd U. N. Symposium, 1976, p.518.

2. Mercado, S., "Movement of Geothermal Fluids and Temperatures Distribution in the Cerro Prieto Geothermal Field, Baja California, Mexico." Paper presented at 2nd U. N. Symposium, 1976, p. 492.

3. Fertl, W. H., and Hammack, G. W., "A Comparative Look at Water Saturation Computations in Shaly Pay Sands," The Log Analyst (March - April, 1972) p. 12.

ACKNOWLEDGMENTS

The assistance of DR. J. Rivera from Comision Federal de Electricidad, Mexico, and Dr. M. Lippman from Lawrence Berkeley Laboratory in obtaining copies of the well logs is greatly appreciated. This study is being sponsored by a research grant from the Geothermal Division of the United States Department of Energy.

TABLE 1

TYPICAL BASIC RECORDED DATA

WELL X-1

Permeable Zone	Depth, ft From	To	(Saraband) ϕ	T, °F	Rt ohm-m	SP mv
1	2570	2625	0.280	385	0.91	-27
2	2658	2695	0.270	410	1.11	-25
3	2748	2782	0.290	420	1.00	-20
4	3085	3110	0.270	450	1.176	-30
5	3145	3180	0.290	460	.91	-28
6	3200	3225	0.295	470	.96	-30
7	3235	3280	0.270	480	.95	-27
8	3590	3613	0.230	500	2.33	-43
9	3694	3715	0.210	520	2.50	-42
10	3780	3806	0.250	530	2.44	-50
11	3923	3945	0.210	540	2.63	-55
12	3980	4020	0.260	550	1.89	-53
13	4100	4140	0.210	555	2.00	-55
14	4155	4180	0.200	570	2.50	-60

TABLE 2

COMPARISON FOR SEVERAL WELLS

Shallow

Well	Depth	R_w (S_p^w)	R_w (R_t^w)	R_w (eqn 5)
X-2	3535-3560	.150	.034	.110
X-3	2785-2830	.110	.022	.091
X-4	2650-2685	.180	.083	.160

Deep

Well	Depth	R_w (S_p^w)	R_w (R_t^w)	R_w (eqn 5)
X-2	4595-4655	.035	.0770	.088
X-3	3715-3760	.07	.080	0.11
X-4	4170-4200	.08	.086	0.095

PERMEABILITY DETERMINATION

Estimation of formation permeability in petroleum exploration using well logs has been a frustrating one. Geothermal systems, in the absence of hydrocarbon phase, present opportunities for further investigations.

The filtration of drilling fluids against a porous and permeable rock is a function of rock porosity and permeability. The depth of mud filtrate invasion then may lead to an estimate of rock permeability. Dual-Induction Laterlog data may be used to compute the radius of invasion.

A study was conducted on the possible application of the above concept. The study included the construction of a wellbore numerical simulator to predict a depth profile of invasion radius for a given permeability column. The invasion profile obtained from Dual-Induction Laterlog was then used for estimation of permeability profile by an iterative technique.

The study showed that for low solid muds the concept may be applicable. Certain properties of drilling fluids needed for the simulation job are not routinely recorded in the field. Fluid loss properties recorded using the API static test are misleading and modified designs of the approach are suggested. In fact, a suitable design was tested for possible field applications.

Various studies conducted under this phase pointed out the feasibility of the proposed technique. Unfortunately, no field example can be presented at this time because of insufficient data about the characteristic of the drilling fluid. This is an area which requires further investigation.

The sequence of papers included here consist of the following:

1. "Permeability Determination in Liquid Dominated Geothermal Reservoirs Using the Dual-Induction Laterlog," I. Ershaghi, E.L. Dougherty, D. Herzberg, and H. Ucok. This paper was presented at the 1978 SPWLA Symposium in El Paso, Texas.

2. "Modeling of Filter Cake Buildup Under Dynamic-Static Conditions," I. Ershaghi, M. Azari, SPE 8902 paper presented at 1980 California Regional Meeting, Los Angeles, CA.

3. "Modeling of Filter-Loss Invasion in an Anisotropic System," B.A. Troesch. Dept. of Mathematics, Univ. of So. Calif.

4. "An Improved Method for Measurement of Filtration Properties of Drilling Fluids," A. Mehdizadeh and I. Ershaghi. Paper presented at the Western Regional SPE Student Paper Contest, Los Angeles, CA (April 1980).

PERMEABILITY DETERMINATION IN LIQUID DOMINATED GEOTHERMAL RESERVOIRS USING THE DUAL INDUCTION LATEROLOG

I. Ershaghi, E. L. Dougherty, D. Herzberg
and H. Ucok

Department of Petroleum Engineering
University of Southern California

ABSTRACT

A method has been developed to estimate the permeability profile in a geothermal well from a Dual Induction-Laterolog, a porosity log, and drilling data. The procedure is based on modeling the invasion of the drilling mud filtrate into the formation and using a history matching technique to arrive at the permeability profile. Input data to the computer model includes basic drilling mud properties, drilling hydraulics, and dimensions of the tubular goods. A permeability profile is assumed for the well and the computer program is run. The objective is to compare the invasion radius computed from the program to that derived from the logging data. The process is then repeated until a satisfactory match is obtained.

INTRODUCTION

Estimation of physical properties of reservoir rock in geothermal systems poses new challenges to existing theories and methods applicable to oil and gas reservoirs. Presence of high temperature limits the utility of existing tools and, even if the tools were available, interpretation of data opens up new frontiers in formation evaluation. Currently efforts are underway to improve the design of tools and make them resistant to the hostile environment in geothermal wellbores. Many researchers have started work on improved or new interpretation methods for estimation of rock and fluid properties from well log data. Baker et al.[1] and Sanyal and Meidav[2] summarized certain difficulties associated with formation evaluation in geothermal reservoirs.

This paper presents a new approach to estimating permeability of liquid-dominated geothermal reservoirs. The proposed technique uses a combination of drilling data together with a dual-induction laterolog. A numerical simulator of wellbore hydraulics during drilling is used to predict invasion profiles for assumed permeability profiles. Comparison of predicted invasion effects to those indicated by the dual-induction laterolog indicates whether or not the assumed permeability profile is reasonable. The method is not believed applicable to oil and gas reservoirs.

STATEMENT OF THE PROBLEM

Permeability of reservoir rock is an important parameter in reservoir assessment. Reservoir engineers need the permeability to calculate deliverabilities, to estimate interference between wells, and to complete an overall reservoir description. By and large, core analysis and measurement

of pressure transients are the most common techniques used in oil field practice to estimate reservoir rock permeability. Attempts to use well logs to estimate formation permeability have resulted in empirical correlations which may not be universally applicable. A review of the literature shows that the logging methods proposed in the past for estimating rock permeability fall into one of the following categories:

1 - methods based on Kozeny equations (electric log)

2 - methods based on acoustic logs

3 - methods based on free fluid index (NML)

4 - methods based on TDT

It is appropriate that a brief review of existing techniques be given here to acquaint the reader with the limitations that these methods may have in geothermal reservoir evaluation.

1 - Permeability from Kozeny equation

A general correlation between rock permeability, porosity and surface area may be written as shown below:

$$K = A \frac{\phi^B}{S_{wi}^C}$$

where

K = single phase permeability

ϕ = porosity

S_{wi} = connate water saturation

A, B, and C = constants

Table 1 shows some of the correlations published by different investigators[3-6]. In the above method it is assumed that the rock contains irreducible water saturation. This concept is valid only in oil and gas reservoirs where hydrocarbon is the dominant phase and water saturation is at its connate level.

Table 1

Permeability Estimates from ϕ and S_w

Correlation	Author(s)	Reference
$K = \frac{C\phi^3}{S_{wi}^2}$	Wyllie and Rose[3]	Jour. Pet. Tech., April, 1950
$K = \frac{A\phi^B}{S_{wi}^C}$	Timur[4]	The Log Analyst, 1968
$K = \frac{A}{S_{wi}^B P_c^C}$	Brown and Husseini[5]	SPWLA Trans. 1977

2 - Methods based on acoustic logs

The use of acoustic logs to estimate permeability has been suggested in the literature. Lebreton et al.[7] proposed the use of an equation of the type:

$$I_e = \alpha' \log_{10} \frac{k}{\mu} + \beta'$$

where α' and β' are approximately constant for a given borehole and $I_e = h_3/h_1$ obtained from the recorded sonic wave train. (h_1 and h_3 are peak amplitudes of two of the first arches.)

Dowling and Boyd[8] also proposed use of the sonic log to estimate formation permeability. In their approach the permeability is estimated from incremental changes in the transit time due to fluid movement caused by the sonic vibrations.

In a recent paper, Staal and Robinson[9] estimated permeability from measurement of the full acoustic wave train; their work is based on the theoretical work of Biot[10] and Rosenbaum[11]. In this technique formation permeability is related to the attenuation of the acoustic wave that corresponds in velocity to the Stonely Wave. Work in this area is in the preliminary stage.

3 - The use of nuclear magnetic log

As discussed by Seever[12], the nuclear magnetic log potentially can provide information about rock permeability.

Timur[13] demonstrated the use of the NML logs for estimation of the specific permeability of a formation from empirical correlations developed

for a given field. The major drawback of this technique is the massive amount of laboratory data required for each case to estimate the empirical coefficients.

4 - Methods based on TDT

Several authors have proposed using the Thermal Decay Time log to make a qualitative or quantitative estimate of permeability. Engelke and Hilchie[14] showed that if the mud filtrate has a higher salinity than the formation water the Neutron Lifetime log together with porosity data may be used to derive a qualitative estimate of the invasion profile and determine the permeable zones. Dowling et al.[15] proposed to alter the natural charged ion spatial distribution in the formation fluids and to measure the resulting thermal neutron decay time characteristics of the formation. Comparison to a reference rock with no alteration provides an estimate of permeability.

The problems associated with the use of the TDT in geothermal reservoirs have not been reported or discussed.

DESCRIPTION OF THE PROPOSED TECHNIQUE

During drilling and prior to running well logs, the drilling fluid percolates into the permeable sections of the wellbore (if wellbore pressure exceeds formation pressure). Mud filtrate displaces the original formation fluid near the wellbore; the mud is filtered out on the rock face and forms a mud cake. Depending upon the composition of the drilling fluid, the sealing properties of the filter cake vary. For oil and gas reservoirs it is imperative that the invasion of mud filtrate be minimized and thus a mud composition with low filter loss is desired. Bentonite, a major ingredient of oil well drilling fluid, has excellent sealing properties. Addition of certain chemicals or materials can further improve the sealing properties of the mud cake and thus minimize invasion of the formation by mud filtrate. Deep invasion in hydrocarbon saturated rocks is undesirable, because the displacement of the mobile hydrocarbon from the vicinity of the wellbore may mask the true potential of a formation. Furthermore, mud filtrate invasion often damages the native producing formation, and may greatly lower the productivity index of the well.

For a liquid dominated system the displacement of formation brine by the mud filtrate will not cause any problem with respect to fluid saturation determination. The estimation of formation water resistivity from electrical logs, however, will be sensitive to the invasion radius of mud filtrate and the problem of formation damage is still at hand.

In addition to the mud composition, the radius of invasion is dependent on rock porosity and permeability and drilling hydraulics. Ignoring the sealing properties of mud and assuming the same pressure gradient for a given rock permeability, the mud filtrate will travel farther into a formation if the porosity is low, and for the same porosity a high permeability rock will allow deeper invasion of filtrate. Since the sealing properties of the mud and the pressure gradient also play important

roles in the filtration process, the following equation may be used to depict the relationship for estimation of invasion radius:

$$r_i = f(mc, \Delta p, t, \phi, K)$$

where r_i = invasion radius

mc = mud composition

Δp = pressure differential between wellbore and formation

t = exposure time

ϕ = formation porosity

K = formation permeability

It seems theoretically possible that if one could estimate invasion radius (dual-induction laterolog) and input t, ϕ, Δp, and a measure of mc, the formation permeability may be obtained from the above equation.

ESTIMATION OF INVASION RADIUS

The use of three resistivity devices (small slam) with different geometric factor has been proposed as a means of estimating invasion radius. This is based on solving the following three simultaneous equations and obtaining the geometrical factors in addition to the correct estimation of R_t.

$$\frac{1}{R_{ILD}} = \frac{G_m}{R_m} + \frac{G_i}{R_i} + \frac{G_t}{R_t} + \frac{G_s}{R_s} \quad \text{(deep induction)}$$

$$\frac{1}{R_{ILM}} = \frac{G_m}{R_m} + \frac{G_i}{R_i} + \frac{G_t}{R_t} + \frac{G_s}{R_s} \quad \text{(medium induction)}$$

$$R_{LL} = G_m R_m + G_{mc} R_{mc} + G_i R_i + G_t R_t \quad \text{(shallow focused)}$$

The above equations may be reduced to three equations containing only R_t, R_i and G_i if one assumes that the borehole and adjacent bed effects are negligible. From the geometric factors, the invasion diameter may be determined depending on the tool specifications. These multiple resistivity devices are available under different names from different service companies. (Dual-Induction Laterolog or Dual-Induction Focused Log). Usually the entire solution process is simplified by the use of charts and nomographs into which the ratios of $\frac{R_{LL}}{R_{ILd}}$ and $\frac{R_{LLM}}{R_{ILd}}$ are entered and the invasion diameter is read directly.

The Dual-Induction Laterologs give an estimate of where the mud filtrate front may be in the formations. An implicit assumption in the use of our method is the existence of sharp frontal movement and negligible dispersion and gravity segregation effects. These logs, however, do not tell us how the mud filtrate reached there.

Various parameters which may play a role in the extent of mud filtrate invasion into a given formation have been the subject of studies by many authors. The first attempt to integrate all such parameters into a simple equation mainly for computer log processing was reported by Breitenbach.[16] He indicated that for a gel-base mud the following equation may be used to estimate the invasion diameter:

$$DI = \frac{D \cdot C'}{\phi} [(0.04643 + 0.00002381\ \Delta p) \cdot API \cdot t^{1/2} + 0.00635\ (BHT - ST)\ t^{1/2} + 0.01495\ V_{mud}\ t^{1/2}] + [1 + 0.0063\ (BHT - ST)] + D^2]^{1/2}$$

where

API = API static filter loss, cc/30 min

BHT = temperature of the formation, °F

ST = surface temperature, °F

C' = dynamic correction factor for gel-base mud

D = borehole diameter, inches

ϕ = porosity, fraction

DI = invasion diameter, inches

Δp = pressure differential, psi

V_{mud} = annular mud velocity, ft/sec

t = time, hrs

As noted by Breitenbach this equation has limited application since it does not include the formation permeability and the initial surge loss into the formation. Furthermore, no explicit and universal technique for estimation of C' (correction for dynamic effect) is given in the above paper. In a subsequent paper Miesch and Albright[17] indicated that the C' may be assumed to be 1 for gel base mud. They also presented correlation equations for estimation of invasion diameter from driller's log parameters. The general form of the correlation may be shown as follows:

points along the wellbore using the second computer program, (MUDFIL). The basic data include a k/h vs time table for the mud cake, mud filtrate viscosity and compressibility and the formation pressure gradient. In addition the porosity profile (from porosity logs) and an assumed permeability profile are needed.

For the assumed permeability profile the invasion radius is determined and compared with the invasion profile obtained from the dual-induction laterolog. If the two do not agree, the assumed permeability profile is adjusted and the computations repeated until a satisfactory match is obtained.

The computation of the filtrate invaded into any segment of the formation during a given time step is done by an iterative procedure. The iteration method is used because the pressure drop across the filter cake is not known.

The main equation which describes the fluid invasion into the formation may be expressed as:

$$\frac{\delta^2 P}{\delta r^2} + \frac{1}{r}\frac{\delta P}{\delta r} = \frac{1}{\eta}\frac{\delta P}{\delta t}$$

where P, r, and t are pressure, radius, and time, respectively and η is the diffusivity constant. $(\eta = \frac{k}{\mu\phi C})$. This equation may be solved for certain boundary conditions. In this study we used the Van Everdingen and Hurst[18] solution which is given in tabular form expressing the dimensionless time t_D vs dimensionless water influx Q(t). The cumulative invasion at any time is then determined from:

$$W_e = B\Sigma\Delta P \times Q(t)$$

where

$$B = 1.119 \times \phi \times C \times r_w^2 \times h$$

Δp = differential pressure at interface between filter cake and formation

The symbol Σ is used here to show the superposition effect.

The computation scheme in the (MUDFIL) program follows the iterative procedure outlined below:

1 - a value for filtrate volume, Q, is assumed for the particular time step,

2 - the expected pressure drop across the mud cake for the given Q is determined using the mud cake k/h values thereby giving the effective pressure against the formation,

$$Log(DI) = A_0 + A_1X_1 + ... + A_{15}X_{15}$$

The coefficients were given for the deep or medium induction logs and X_1 through X_{15} represent formation and rock properties. Properties used included depth, porosity, R_w, R_m, temperature, R_{mf}, BHT, mud weight, water loss (API), hole diameter and the resistivity from an induction log. The correlations were based on 676 zones from 26 wells and the average absolute deviation for estimation of D_i was reported at 41.8 percent.

OTHER INPUT PARAMETERS

The complete history of drilling process for any segment of the borehole may be simulated by a computer program. The program requires estimate of drilling time, tripping time, and the onset of static conditions in the wellbore. In addition mud density, circulation velocity, dimensions of drill pipe, drill collar and the wellbore itself are needed. The program estimates the flow regime in different segments of the circulation path and determines the effective pressure against the formation.

The cumulative volume of filtrate invaded into permeable zones as a function of time is then computed. To do this a measure of mud cake permeability-thickness ratio is needed which may be obtained from laboratory tests on core samples. Volume of filtrate invaded is then translated into the radius of invasion using a knowledge of formation porosity.

DESCRIPTION OF THE SIMULATOR

The numerical simulator used in this study consists of two computer programs. The first one (MUDPRS) is designed to model the wellbore hydraulics during drilling and estimate the complete history of mud column pressure against the drilled portion of the formation. The pressure data generated from this program is then used in the second program (MUDFIL) together with the properties of the formation and the mud cake to derive the estimated invasion profile.

Estimation of Pressure Profile

The pressure in the mud column and against any point of the formation is a function of depth, mud density, and the circulation rate. When the mud column is in static condition, a circulation rate of zero is used in the computations. For the dynamic conditions (during drilling) the circulation pressure is obtained from accounting of the pressure losses in the system.

The input data for this computer program consists of tubular dimensions and lengths, mud properties, circulation rate, drilling rate and the wellbore radius.

Estimation of the Invasion Radius

The pressure profile vs. time is obtained from the first program and by a superposition method the invasion radius is computed for different

3 - for the given time step the dimensionless time and the corresponding Q(t) from the Van Everdingen and Hurst solution is determined,

4 - from the Q(t) the amount of influx is determined and compared with the assumed value, $\underline{Q}$,

5 - the process is repeated until the two influx values match within a given tolerance,

6 - by using the principle of superposition the cumulative influx is determined and translated in terms of invasion radius.

The basic wellbore parameters used in the simulator runs shown in this paper are given in Table 2. For simplicity it was assumed that the dynamic filtration prevails without any pause until the entire section is drilled through. The total static period before the commencement of the logging was ten hours.

NO MUD CAKE

In the absence of any mud cake (such as when drilling with water) the invasion radius is a function of formation permeability, porosity, and the time of exposure. Fig. 1 shows the invasion profile for a 500 ft. layer with uniform permeability (0.1 md) and porosity (0.2). The radius of invasion is largest at the top of the section, which has been exposed to a longer period of invasion. For higher formation permeabilities drilling fluid will invade farther into the formation. This fact is demonstrated in Fig. 2 for permeability varying from 0.1 md to 1000 md. The porosity of the formation also affects the radius of invasion significantly. Fig. 3 shows that for a section with uniform permeability of 10 md, changing the porosity from 0.20 to 0.1 increases the invasion radius.

The cases discussed above illustrate that in the absence of a mud cake, the invasion radius may vary from a fraction of a foot to 50 feet or higher depending on formation properties and drilling hydraulics. As long as the invasion radius does not extend beyond the depth of investigation of the deep induction tool, the method proposed in this paper may be used to estimate the formation permeability profile. The results shown above imply that for drilling with water the rock permeability must be low ($<10_{md}$) to limit the invasion radius.

WITH MUD CAKE

As is customary, the drilling fluid contains bentonite or other sealing agents to form a cake with low permeability which impedes invasion of the mud filtrate into permeable layers. Particle invasion before the mud cake is fully established will also cause a reduction in permeability in the first few inches of the formation. In this paper we assume that the effect of such permeability alteration is included in the overall permeability barrier associated with the mud cake.

The effect of the mud cake needs to be carefully evaluated in light of formation permeability and the mud composition. The two major questions are the way the mud composition, on one hand, and formation permeability on the other influence the buildup and the properties of the mud filter cake.

Effect of Mud Composition

The concentration of any clay material or other sealing agents in the mud directly affects the filter cake permeability. Since, for the purpose of this paper and the application method discussed here, we are more concerned with the permeability thickness ratio of the filter cake than with the permeability or thickness separately, we shall examine the sealing property of the mud cake in terms of k/h ratio. (Note that h is mud cake thickness.)

The rate of filtration through an already established mud cake is directly proportional to k/h. Therefore, a decreasing trend in k/h indicates reduction of filtrate throughput.

For comparative studies a static API filter press is normally used to study mud cake k/h variation versus time for different mud compositions. The method of analysis consists of plotting cumulative filtrate volume versus time. Using the slope of the plot in the Darcy equation will result in an estimation of k/h versus time.

Fig. 4 shows an API static test results for three muds with bentonite concentration of 10, 50 and 100 g/liter. As it is expected, increasing bentonite content reduces the k/h ratio significantly.

Unfortunately API static test data may not represent actual wellbore conditions. As discussed by Outmans[19], Ferguson and Klotz[20], Krueger[21] and others there are several stages of filtration in the borehole. A typical filtration schedule may be as illustrated in Fig. 5. From this plot it follows that the k/h ratio may go up or down depending on the stage of filtration. As discussed by Horner et al.[22], the only way to determine the dynamic filtration behavior of a given drilling mud is to run a dynamic test. No other test, such as the API static test is truly representative of actual downhole behavior. Studies of dynamic filtration reported by Ferguson and Klotz[20], Krueger[21], and others[23,24] show that the three main factors controlling the volume of filter loss are mud composition, pressure differential and rock permeability. Mud composition and (mainly) the matrix grain sizes determine the degree of particle invasion or pore plugging[25]. Pressure differential acts as the driving force and affects mud cake compressibility. The role of formation permeability is, however, somewhat obscure. For high permeability rocks the initial spurt loss is substantial, and there is a rapid buildup of the mud cake. Large pores of such rock also lead to particle invasion and possible internal rock permeability reduction. Subsequently the mud column acts against a low permeability filter cake and the water loss becomes negligible. For low permeability rock the initial spurt loss is low, and the transition between the formation and the mud column is a thickened mud with properties between filter cake and mud slurry. The permeability of this thickened mud is intuitively

larger than the permeability of the mud cake. Fig. 3 of the Horner et al.[22] paper shows the significance of rock permeability on cumulative dynamic filtration.

ESTIMATION OF MUD CAKE k/h RATIO

To obtain typical values for k/h ratio we tested the utility of running API static filter tests by comparing results to dynamic filtration data reported in the literature. One significant observation is that the resistance of the filtering medium affects filtration behavior. Static filtration against permeable rocks results in different filtration properties than those predicted by the API test for the same mud.

Currently we are building our own dynamic test facility for further testing of drilling muds. In the absence of dynamic filtration data, we used the data presented by Ferguson and Klotz, Bezemer and Havenar[26] and Krueger[21].

As discussed by Ferguson and Klotz[20] the major fraction of the total filtrate that invades the formation is under dynamic conditions; static filtration contributes only from 10 to 30 percent. From the data presented in Fig. 4 of Ferguson and Klotz we estimated that the k/h ratio during dynamic filtration with bentonite mud drops from an average of 0.00195 md/cm to 0.000653 md/cm. Krueger's data also show an average dynamic fluid loss rate of 0.5 ml/hr/in^2. Table 3 shows a typical k/h ratio one might expect for a high bentonite content mud and for an average rock permeability. Obviously, the concentration and particle size of the clay or other sealing materials or water loss additives will influence the k/h ratio.

The ideal test would be to conduct a dynamic-static filtration test using rock permeabilities from 1 md to 1000 md (not necessarily rock samples from the formation) and input three or more tables to the simulator and interpolate for permeabilities in between.

In the absence of reliable k/h ratio, as will be shown below, the proposed technique will result in a qualitative profile of formation permeability.

Results of Similator Runs with Mud Cake

To illustrate the simulation we assumed a permeable section 500 ft. thick with permeabilities varying from 1 md to 1000 md (as illustrated in Fig. 6) and porosities ranging from 0.05 to 0.35 (see Table 4). We ran the simulator assuming the same k/h ratio applied to all rock permeabilities. To study the effect of changing flow properties of the mud cake, we made a series of runs in which the k/h values shown in Table 3 were multiplied by a (constant) factor varying from 0.01 to 100. The invasion profiles for several factors are shown in Fig. 6. With higher permeability mud the invasion profile is very similar to the formation permeability profile. On the other hand, for lower values of mud cake permeability the invasion profile tends to smooth out and no longer resembles the formation permeability profile. In fact, when the k/h ratio is reduced by a factor of 0.01 there seems to be a trend reversal with the low permeability rocks showing

deeper invasion. This confounding effect is caused by the shape of the assumed porosity profile. The low permeability zone in the middle of the section was assumed to have a low porosity with a consequent increase in invasion radius. If one assumes the same porosity (0.1) for the entire section, regardless of the magnitude of k/h ratio, the calculated invasion radius is smaller in the low permeability section as shown in Fig. 7.

The exposure time, the length of time the borehold wall is exposed to drilling fluid, also significantly affects radius of invasion. Because the mud cake properties when the filling fluid is circulating differ greatly from the properties when the fluid is not circulating, exposure time during both flow regimes (dynamic and static, respectively) must be specified to our program. Fig. 8 shows for the 500-ft. section the calculated invasion radius for two exposure times. Increasing exposure time from 10 hours (500 ft/50 ft/hr) to 25 hours (500 ft/20 ft/hr) increased invasion radius by about 30 percent.

MUD PROBLEMS IN GEOTHERMAL DRILLING

Field experience indicates that during the drilling of geothermal wells drilling fluid may undergo serious degradation. Thermal degradation of the organic compounds affects viscosity and filter loss properties. Also, the high temperatures may cause the mud to solidify and result in drilling problems. Remont et al.[27] reported on the stability and properties of some commercially available high temperature muds. Their findings indicate that most of the water base muds fail to retain their functional properties at temperatures above 350°F. In a subsequent publication Remont et al.[28] presented formulation of an improved drilling fluid suitable for geothermal application. From their data, indications are that the new formulation may retain its viscosity and water loss properties even after static aging at 500°F. In brief the new formulation calls for substitution of sepiolite for a portion of the bentonite. Furthermore, use of brown coal and sodium polyacrylate was suggested to improve filtration control characteristics. Sepiolite, a naturally occurring clay mineral, has a needle-like structure which makes it less effective than bentonite in filtration control.

As the newly formulated muds for geothermal drilling tend to be lower in solid content and somewhat higher in filtration losses, the technique presented in this paper is potentially more applicable with these newer muds.

SUMMARY AND CONCLUSIONS

We have presented a new approach for estimating formation permeability profile using a combination of several data bases which are and should be available from the drilling operation. The proposed technique consists of a wellbore simulator making use of drilling hydraulics data and mud composition hand in hand with well log data to derive a quantitative, or at least a qualitative, estimate of the permeability profile. The application of the technique requires a knowledge of dynamic filtration behavior of the drilling mud, which in our opinion should become a routine test replacing the inaccurate and rather meaningless API test.

The proposed technique is most applicable to liquid dominated geothermal reservoirs for which low solid muds are preferred and the formation contains only one fluid. Muds with medium to low sealing properties may provide invasion profiles which are related to the formation permeability distribution.

NOMENCLATURE

c = filtrate compressibility, psi^{-1}

G = geometric factor

h = mud cake thickness, cm

H = formation thickness, ft

k = filter cake permeability, md

K = formation permeability, md

P_c = capillary pressure, psi

Δp = pressure differential

Q = cumulative filter loss, cc

q = flow rate, cc/sec

$Q(t)$ = dimensionless influx (from Van Everdingen and Hurst)

R_t = resistivity of the uninvaded zone, ohm-m

R_i = resistivity of the invaded zone, ohm-m

r_i = invasion radius, ft

r_w = wellbore radius, ft

S_{w_i} = interstitial water saturation

t = time

W_e = cumulative invasion

ϕ = porosity, fraction

μ = filtrate viscosity, cp

η = diffusivity constant

ACKNOWLEDGEMENT

This study was supported by a grant from the Geothermal Division of the United States Department of Energy. Messrs. M. Azari and J. Luther assisted in the experimental work.

REFERENCES

1. Baker, L. E., Campbell, A. B., and Hughes, R. L.: "Geothermal Well Logging: An Assessment of the State of the Art," The Log Analyst (Nov.-Dec., 1975) 21-24.

2. Sanyal, S. K., and Meidav, H. T.: "Important Considerations in Geothermal Well Log Analysis," SPE 6535, paper presented at 47th Annual California Regional Meeting of SPE in Bakersfield, Calif. (April 13-15, 1977).

3. Wylie, M. R. J., and Rose, W. D.: "Some Theoretical Considerations Related to the Quantitative Evaluation of the Physical Characteristics of Reservoir Rock from Electric Log Data," Jour. Pet. Tech. (April, 1950).

4. Timur, A.: "An Investigation of Permeability, Porosity and Residual Water Saturation Relationships for Sandstone Reservoirs," The Log Analyst, vol. 9, no. 4 (July-August, 1968).

5. Brown, A., and Husseini, S.: "Permeability from Well Logs Shaybah Field, Saudi Arabia," SPWLA Transaction (1977) Part Q.

6. Barlai, Z.: "Determination of Permeability and Specific Surface Area of the Pore Channels from Well Logs in Fine Grained Sandstones," SPWLA Transaction (1976) Part C.

7. Lebreton, F., Sarya, J. P., and Moriher, P.: "Acoustic Method and Device for Determining Permeability Logs in Boreholes," U.S. Patent 3,622,969 (Nov. 23, 1971).

8. Dowling, A. J., and Boyd, J. F.: "Acoustic Permeability Log Utilizing Differential Travel Time Measurements," U. S. Patent 3,900,826 (Aug. 19, 1975).

9. Staal, J. J., and Robinson, J. D.: "Permeability Profile from Acoustic Logging," SPE 6821, paper presented at the 52nd Annual Fall Meeting of SPE in Denver, Colorado (Oct. 9-12, 1977).

10. Biot, M. A.: "Propagation of Elastic Waves in a Cylindrical Bore Containing a Fluid," Jour. of Applied Physics, vol. 23, no. 9 (Sept., 1952) p. 997.

11. Rosenbaum, J. H.: "Synthetic Microseismograms: Logging in Porous Formations," Geophysics, vol. 39 (Feb., 1974) 14.

12. Seevers, D. O.: "A Nuclear Magnetic Method for Determining the Permeability of Sandstones," SPWLA 7th Annual Symposium Transactions, pp. L1-L14, 1966.

13. Timur, A.: "Producible Porosity and Permeability of Sandstones Investigated Through Nuclear Magnetic Resonance Principles," The Log Analyst (Jan.-Feb., 1969) p. 3.

14. Engelke, C. P., and Hilchie, D. W.: "A New Qualitative Permeability Indicator," SPWLA Transaction (1971) Part M.

15. Dowling, D. J., and Boyd, J. F.: "Permeability Log Using New Lifetime Measurements," U.S. Patent 3,890,502 (June 17, 1975).

16. Breitenbach, E. A.: "A New Technique for Approximating Drilling Fluid Filtration," SPWLA Transaction (1965) Part I.

17. Miesch, E. P., and Albright, J. C.: "A Study of Invasion Diameter," SPWLA Transaction (1967) Part O.

18. Van Everdingen, A. F., and Hurst, W.: "The Application of the Laplace Transformation to Flow Problems in Reservoirs," Trans. AIME vol '86 (1949) 305.

19. Outmans, H. D.: "Mechanics of Static and Dynamic Filtration in the Borehold," Soc. Pet. Eng. Jr. (Sept., 1963) p. 236.

20. Ferguson, C. K., and Klotz, J. A.: "Filtration from Mud During Drilling," Trans. AIME (1954) 29.

21. Krueger, R. F.: "Evaluation of Drilling-Fluid Filter-Loss Additives Under Dynamic Conditions," JPT (Jan., 1963) 90.

22. Horner, V., White, M. M., Cochran, C. D., and Deily, F. H.: "Microbit Dynamic Filtration Studies," JPT (1957) 183.

23. Prokop, C. L.: "Radial Filtration of Drilling Mud," Trans. AIME (1952) 5.

24. Bezemer, C., and Havenar, I.: "Filtration Behavior of Circulating Drilling Fluids," Soc. Pet. Eng. Jr. (Dec., 1966) p. 292.

25. Krueger, R. F., and Vogel, L. C.: "Damage to Sandstone Cores by Particles from Drilling Fluids," API Drilling and Prod. Prac. (1954) 158.

26. Remont, L. J., Rehm, W. A., MacDonald, W. J., and Maurer, W. C.: Evaluation of Commercially Available Geothermal Drilling Fluids, Sandia Laboratories Report (SAND 77-7001) April, 1977.

27. _____: Improved Geothermal Drilling Fluids, Energy Research and Development Administration (IDO/1603-1) June, 1977.

Table 2

Basic Data

Mud density	=	9 ppg
Drill pipe O.D.	=	5"
Drill pipe length	=	40'
Drill collar O.D.	=	7"
Collar length	=	30'
r_w	=	5.875"
Circulation rate	=	500 gpm
Formation pressure gradient	=	0.460 psi/ft
μ (filtrate)	=	0.6 cp
c	=	3×10^{-6} psi^{-1}
U (mud)	=	40 cp
Drilling rate	=	10 ft/hr (except for sensitivity studies)

Table 3

Mud Cake k/h Ratio Used For The Example Run

Time, hrs	k/h, md/cm
0.2	0.0075
0.4	0.0055
0.6	0.0041
0.8	0.0032
1.0	0.0026
1.2	0.0022
1.4	0.0020
1.6	0.0018
1.8	0.0017
2.0	0.0015
2.2	0.0012
2.4	0.0010
2.6	0.0009
2.8	0.0009
>2.8	0.0009

Table 4

Variable Porosities For The Example Run

k,md	ϕ
1	0.05
10-20	0.10
50	.17
100	.20
200	.25
300	.28
400-500	.30
1000	.35

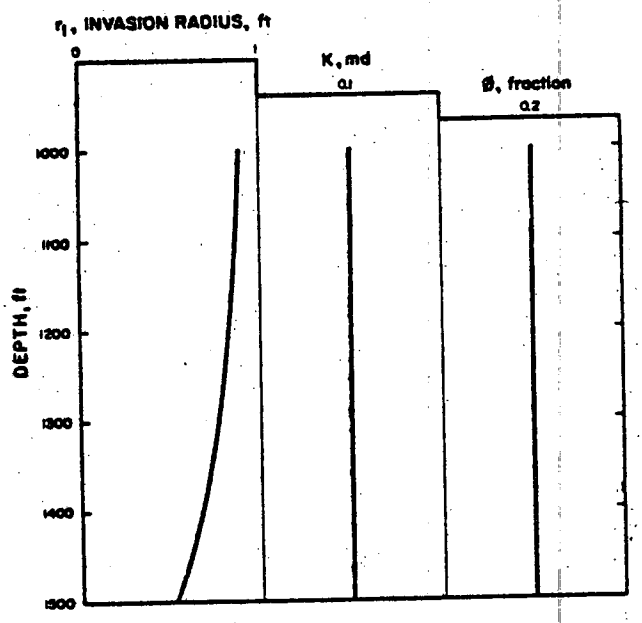

Fig. 1 Invasion Profile for a Uniform Permeability and Porosity Section (No Mud Cake).

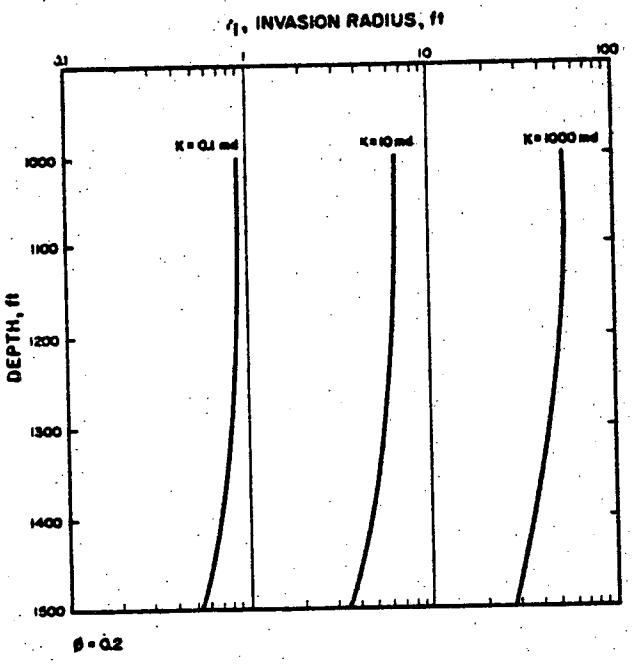

Fig. 2 Effect of Formation Permeability on Invasion Radius (No Mud Cake).

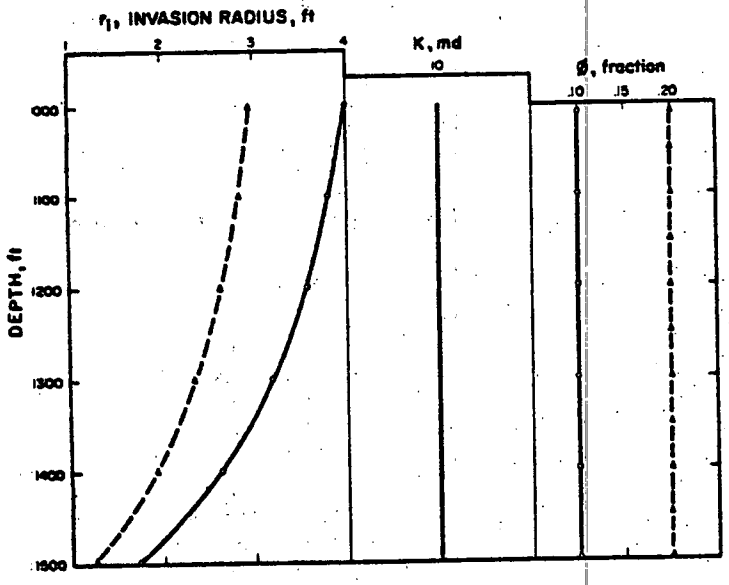

Fig. 3 Effect of Formation Porosity on Invasion Radius (No Mud Cake).

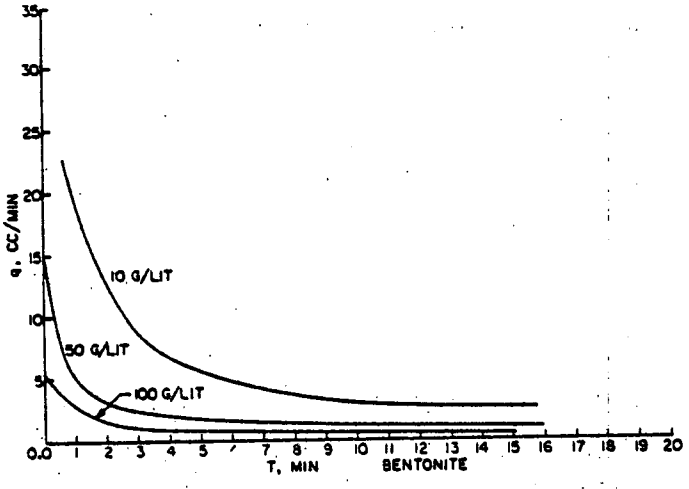

Fig. 4 Effect of Bentonite Concentration on the Filtration Rate in a Static API Test.

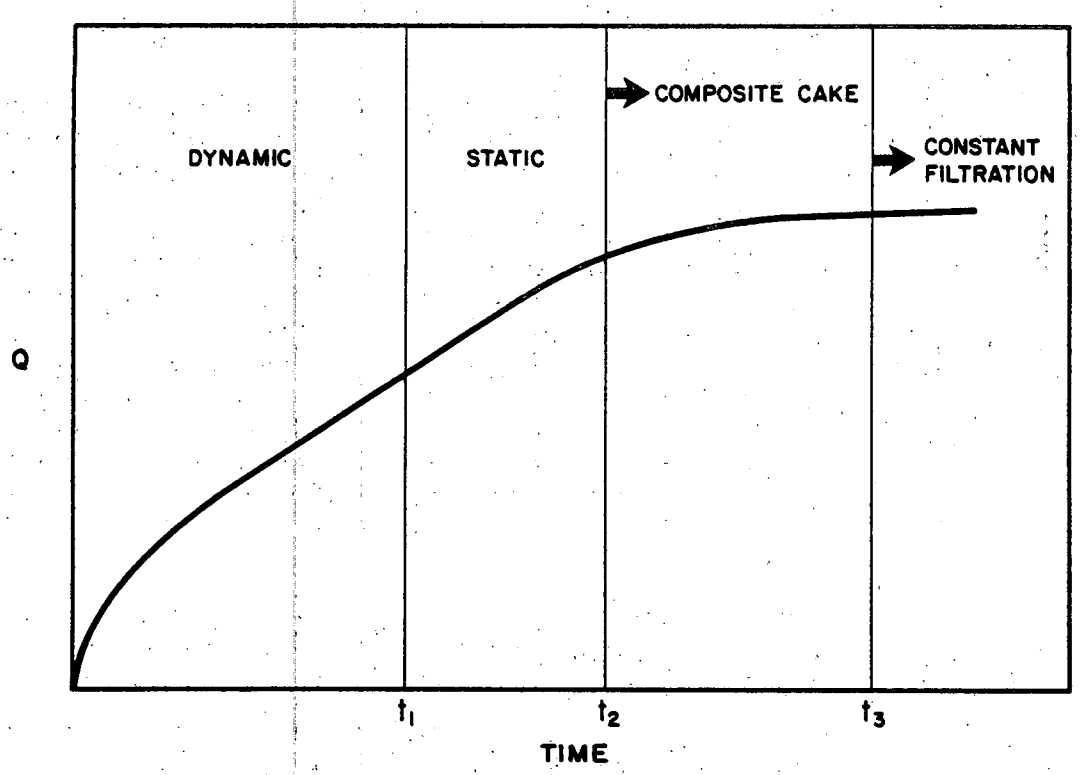

Fig. 5 Typical Mud Filtration Schedule During a Drilling Operation.

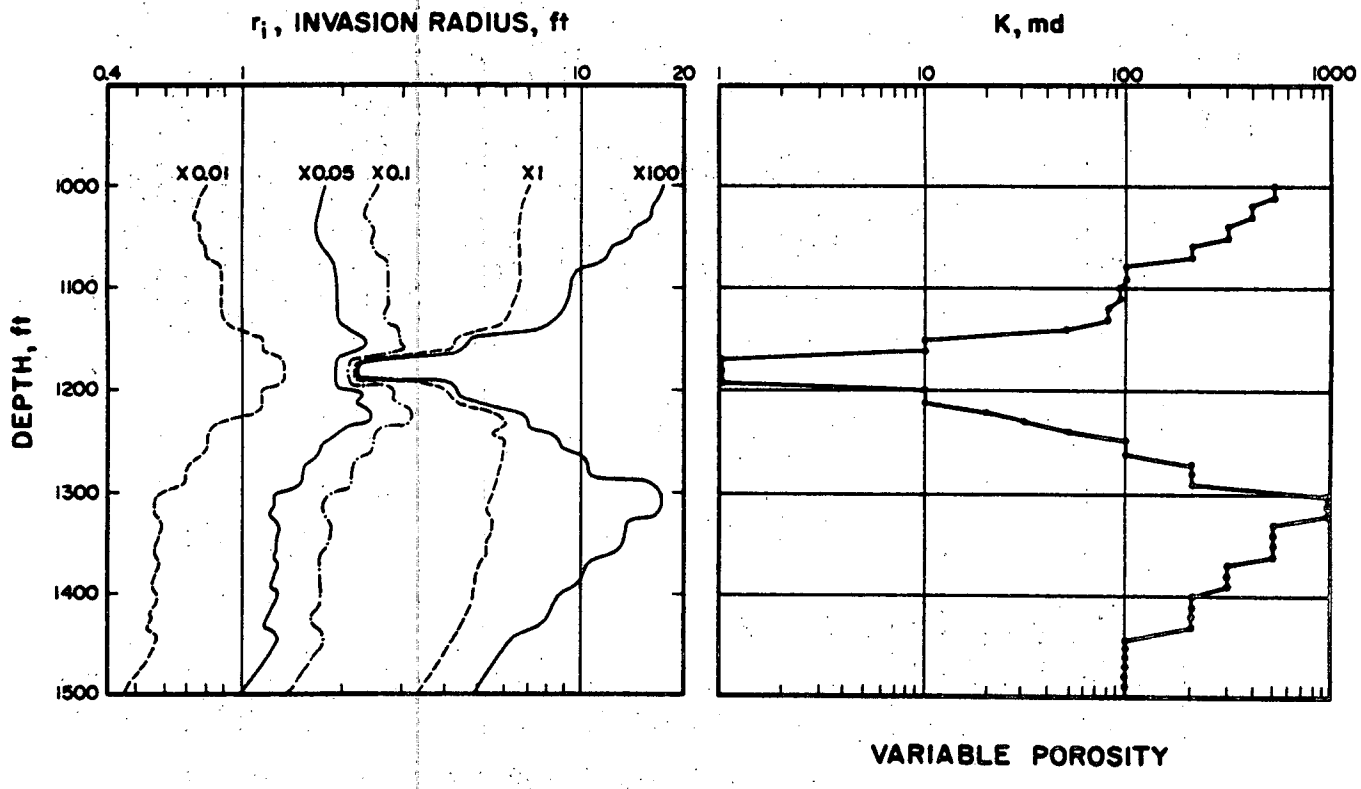

Fig. 6 Effect of Mud Cake Permeability-Thickness Ratio (k/h) on Invasion Radius (Non-Uniform Porosity).

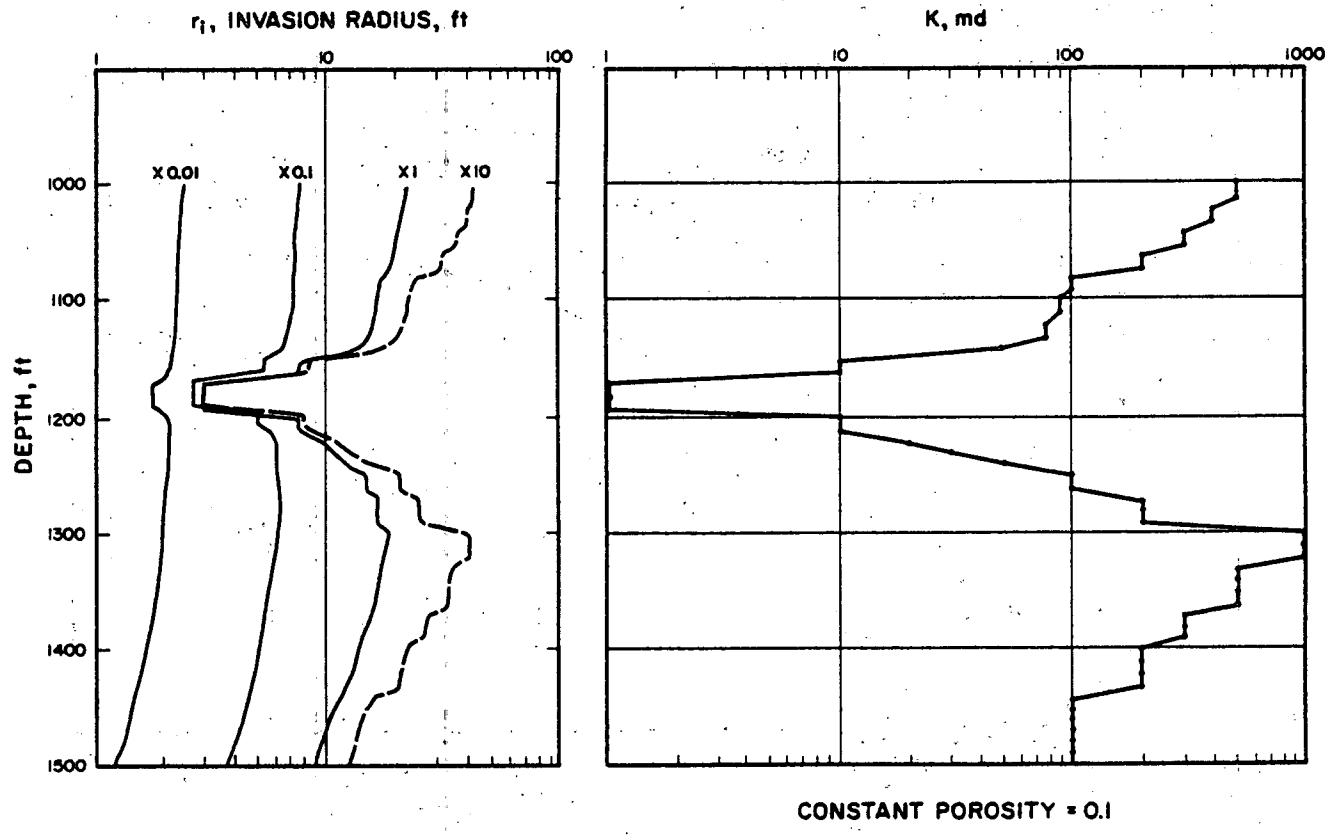

Fig. 7 Effect of Mud Cake Permeability-Thickness Ratio (k/h) on Invasion Radius (Uniform Porosity).

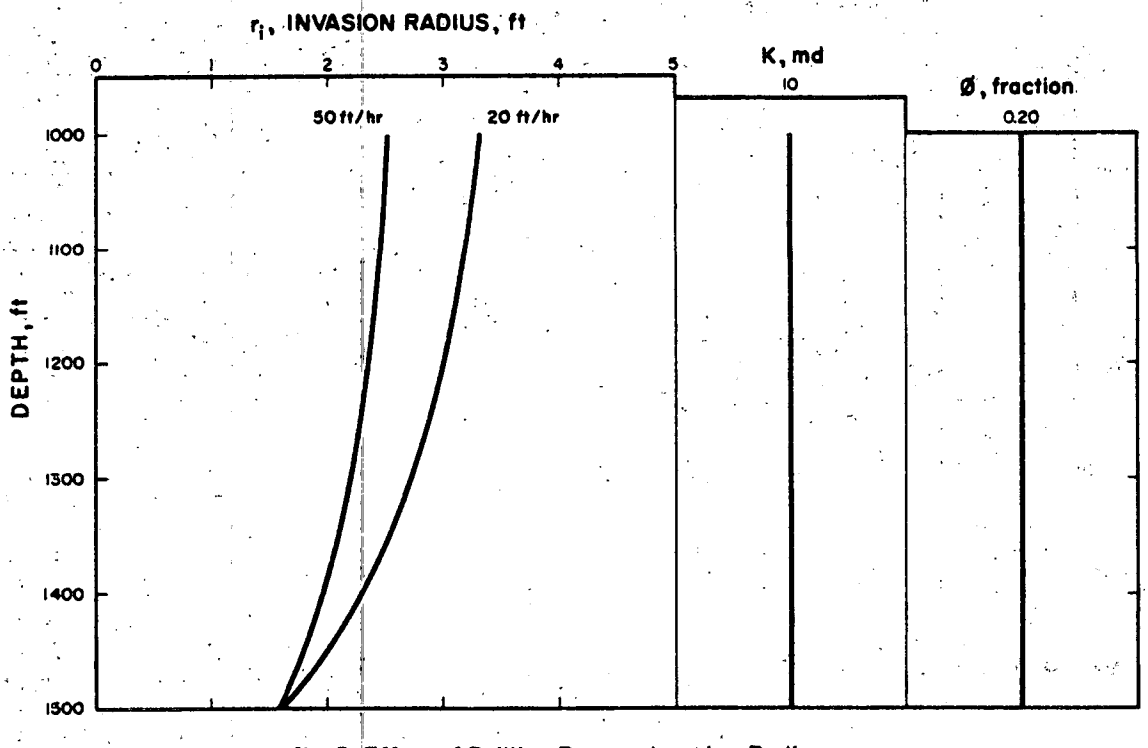

Fig. 8 Effect of Drilling Rate on Invasion Radius (Uniform Permeability and Porosity with Mud Cake).

SPE 8902

MODELING OF FILTER CAKE BUILDUP UNDER DYNAMIC-STATIC CONDITIONS

by Iraj Ershaghi and Mehdi Azari,
University of Southern California

This paper was presented at the 1980 50th Annual California Regional Meeting of the Society of Petroleum Engineers of AIME held in Los Angeles, California, April 9-11, 1980.

ABSTRACT

A method is discussed whereby the numerical solution of equations describing the filtration process of drilling fluid may be used for prediction of cake buildup and filtrate volume into a given zone. The data required for the simulation study include estimation of cake permeability during the dynamic phase, filtrate viscosity, cake compressibility and porosity, and pressure differential against the formation.

Application of the technique allows sensitivity analysis of important parameters controlling the filtration process in a given operation. Furthermore, estimation of invasion radius may be made in advance for determination of optimum timing for logging and improvements in log interpretations. This will allow the design of the best mud composition for a given application.

INTRODUCTION

Fundamental studies on the mechanics of drilling fluid filtration in the borehole have been reported by Prokop[1], Krueger and Vogel[2], Ferguson and Klotz[3], Bezemer and Havenaar[4], and several other investigators[5-7]. Additional laboratory work was recently reported by Simpson[8]. The only paper describing the filtration process in analytical terms was published by Outmans[9]. No quantitative use of the above analytical contribution has been discussed in the literature.

There is continued interest on part of the petroleum industry in minimizing formation damage during the drilling operation. Improved techniques and correlation[10] and simulation capabilities for describing the filtration process are needed for prediction of optimum drilling programs and drilling fluids to ensure minimization of damage to producing formations.

A complete simulation of the filter cake buildup requires extensive laboratory data on the behavior of a given mud under simulated borehole conditions. The method discussed in this paper is an attempt to minimize the extent of laboratory data requirement by the application of numerical modeling techniques to the solution of the equations describing the filtration process.

References and illustrations at end of paper.

Description of the Problem

As described by Ferguson and Klotz, during the dynamic phase of drilling, the rate of mud filtration against the formation gradually approaches a constant value and an equilibrium filter cake is established. Subsequent to the dynamic phase, when the drilling stops, filtration of mud through the already deposited cake continues and the filter cake itself goes through a phase of gradual change in its properties.

Prediction of the filter cake buildup and filtration rate during the initial dynamic phase is theoretically possible as shown by Outmans. In this study, however, it is assumed that the dynamic filtration data are available from actual laboratory tests on rock samples. Our effort is mainly focused on understanding the subsequent filtration through the filter cake once the drilling stops. Of interest are the roles that the cake thickness, permeability, compressibility, and the pressure differential may play in the rate of filter cake buildup and the rate of filtration.

Mathematical Model

As shown by Outmans, filtration through a deposited cake under dynamic conditions may be described by the following equations:

$$\frac{\partial^2 P_{DS}}{\partial x^2} = \frac{\mu}{c}\frac{\partial P_{DS}}{\partial t} \quad 0 < x < h(t) \quad t > 0 \qquad \ldots (1)$$

$$P_{DS}(x,0) = -a_1 \frac{P^{-\nu+1}}{-\nu+1}\left(1 - \frac{x}{H}\right) \qquad \ldots (2)$$

$$0 < x < H = h_0$$

$$P_{DS}(0,t) = -a_1 \frac{P^{-\nu+1}}{-\nu+1} \quad \ldots (3)$$

$$P_{DS}(h,t) = 0 \quad \ldots (4)$$

$$\frac{dh}{dt} = b \frac{c}{\mu} \frac{\partial P_D}{\partial x}(h,t) \quad \ldots (5)$$

(See the nomenclature at the end.)

Numerical solution of the above equations was not presented by Outmans. These equations are solved here for some hypothetical cases to gain a better insight into the factors controlling the filtration process. The problem is solved for a one dimensional system which is a fair representation of the filter cake buildup process in a borehole, Fig. 1.

Equations 1-5 are solved numerically for a cake of thickness h_0 using the Crank-Nicholson approach. In general the P_{DS} equation is solved under the given initial and boundary conditions. Then the rate of the filter cake buildup (dh/dt) is determined from equation 5. The filtration rate, q, is obtained from the following equation:

$$q = \frac{k}{a_1 \mu} \frac{\partial P_{DS}(0,t)}{\partial x} \quad \ldots (6)$$

and the cumulative filtration is computed using:

$$Q = \int_0^t q\,dt \quad \ldots (7)$$

Initial values required are the thickness, permeability, and the cumulative filtration per unit area of the existing cake plus the differential pressure and the mud properties (a_1, ν, b, k, μ).

The numerical solution approach allows overall sensitivity studies on the effect of various mud properties and borehold pressure on the filtration process.

Data Requirements

To apply the simulator described here to a given drilling operation, the following data need to be furnished from laboratory tests or available correlations:

1. Filtrate viscosity, μ
2. Filter cake compressibility, (a) (versus solid pressure). The degree of flocculation of particles in the presence of a given electrolyte controls the dependence of (a) on pressure. This information may be obtained using the compression technique discussed by Grace[12]
3. Filter cake permeability, k. Dynamic tests in a modified API filter press[13] or other similar devices may be used to derive k. It is recommended that filtration tests be actually conducted against permeable rocks (various permeabilities).
4. Specific filter cake volume, b.

$$b = \frac{1 - \phi_s}{\phi_s - \phi_c}$$

ϕ_s = porosity of suspension = 1 - S

S = solid concentration

ϕ_c = filter cake porosity which may be obtained from techniques discussed by Grace[12] and Tiller and Cooper[11].

5. Initial values of cake thickness, h and filtrate volume, Q. These may be obtained from the dynamic tests.
6. ν (exponent from the slope of log a vs. log P_s)

Data for the base case used in this study are shown in Table 1.

Results and Discussion

Consider a filter cake of thickness h_0 formed during the dynamic filtration process. Subsequent filtration through the cake as a function of time is modeled and shown for various cake permeabilities and thicknesses. Figure 2 shows the initial porosity profile in the cake and the changes after several time steps. The gradual compaction of the cake with time can be seen from these plots. For the same cake the solid pressure distribution is computed and shown in Fig. 3. Again the model illustrates the solidification process under the imposed pressure gradient. The initial porosity distribution was obtained from the technique discussed by Tiller and Cooper[11] and Grace[12].

The permeability of the cake is a very important factor in controlling the rate of follow-up filtration. Filter cake permeabilities were obtained from studies conducted by Mehdizadeh[13]. For typical cake permeabilities ranging from 10^{-5} darcies to 10^{-7} darcies, the computed cumulative thickness of the cake versus time is shown in Fig. 4. The growth rate of the cake thickness can be greatly inhibited if the cake permeability is designed in the order of 10^{-7} darcies or less. The thickness of the original cake under similar permeability conditions has the same effect on the cumulative throughput. This can be seen from Fig. 5. As illustrated in Fig. 6 and 7 the permeability of the cake has the upper hand control on the rate of filtration and thus the cumulative throughput.

The model can be used to study the effect of filtrate properties on the cumulative filtration. Under equal conditions, the viscosity of the filtrate can have substantial effect on the filtration process. This effect becomes more noticeable with time, Fig. 8. The rate of cake buildup for the two cases studied are shown in Fig. 9.

Pressure gradient across the cake has only a minor effect on the filtration process. As shown in

Fig. 10, reducing the ΔP from 350 psi to 147 psi for the base case causes a reduction of only .005 cc/cm^2 in the cumulative throughput. A similar observation can be made about the cake thickness, Fig. 11. The modeling technique discussed here, using some basic laboratory data for the dynamic filtration properties of a given mud, can potentially help the drilling engineer in predicting the growth rate of filter cake and the filtration rate for a given operation. Such prediction capability will be helpful in the screening of various mud compositions. In addition, optimum time for well logging may be predicted from the model study.

The method discussed requires laboratory data ordinarily not available at the wellsite. Such information should become an integral part of the drilling fluid testing program.

Laboratory data, such as the filtration properties of a given mud measured against porous rocks (rather than a filter paper), should be made available to the drilling engineer. A modified API cell using the dynamic process should replace standard static tests. Properties of the deposited cake such as its permeability should be determined on a routine basis. Compressibility data on various mud compositions may be made available for general use.

CONCLUSIONS

The simulation technique described in this paper is a step in the proper design and selection of drilling fluid composition. The simulation approach requires data on the properties of filter cake which traditionally have not been made available to the drilling engineer on a routine basis. The application of the technique results in estimation of filter cake thickness, filtrate volume, and depth of invasion for a given permeable zone.

Sensitivity studies conducted using this technique show that the cake permeability and the filtrate viscosity are the two important factors controlling the filtration process.

ACKNOWLEDGMENT

This study was conducted as a part of research project supported by the Geothermal Division of the U. S. Department of Energy.

NOMENCLATURE

a = local filter cake compressibility, $M^{-1}Lt^2$

a_1 = (a) at one psi solid pressure, $M^{-1}LT^2$

b = specific filter cake volume = $\frac{1 - \phi_s}{\phi_s - \phi_c}$

c = coefficient of consolidation = $\frac{k_1}{a_1}$

$h(t)$ = thickness of cake at time t, L

H = thickness of dynamic cake at equilibrium, L

k = cake permeability, L^2

s = volumetric solid concentration

t = time

P_s = solid pressure

P_{DS} = dimensionless function of solid pressure = $-\int_o^{P_s} a \cdot dP_s$

q = rate of filtration (L^3T^{-1})

Q = filtrate volume per unit area, LT^{-1}

x = distance from the base of filter cake

$X_D = \frac{x}{H}$ dimensionless distance

μ = filtrate viscosity

$\phi_s = 1 - s$ = porosity of suspension

ϕ_c = filter cake porosity

ν = slope from the plot of a vs. P_s ($a = a_1 \cdot P_s^{-\nu}$)

REFERENCE

1. Prokop, C. L., "Radial Filtration of Drilling Mud," TAIME, Vol. 195 (1952) 5.

2. Krueger, R. F. and Vogel, L. C., "Damage to Sandstone Cores by Particle from Drilling Fluids," API Drilling and Production (1954) 158.

3. Ferguson, C. K. and Klotz, J. A., "Filtration from Mud During Drilling," TAIME, Vol. 201 (1954) 29.

4. Bezemer, C. and Havenaar, I., "Filtration Behavior of Circulating Drilling Fluids," SPEJ (Dec. 1966) 292-298.

5. Horner V., White, M. M., Cochran, C. D., and Deily, F. H., "Microbit Dynamic Filtration Studies," TAIME, Vol. 210 (1957) 183.

6. Krueger, R. F., "Evaluation of Drilling-Fluid Filter-Loss Additive Under Dynamic Conditions," JPT (Jan. 1963) 90.

7. Lawhon, C. P., Evans, W. M., and Simpson, J. P., "Laboratory Drilling Rate and Filtration Studies of Clay and Polymer Drilling Fluids," TAIME, Vol. 240 (1967) 688.

8. Simpson, Jay P., "Drilling Fluid Filtration Under Simulated Downhole Conditions," SPE 4779, SPE Symposium on Formation Damage Control, New Orleans (Feb. 7-8, 1974).

9. Outmans, H. D., "Mechanics of Static and Dynamic Filtration in the Borehole," SPEJ (Sept. 1963) 236.

10. Hassen, B. R., "New Technique Estimates Drilling Filtrate Invasion," SPE 8791, Fourth SPE Symposium on Formation Damage Control, Bakersfield, CA (Jan. 28-29, 1980).

11. Tiller, F. M., and Cooper, H. R., "The Role of Porosity in Filtration: Part V. Porosity Variation in Filter Cakes," AIChE Journal, Vol. 8 (1962) 445.

12. Grace, H. P., "Resistance and Compressibility of Filter Cake," Chem. Engin. Prog., Vol. 49 (1953) 303.

13. Mehdizadeh, A., "Dynamic Filtration Behavior of Drilling Fluids Against Porous Rocks," MS report, University of Southern California (Feb. 1980).

TABLE 1

DATA USED IN THE BASE CASE

μ = 0.8 cp	b = .23
Δp = 350 psi	ν = .77
k = 10^{-6} darcies	h_0 = .2 cm
a = 7 x 10^{-4} psi^{-1}	Q_D = .3 mL/cm^2

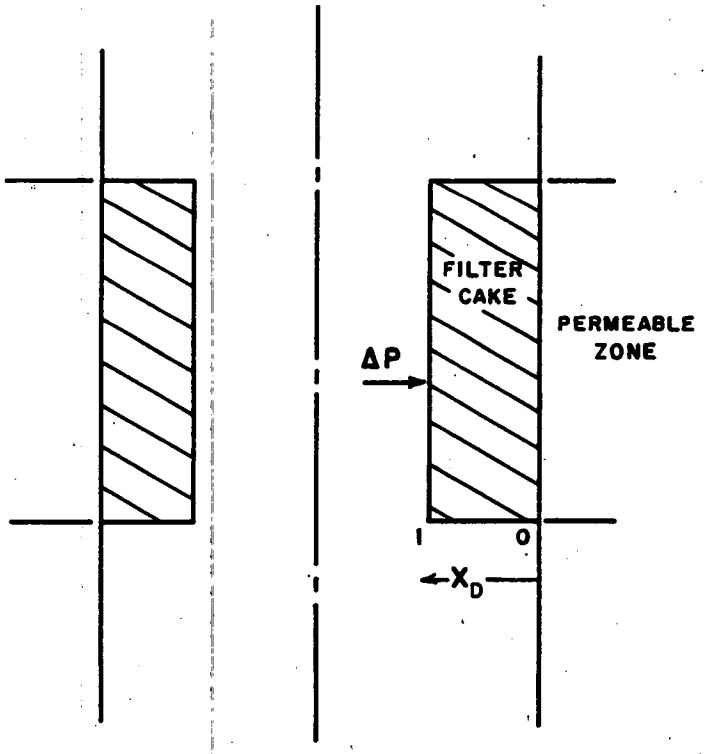

Fig. 1 - Schematic diagram of mud cake model.

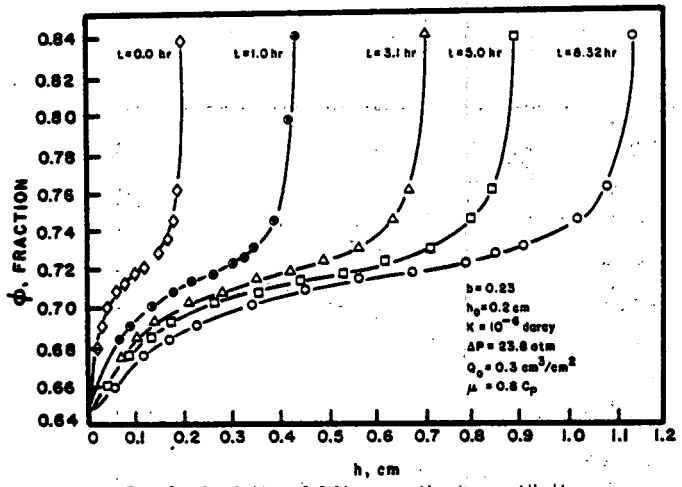

Fig. 2 - Simulation of filter porosity change with time.

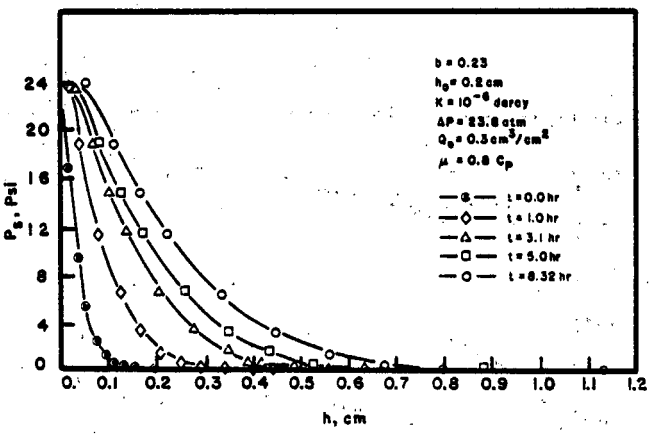

Fig. 3 - Simulation of solid pressure change in filter cake with time.

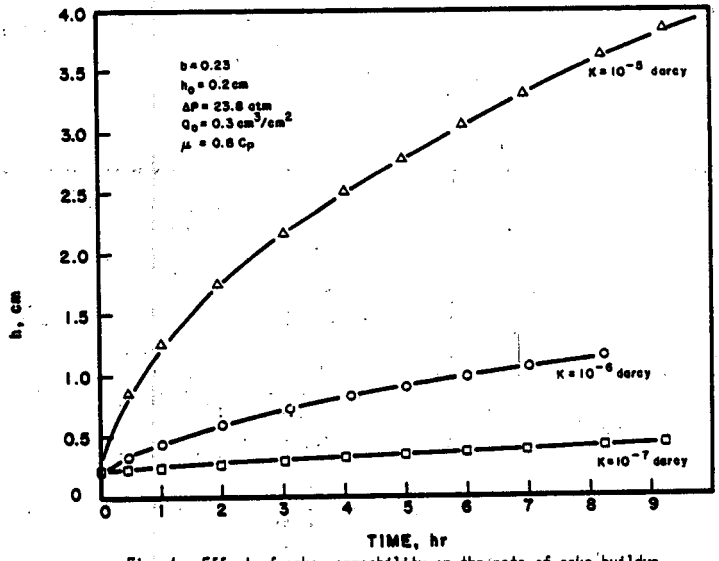

Fig. 4 - Effect of cake permeability on the rate of cake buildup.

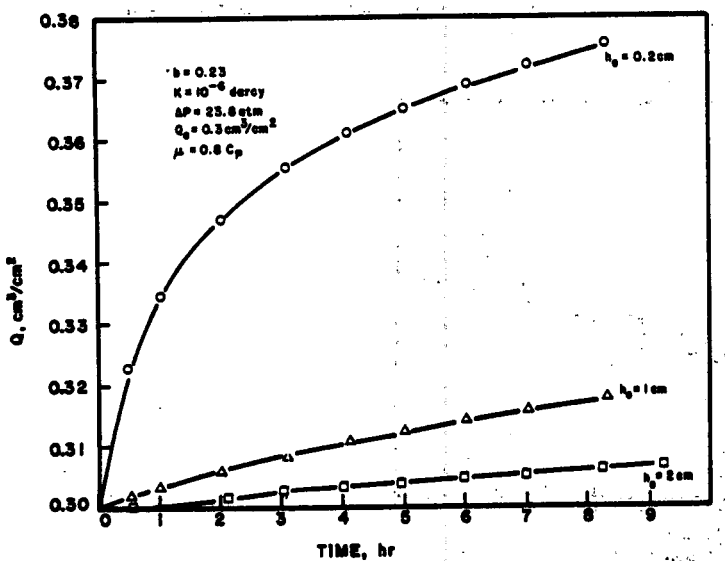

Fig. 5 - Effect of initial cake thickness on filtrate volume.

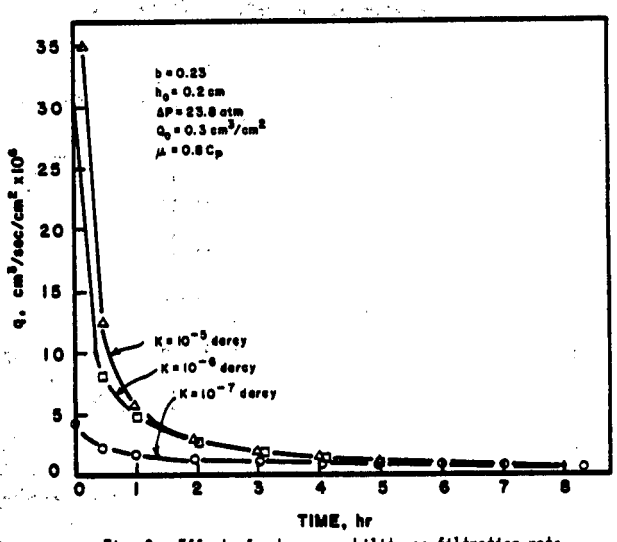

Fig. 6 - Effect of cake permeability on filtration rate.

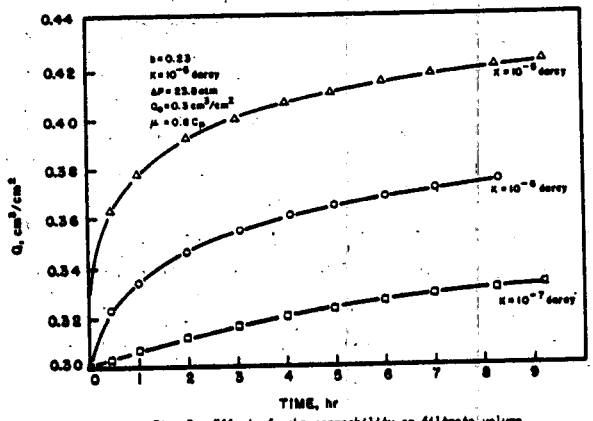

Fig. 7 - Effect of cake permeability on filtrate volume.

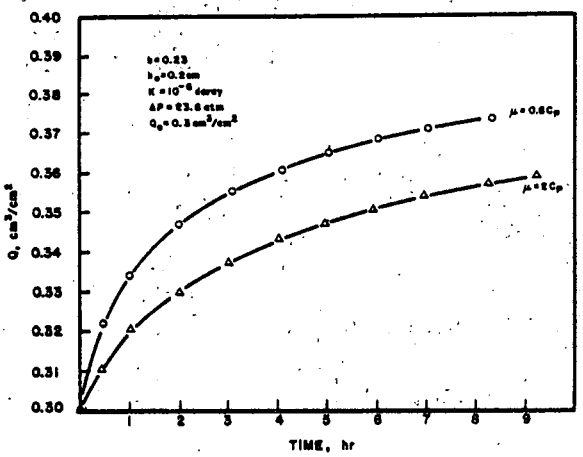

Fig. 8 - Effect of filtrate viscosity on filtrate volume.

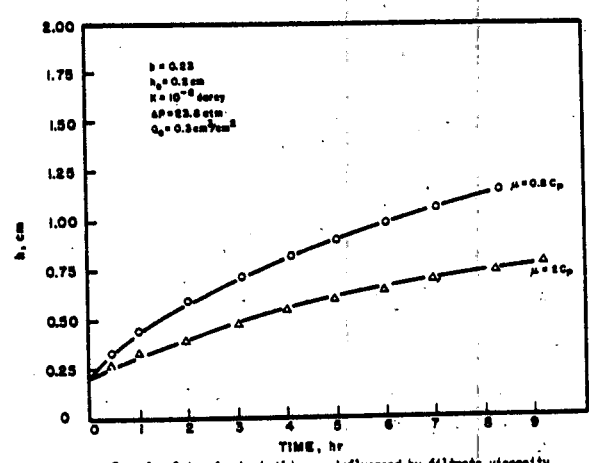

Fig. 9 - Rate of cake buildup as influenced by filtrate viscosity.

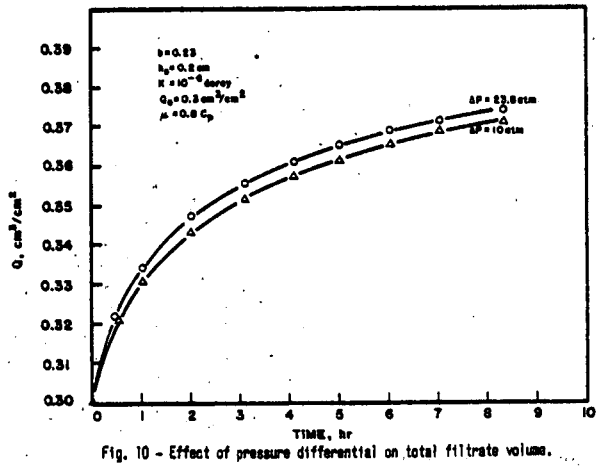

Fig. 10 - Effect of pressure differential on total filtrate volume.

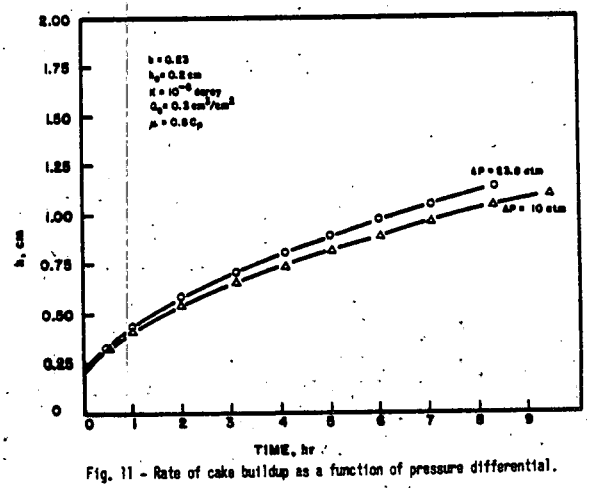

Fig. 11 - Rate of cake buildup as a function of pressure differential.

MODELING OF FILTER-LOSS INVASION IN AN ANISOTROPIC SYSTEM

B.A. Troesch

ABSTRACT

Given pressure profile data in the borehole during drilling, the two-dimensional elliptic partial differential equation for pressure distribution around the wellbore is solved by successive overrelaxation. The invasion front of the mud filtrate is then obtained versus time from the pressure gradient data computed in the anisotropic medium.

INTRODUCTION

The use of invasion radius profile to estimate formation permeability was discussed by Ershaghi et. al. Dimensionless solution of the hydraulic diffusivity equation for a homogeneous system as tabulated by Van Everdingen and Hurst was used by these authors to estimate the invasion profile. In this treatment, the flow is assumed to lie independent of the azimuth. The basic equation also expresses the assumption that the layers may be treated independent of each other.

In this paper the solution of the governing equation is sought for an anisotropic medium.

For the development of the present program, the assumption of axial symmetry is retained, i.e., the solution is independent of the azimuthal angle. On the other hand, the time history of the motion of the invasion front should be treated differently. At each time step the pressure distribution in the reservoir is computed and the motion of the front is then determined from Darcy's law. Therefore, the time does not appear in the differential equation anymore. Under these assumptions, it is no longer possible to treat the horizontal layers of the reservoir separately (see below), so that the elliptic partial differential equation for the pressure in the independent variables r (radial direction) and z (depth measured downwards) has to be solved. This leads to a problem that differs considerably from the approach used in (1), especially with respect to computer time and also, to some extent, in storage requirements. If the drilling depth is small, in the approach (1) only the affected layers must

be computed, whereas in the two-dimensional approach the pressure in the entire reservoir must be found. Of course, gravity effects, steam formation, temperature variations, and capillarity are neglected here too.

2. THE BASIC EQUATION

Originally, it was considered to base the computation on the equations given in (3). For our purpose, they can be simplified to a one-phase system for the potential, and both the source term and the time-dependent saturation term can be dropped. This leaves a time-independent equation for the potential anisotropic medium. However, the difference in density between the mud filtrate and the formation brine is so small that gravity effects may also be neglected. Under these assumptions, the equation reduces to the form given in (4, Chapter 2) namely

$$\frac{1}{r}\frac{\partial}{\partial r}\left(\frac{k_h}{\mu} r \frac{\partial p}{\partial r}\right) + \frac{\partial}{\partial z}\left(\frac{k_v}{\mu}\frac{\partial p}{\partial z}\right) = 0$$

where k_h, k_v are the permeabilities in the horizontal and vertical direction respectively, and μ is the viscosity is taken to be constant, i.e., temperature effects are neglected, and if the permeabilities are independent of the radial coordinate, then

$$\frac{k}{\mu}\frac{1}{r}\frac{\partial}{\partial r}\left(r\frac{\partial p}{\partial r}\right) + \frac{\partial}{\partial Z}\left(\frac{\alpha k}{\mu}\frac{\partial p}{\partial z}\right) = 0$$

with $k(z) = k_h(z)$, $k_v(z) = \alpha(z)k(z)$. The factor $\alpha(z)$ measures the anisotropy of the medium.

For the volumetric rate of flow $\underline{u}$, with the radial component u and the vertical component v, Darcy's law furnishes

$$u = -\frac{k}{\mu}\frac{\partial p}{\partial r},$$

$$v = -\frac{\alpha k}{\mu}\frac{\partial p}{\partial z}.$$

The geometrical displacement of the invasion front between the mud filtrate and the formation brine during the time interval Δt is therefore (the porosity ϕ is assumed to be constant)

$$\Delta r = -\frac{k}{\mu\phi}\frac{\partial p}{\partial r}\,\Delta t$$

$$\Delta z = -\frac{\alpha k}{\mu\phi}\frac{\partial p}{\partial z}\,\Delta t.$$

In summary, with

$$f(z) = k(z)/\mu\phi$$

$$g(z) = \alpha(z)k(z)/\mu\phi$$

solve

$$\frac{1}{r}\frac{\partial}{\partial r}\left(r\,\frac{\partial p}{\partial r}\right) + \frac{1}{f}\frac{\partial}{\partial z}\left(g\,\frac{\partial p}{\partial z}\right) = 0 \qquad (1)$$

for the pressure p. The boundary conditions are

p(z) prescribed in the formation,

$\partial p/\partial r = 0$ (no-flow condition) below the borehole,

$\partial p/\partial z = 0$ (no-flow condition) at the top of the reservoir,

$p = 0$ for $r^2 + z^2 \to \infty$

The front displacement during Δt is then

$$\Delta r = -f\,\frac{\partial p}{\partial r}\,\Delta t$$

$$\Delta z = -g\,\frac{\partial p}{\partial z}\,\Delta t. \qquad (2)$$

We observe that the method preserves a sharp front at all times, i.e., no smearing out of the front can occur as it may happen in an alternate formulation.

Whereas equation (2) is a relatively straightforward evaluation, the partial differential equation (1) is discretized and the resulting algebraic system solved by successive overrelaxation.

3A. The Solution of the Algebraic Problem

Among the methods suitable for the solution of the resulting large algebraic system of equations are the direct Gauss elimination method, the successive overrelaxation method, and the alternative direction implicit iterative method. These basic methods are used with many variations in actual implementations. For instance, one device (cf. [7]) is a rearrangement of the equations which leads to the most beneficial structure of the coefficient matrix. However, this optimization of the matrix structure is not trivial and has not been carried out. For the Gauss elimination, the matrix is therefore too large and not of sufficiently small band width. The alternating direction implicit iterative method is also not particularly suitable for our case, because of the irregular mesh and nonconstant coefficients [8]. Therefore, the successive overrelaxation approach is implemented. Since the coefficient matrix does not depend on the solution it can be computed once and for all, so that the implementation of the method becomes reasonably short. The overrelaxation procedure requires quite a large number of iterations. However, since the pressure changes from one time step to the next is smooth, it is important to use as the initial guess the pressure distribution of the previous time step.

4. The Derivation of the Difference Equations

The finite difference equations are based on the five-point star with equal meshsize in the z-direction, z increasing downwards, but unequal meshsized in the r-direction, as shown in the figure.

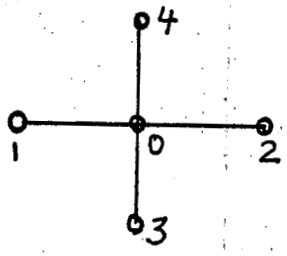

The numbering of the points is local for the derivation and will be changed to the usual double subscripts in the programming implementation.

The terms involving the z-derivatives are simpler. If we denote the meshsize in the z-direction by Δ, then over the interval 0-4

$$g(z)\partial p/\partial z = (p_o - p_4)\ (g_o + g_4)/2\Delta$$

and over the interval 3-0

$$g(z)\partial p/\partial z = (p_3 - p_o)\ (g_3 + g_o)/2\Delta$$

Hence

$$\frac{1}{f(z)}\ \frac{\partial}{\partial z}\ \left(g(z)\ \frac{\partial p}{\partial z}\right) = \left\{p_3(g_3 + g_o) - p_o(2g_o + g_3 + g_4) + p_4(g_o + g_4)\right\}/2f_o\Delta^2$$

For the derivative in the r-direction we have to choose a quadratic function through the three points 1, 0, 2:

$$p_1 = ar_1^2 + br_1 + c$$

$$p_o = ar_o^2 + br_o + c$$

$$p_2 = ar_2^2 + br_2 + c,$$

and hence $p_r = 2ar + b$

and $1/r\ (rp_r)_r = 4a + b/r.$

If we denote

$$r_o - r_1 = \Delta_-$$

$$r_2 - r_o = \Delta_+$$

then

$$p_2 - p_o = (a\,(r_2 + r_o) + b)\,\Delta_+$$

$$p_o - p_1 = (a\,(r_o + r_1) + b)\,\Delta_-.$$

The determinant of this system for a and b is

$$r_2 - r_1 = \Delta_+ + \Delta_- = \Delta_s$$

with the obvious notation.

Therefore, we obtain

$$a = \frac{1}{\Delta_s}\begin{vmatrix} (p_2 - p_o)/\Delta_+ & 1 \\ (p_o - p_1)/\Delta_- & 1 \end{vmatrix} = \left\{(p_2 - p_o)/\Delta_+ - (p_o - p_1)/\Delta_-\right\} \Big/ \Delta_s$$

and

$$b = \frac{1}{\Delta_s}\begin{vmatrix} r_2 + r_o & (p_2 - p_o)/\Delta_+ \\ r_o + r_1 & (p_o - p_1)/\Delta_- \end{vmatrix}$$

$$= \left\{(r_2 + r_o)\;\;(p_o - p_1)/\Delta_- - (r_o + r_1)\;\;(p_2 - p_o)/\Delta_+\right\} \Big/ \Delta_s\,.$$

These expression are now inserted into the approximation for $1/r(rp_r)_r$, and the terms properly collected. After some simplification we obtain

$$\frac{1}{r}(rp_r)_r = \frac{1}{\Delta_s}\left\{p_1\;\left(\frac{2}{\Delta_-} - \frac{\Delta_+}{r_o\Delta_-}\right) + p_o\;\left(-\frac{2}{\Delta_+} - \frac{2}{\Delta_-} + \frac{\Delta_+}{r_o\Delta_-} - \frac{\Delta_-}{r_o\Delta_+}\right)\right.$$

$$\left. + p_2\;\left(\frac{2}{\Delta_+} + \frac{\Delta_-}{r_o\Delta_+}\right)\right\}.$$

Together with the formula for the z-derivatives the approximation to the differential equation is readily obtained and solved for the pressure at the center of the star

$$p_o = (c_1 p_1 + c_2 p_2 + c_3 p_3 + c_4 p_4)/(c_1 + c_2 + c_3 + c_4)$$

with

$$c_1 = (2 - \frac{\Delta_+}{r_o}) \frac{\Delta^2}{\Delta_s \Delta_-}$$

$$c_2 = (2 + \frac{\Delta_-}{r_o}) \frac{\Delta^2}{\Delta_s \Delta_+}$$

$$c_3 = (g_o + g_3)/2\ f_o$$

$$c_4 = (g_o + g_4)/2\ f_o .$$

This represents the formula for the overrelaxation procedure, where the new pressure value p_o at the center of the five-star is computed from the pressure at the surrounding points from the previous iteration.

At the surface of the region under investigation ($z = 0$) the normal derivative $\partial p/\partial z$ must vanish, since it is assumed here that no flow takes place through it. The corresponding finite difference approximation is obtained by observing that all the values at point 4 are equal to those at point 3. This leads to

$$p_o = (c_1 p_1 + c_2 p_2 + c_3 p_3)/(c_1 + c_2 + c_3)$$

with

$$c_1 = (2 - \frac{\Delta_+}{r_o}) \frac{\Delta^2}{\Delta_s \Delta_-}$$

$$c_2 = (2 + \frac{\Delta_-}{r_o}) \frac{\Delta^2}{\Delta_s \Delta_+}$$

$$c_3 = (g_o + g_3)/f_o .$$

The no-flow condition, i.e., $\partial p/\partial r = 0$ also applies to the points at the well radius below the formation. In this case the virtual point 1 is arbitrary, and we choose it at the same distance from point 0 as point 2, so that $\Delta_- = \Delta_+$, $\Delta_s = 2\Delta_+$, and also set $p_1 = p_2$. Then p_o becomes

$$p_o = (c_2 p_2 + c_3 p_3 + c_4 p_4)/(c_2 + c_3 + c_4)$$

with

$$c_2 = 2\,\Delta^2/\Delta_+^2$$

$$c_3 = (g_o + g_3)/\,2f_o$$

$$c_4 = (g_o + g_4)/\,2f_o .$$

Since the pressure at the borehole inside the mudcake is assumed known, and at the other two edges of the reservoir is replaced by the pressure at infinity, i.e., $p = 0$, the finite difference formulation of the problem is complete.

For the programming implementation the mnemonic nomenclature shown in the figure has been used, for instance, $C_1 = C_W$ etc.

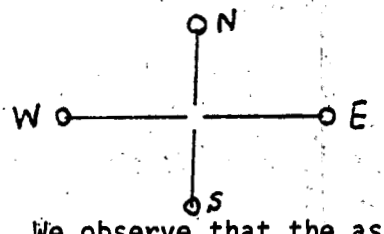

We observe that the assumption that the reservoir properties do not vary in the radial direction has led to a significant simplification, if the meshsize in the z-direction is chosen to be constant. The coefficients C_W, C_E depend only on r, and the coefficients C_S, C_N only on z, and these vectors can be set up before the start of the successive overrelaxation.

5. The Overall Mesh. Nomenclature

The mesh is shown in the figures below. The general index used is J, with the index in the Horizontal direction JH, and its Maximum value JHM,

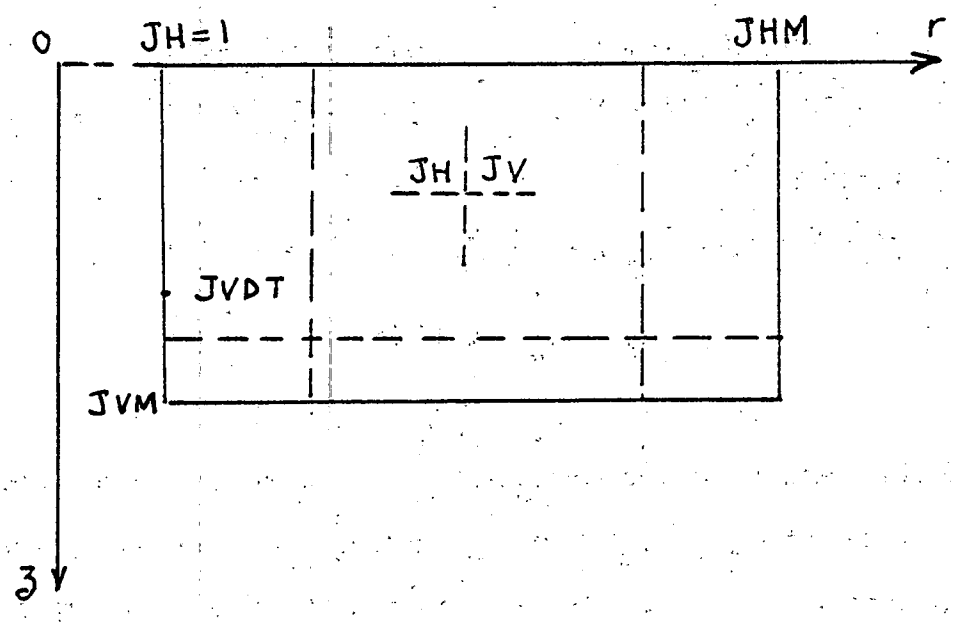

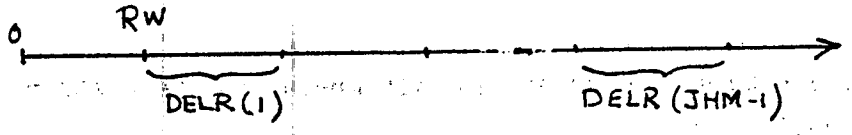

and the index in the vertical direction JV with the maximum JVM. Similarly, the meshpoint at the bottom of the bore hole, i.e., the deepest point for which pressure data is furnished, is denoted by JVDT.

The constant meshsize Δ in the z-direction is called DELZ, while the variable r-mesh is chosen with the index at its left endpoint. This means that at the point JH the Δ_+ is DELR(JH) and Δ_- is DELR(JH-1). The distribution of the r-mesh is specified by the fucntion DELRFC. As the formulas above show, only the mesh ratios are needed, and they are locally called

$$DELE = \Delta_+/\Delta$$

$$DELW = \Delta_-/\Delta$$

and their sum

$$DELS = (\Delta_+ + \Delta_-)/\Delta = \Delta_s/\Delta.$$

6. The Overrelaxation Procedure

In an iteration step (counted by the index IC) the new pressure P is computed from the previous pressure PREVP according to the formulas above. The maximum number of iterations is NIT. The pressure P itself is prescribed at the bore hole, namely the pressure data PDATA inside the mud cake, and it vanishes at the two outer edges.

7. The Motion of the front

The invasion radius is computed at horizontal levels Δz apart, i.e., at the levels where pressure results are available. The motion of the front between the mud filtrate and the formation brine is computed from the permeability, the viscosity, the porosity, and the pressure gradient. Since the motion of the front is two-dimensional, the computation of the invasion radius becomes somewhat involved.

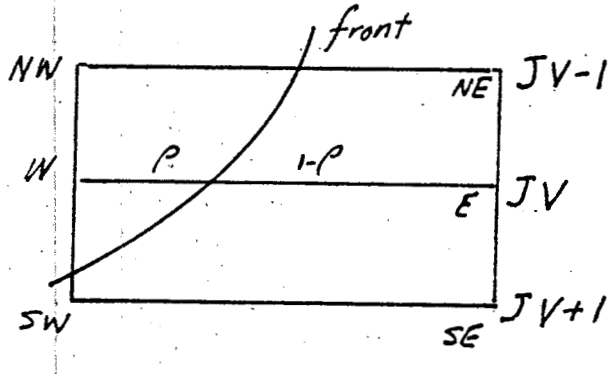

For the computation of the velocity vector of the front, the pressure gradient is needed. We express it again by a local nomenclature as shown in the figure above. The r-component of grad p (called PGRDR) is computed as

$$\partial p/\partial r = (p_E - p_W)/\Delta_W$$

where Δ_W is the meshsize in r, belonging to the left endpoint (see above); the z-component of the pressure gradient (called PGRDZ) is computed as the weighted average between the two adjacent meshlines (the meshsize Δ in z is constant). Let the present position of the front be inside the r-interval with the ratio $\rho(z)$ (called RATIO), then

$$\partial p/\partial z = (1 - p)\,(p_{SW} - p_{NW})/2\Delta + p(p_{SE} - p_{NE})/2\Delta.$$

Since the front will normally move to the right and downwards, the upward front point is used to determine the front displacement on a constant z-line (see figure, for the line JV).

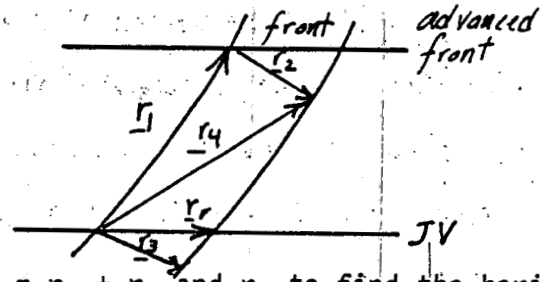

The vector $\underline{r}_1$ is known at the beginning of the displacement of the front. With the displacement vectors $\underline{r}_2$ and $\underline{r}_3$ we interpolate between $\underline{r}_4 = \underline{r}_1 + \underline{r}_2$ and $\underline{r}_3$ to find the horizontal displacement $\underline{r}_r$:

$$\underline{r}_r = \underline{r}_3 + \beta \underline{r}_4$$

or in the components

$$r_r = r_3 + \beta r_4, \quad z_r = z_3 + \beta z_4.$$

This determines the factor (called FACTR)

$$\beta = -z_3/z_4$$

and the displacement r_r to be added to the previous front position (called RADD)

$$r_r = r_3 - z_3 r_4/z_4.$$

The velocity components u,v in the r and z direction, respectively, are

$$u = -f\phi\partial p/\partial r$$

$$v = -g\phi\partial p/\partial z,$$

so that the displacements $\underline{r}_2$ and $\underline{r}_3$ on the two lines turn out to be, after a time increment of Δt,

$$u = -f\partial p/\partial r\ \Delta t$$

$$z = -g\partial p/\partial z\ \Delta t$$

These increments are called GRDRR and GRDRZ in the program, and are used to compute β and hence the desired invasion radius (called RFR) at $t + \Delta t$.

In order to compute the pressure gradient for the front motion, it is necessary to determine the present position of the front with respect to the mesh. This is accomplished by simply comparing the invasion radius with the mesh points in the r-direction in turn. The front index (called JFR) denotes the nearest meshpoint inside the front.

BIBLIOGRAPHY

1. I. Ershaghi, E.L. Dougherty, D. Herzberg, and H. Ucok, Permeability Determination in Liquid Dominated Geothermal Reservoirs Using the Dual Induction Laterolog, Department of Petroleum Engineering, University of Southern California, Progress Report No. 1.
2. Van Everdingen, A.F., and Hurst, W., The Application of the Laplace Transformation to Flow Problems in Reservoirs, Trans. AIME, Vol. 186 (1949) 305.
3. MacDonald, R.C., Methods for Numerical Simulation of Water and Gas Coning, reprinted in SPE Reprint Series No. 11, Numerical Simulation, 1973.
4. Matthews, C.S., and Russell, D.G., Pressure Buildup and Flow Tests in Wells, Henry L. Doherty Series, Vol. 1, SPE, 1967.
5. Breitenbach E.A., Thurnau D.H., and Van Pooen, H.K., Solution of the Immiscible Fluid Flow Simulation Equations, Reprint, SPE Reprint Series No. 11, Numerical Simulation, 1973.
6. Cavendish, J.C., Price, H.S., and Varga, R.S., Galerkin Methods for the Numerical Solution of Boundary Value Problems, Reprint, SPE Reprint, Series No. 11, Numerical Simulation, 1973.
7. Mercer, J.W., and Faust, C.R., Numerical Simulation of Geothermal Reservoirs, USC Short Course, Summer 1977.
8. Wasserman, M.L., Private communication.

APPENDICES

A. Some Theoretical Remarks

1. The reduction to the Laplace equation.

The basic equation (1)

$$\frac{1}{r}\frac{\partial}{\partial r}\left(r\frac{\partial p}{\partial r}\right)+\frac{1}{f(z)}\frac{\partial}{\partial z}\left(g(z)\frac{\partial p}{\partial z}\right)=0$$

where $f(z) = k/\mu\phi$

$g(z) = \sigma k/\mu\phi$

can be transformed by introducing the new independent variable

$$\zeta = \int^z dt/\sqrt{\alpha(t)}.$$

Then $\frac{\partial}{\partial z} = \frac{1}{\sqrt{\alpha(z)}}\frac{\partial}{\partial \zeta}$

and hence

$$\frac{1}{f}\frac{\partial}{\partial z}\left(g(z)\frac{\partial p}{\partial z}\right) = \frac{\mu\phi}{k\sqrt{\alpha}}\frac{\partial}{\partial \zeta}\left(\frac{\sqrt{\alpha}\,k}{\mu\phi}\frac{\partial}{\partial \zeta}\right).$$

If the function $\alpha(z)$ can be chosen in such a way $\alpha\, k/\mu\phi$ is constant, then the basic equation reduces to the Laplace equation $\frac{1}{r}\frac{\partial}{\partial r}\left(r\frac{\partial p}{\partial r}\right)+\frac{\partial^2 p}{\partial \zeta^2}=0$ for which many properties are known, in particular the fundamental solution (see, e.g. [9]) and the behavior at infinity.

The equation is also simplified, though not so drastically, if we apply the same transformation to z and set

$$\sqrt{\alpha}\;k/\mu\phi = A\exp(q(\zeta)).$$

In this case we obtain

$$\frac{1}{f}\frac{\partial}{\partial z}\left(g\frac{\partial p}{\partial z}\right) = \exp(-q)\frac{\partial}{\partial \zeta}\left(e^{q}\frac{\partial p}{\partial \zeta}\right)$$

and the differential equation transforms into

$$\frac{1}{r}\frac{\partial}{\partial r}\left(r\frac{\partial p}{\partial r}\right) + \frac{\partial^2 p}{\partial \zeta^2} + \frac{dq}{d\zeta}\frac{\partial}{\partial \zeta} = 0$$

The first derivative term can be eliminated, if we introduce the new dependent variable v by setting

$$p = ve^{-q(\zeta)/2}.$$

The resulting equation becomes then

$$\frac{1}{r}\frac{\partial}{\partial r}\left(r\frac{\partial v}{\partial r}\right) + \frac{\partial^2 v}{\partial \zeta^2} - \left(\frac{1}{2}\frac{d^2q}{d\zeta^2} + \frac{1}{4}\left(\frac{dq}{d\zeta}\right)^2\right)v = 0.$$

If now $\frac{1}{2}\frac{d^2q}{d\zeta^2} + \frac{1}{4}\left(\frac{dq}{d\zeta}\right)^2 = -a^2$

where a^2 is constant, we obtain

$$\nabla^2 v + a^2 v = 0$$

a Helmholtz-type equation which has been investigated in the literature [11]. The integration of the nonlinear equation for q can be carried out with the results

$$q(\zeta) = \ln \cosh^2 a(\zeta - \zeta_o)$$

so that the pressure and the new dependent variable are related by

$$p = v \operatorname{sech} a(\zeta - \zeta_o).$$

Although these transformations might shed some light on the situation in very special cases they are unfortunately not applicable to real reservoirs where the formation properties cannot be chosen freely. We have therefore not pursued this line of investigation.

The partial differential equation (1) appears to be amenable to the method of separation of variables. The equation itself is indeed separable and the domain consists of coordinate lines. However, the boundary conditions at the wellbore are of mixed type and the method breaks

down (cf. [10]. The situation is different, if the boundary condition below the wellbore were to be approximated by $p = 0$. Under these assumptions, an attempt was made to obtain a solution by superposition, but the problem remains untractable unless further restrictions are imposed.

It should be mentioned that the assumption of incompressible fluids, although apparently quite reasonable for the injection fluid and the formation brine, has important mathematical consequences. The basic equation (1) does then not contain any time derivatives as did the basic equation in [1]. This immediately precludes the possibility to treat the problem in separate layers. The differential equation (1) would then reduce to the ordinary differential equation

$$\frac{1}{r}\frac{d}{dr}\left(r\frac{dp}{dr}\right) = 0$$

with the unique solution

$$p(r) = C_1 + C_2 \log r$$

and this solution cannot be adjusted to the boundary conditions $p(\infty) = 0$ and the prescribed pressure at the borehole.

B. The Boundary Conditions at Infinity

For the numerical solution of a partial differential equation in an infinite domain, it is necessary to restrict the solution to a finite domain. The boundary conditions at infinity are then imposed at the boundary of this finite domain of computation. Since more appropriate boundary conditions may be imposed, if the behavior of the solution, for instance the rate of decay, at large distances from the origin is known, a first step to compute this decay is outlined here. Similar considerations have proved successful for ordinary differential equations (cf. [11]) and for

hyperbolic partial differential equations [12], [13]. In the simplest case of constant formation properties, it is confirmed that the pressure decays inversely proportional to the distance from the pressure source.

We assume that the pressure behaves like

$$p \sim (r^2 + z^2)^{-\frac{1}{2}} F(z/r)$$

Then a straightforward computation leads to

$$\frac{1}{r}(rp_r)_r = -2R^{-3}F + 3r^2R^{-5}F + 2(z/r)R^{-3}F' + (z^2/r^4)R^{-1}F'' + (z/r^3)R^{-1}F'$$

and

$$\frac{\partial}{\partial z}\left(g \frac{\partial p}{\partial z}\right) = g_z (R^{-1}F'/r - zR^{-3}F) + g (3z^2R^{-5}F - R^{-3}F - 2(z/r) R^{-3}F' + R^{-1}F''/r^2)$$

where $R^2 = r^2 + z^2$.

For the special case of an isotropic and homogeneous formation permeability we have $g_z = 0$ and $g/f = 1$, and hence $F(z/r)$ = constant represents a solution $p \sim 1/R$:

$$f \frac{1}{r}(rp_r)_r + (gp_z)_z = (-2R^{-3} + 3r^2R^{-5} + 3z^2R^{-5} - R^{-3}) F = 0.$$

In the general case we assume that the anisotropic facotor α and the permeability k tend to constant values, α_o and k_o, as z gets very large. Then we obtain again $g_z = 0$ and $g/f = \alpha_o$. Setting $\tan\theta = z/r$, the final equation for the angular dependence of the pressure becomes eventually

$$\sec^2\theta(\alpha_o + \tan^2\theta)F'' + \tan\theta(2 - 2\alpha_o + \sec^2\theta)F' + (3\cos^2\theta + 3\alpha_o \cdot \sin^2\theta - 2 - \alpha_o) F = 0$$

For the solution of this rather complicated ordinary differential equation one has to resort to numerical integration. This clearly indicates that it is quite difficult to compute the pressure decay far away from the pressure source in an inhomogeneous medium.

AN IMPROVED METHOD FOR MEASUREMENT OF FILTRATION PROPERTIES OF DRILLING FLUIDS

A. Mehdizadeh and I. Ershaghi

INTRODUCTION

During drilling operation by the rotary method, drilling mud is filtered against permeable beds. Mud filtrate invades the formation to a certain distance depending on properties of the formation and the pressure differential against the formation. Prediction of filtration properties of a given mud under downhole conditions is an important part of an overall plan in minimizing damage to producing formations.

Ample evidence exist in the literature pointing out to the inadequacy of conventional filter cells.[1-3] Dynamic filtration tests simulating downhole conditions indicate filtration properties of drilling fluid may not be predicted accurately from static tests. Physical models to simulate borehole conditions are often not readily available for routine field application.

Because of the need for some actual dynamic filtration test data for use in mathematical modeling reported in this publication, we modified the API cell and constructed a portable unit which can provide improved estimates of filter loss data. This section of the report is aimed at describing the design and presenting some typical dynamic filtration measurement.

Description of the Proposed Design

The conventional filtration cell proposed by the American Petroleum Institute (API) was modified as described below:

1. The bottom of the cell is equipped with a core holder which can hold cores one inch in diameter and up to 1/2 inch in thickness. The core material is used as a filter media.
2. To create continuous agitation of the mud sample, a heavy duty electric stirrer is fitted through the top of the cell. The shaft passes through a seal bearing designed to withstand 200 psi pressure. Constant speed stirring is provided by an 1/50 h.p. motor. Speed adjustments are made using a special tape wound rheostat with a calibrated dial.

A cross-sectional view of the modified cell is shown in Fig. 1.

Experimental Test Results

Various filtration tests were conducted using the modified cell to investigate the dynamic and static filtration behavior of water-base muds. The composition was mainly bentonite in water ranging in concentration from 20 to 40 lb/bbl. Salt concentrations were as high as 3 lb/bbl. Static tests were run at a pressure of 50 psi and the cumulative filtrate volume was recorded with time. Dynamic tests were run at rotational speeds ranging from 30 to 50 R.P.M. under similar pressure.

Experiments conducted using filter paper indicate higher filtration losses under dynamic conditions, Fig. 2. Changing the filter medium to a piece of rock sample (Berea Sandstone) and working with lower mud concentration results in the same relationship between the dynamic and static tests, Fig. 3. However, the cumulative filtration for similar elapsed times are much lower when rocks are used as filters. The permeability of the rock seems to have little influence on the cumulative filter loss. As shown in Fig. 4, for a permeability range from 250 md to 550 md the results are very close. Rocks of much lower or much higher permeabilities were not investigated. Intuitively one expects some changes at such extremities.

From the cake buildup on core samples, estimates of cake permeability were made using a series model of the Darcy's law. Typical values were in the range of 0.0060 md.

The proposed filter cell is one step improvement beyond the conventional API cell used in the industry. The improvements offered by the proposed design are the ability to measure filtration loss of drilling fluids against rock samples rather than filter paper, conducting the test under non-static mud condition, and estimating filter cake permeability for numerical simulation of borehole dynamics during the drilling operation.

REFERENCES

1. Benzemer, C. and Havenaar, I., "Filtration Behavior of Circulating Drilling Fluids," Soc. Pet. Eng. Jour. (Dec. 1966) 292-298.
2. Ferguson, C. K. and Klotz, J. A., "Filtration from Mud During Drilling," Trans. AIME, Vol. 201 (1954) 29.
3. Hassen, B. R., "New Technique Estimates Drilling Filtrate Invasion," SPE 8791, 4th SPE Symposium on Formation Damage Control, Bakersfield, CA (Jan. 28-29, 1980).

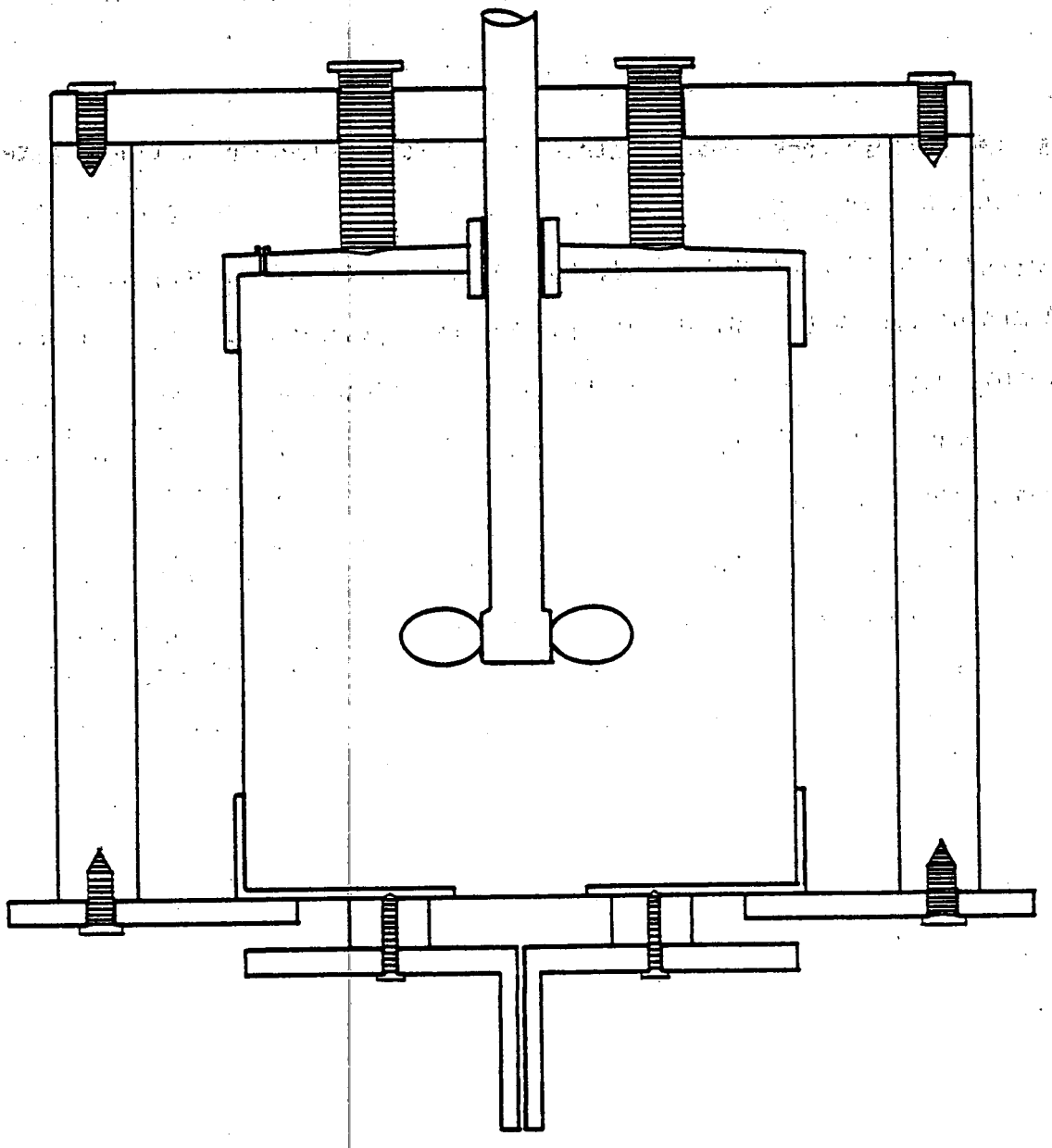

Fig. 1- Cross Sectional View of the Proposed Modified API Filter Cell.

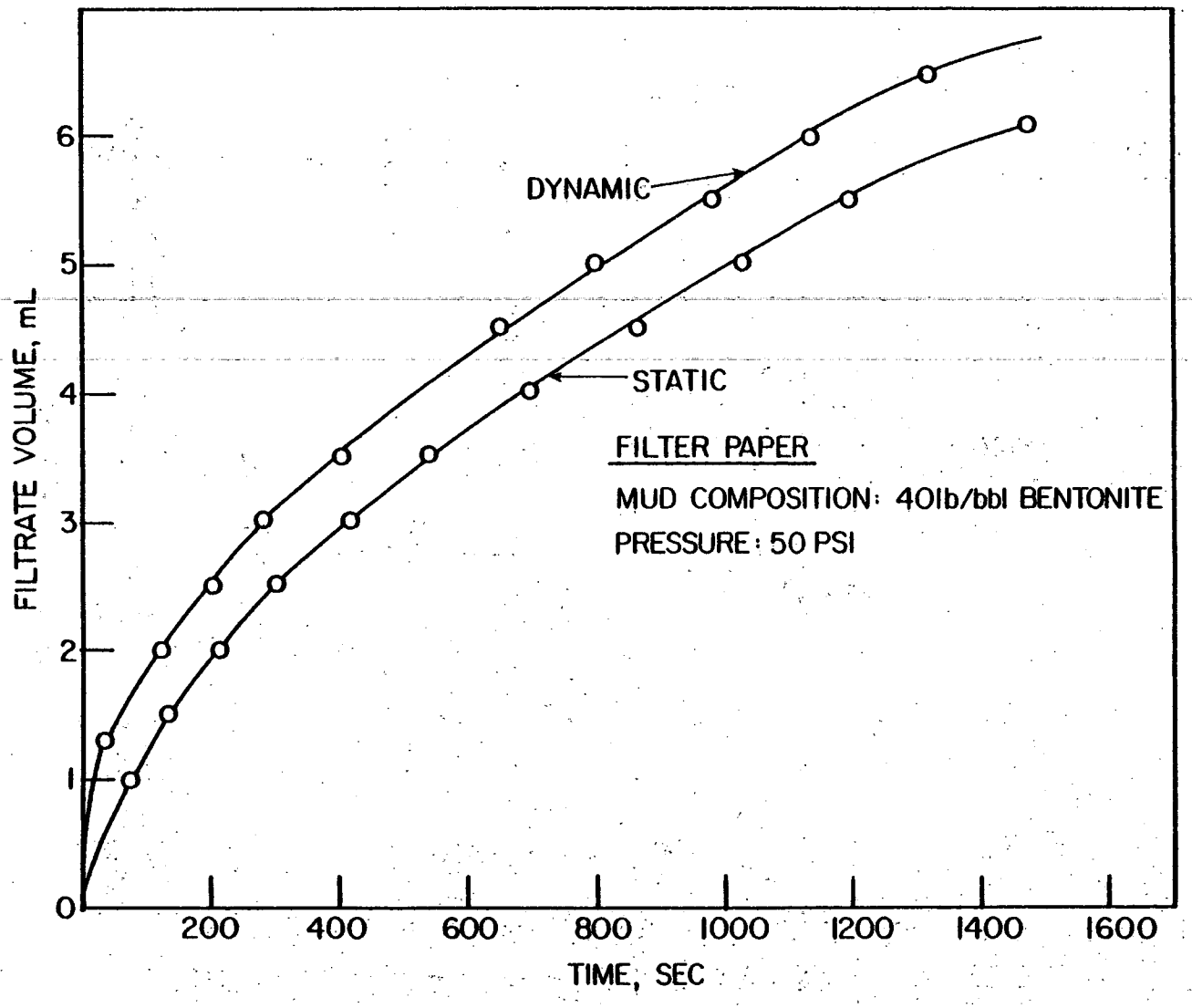

Fig. 2- Comparison of Static and Dynamic Filtration using Filter paper.

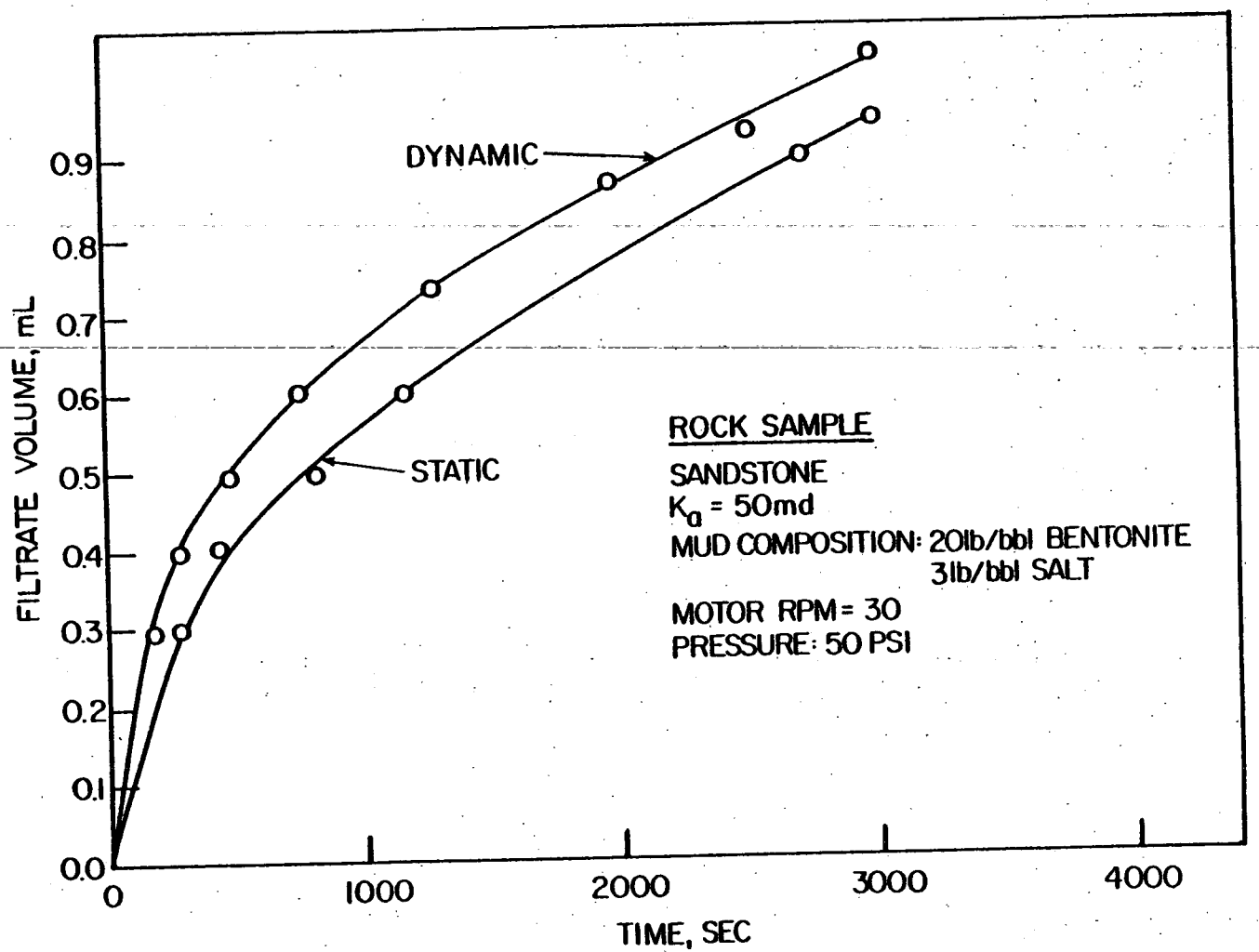

Fig. 3- Static and Dynamic Filtration using a Permeable Rock as a Filter Medium.

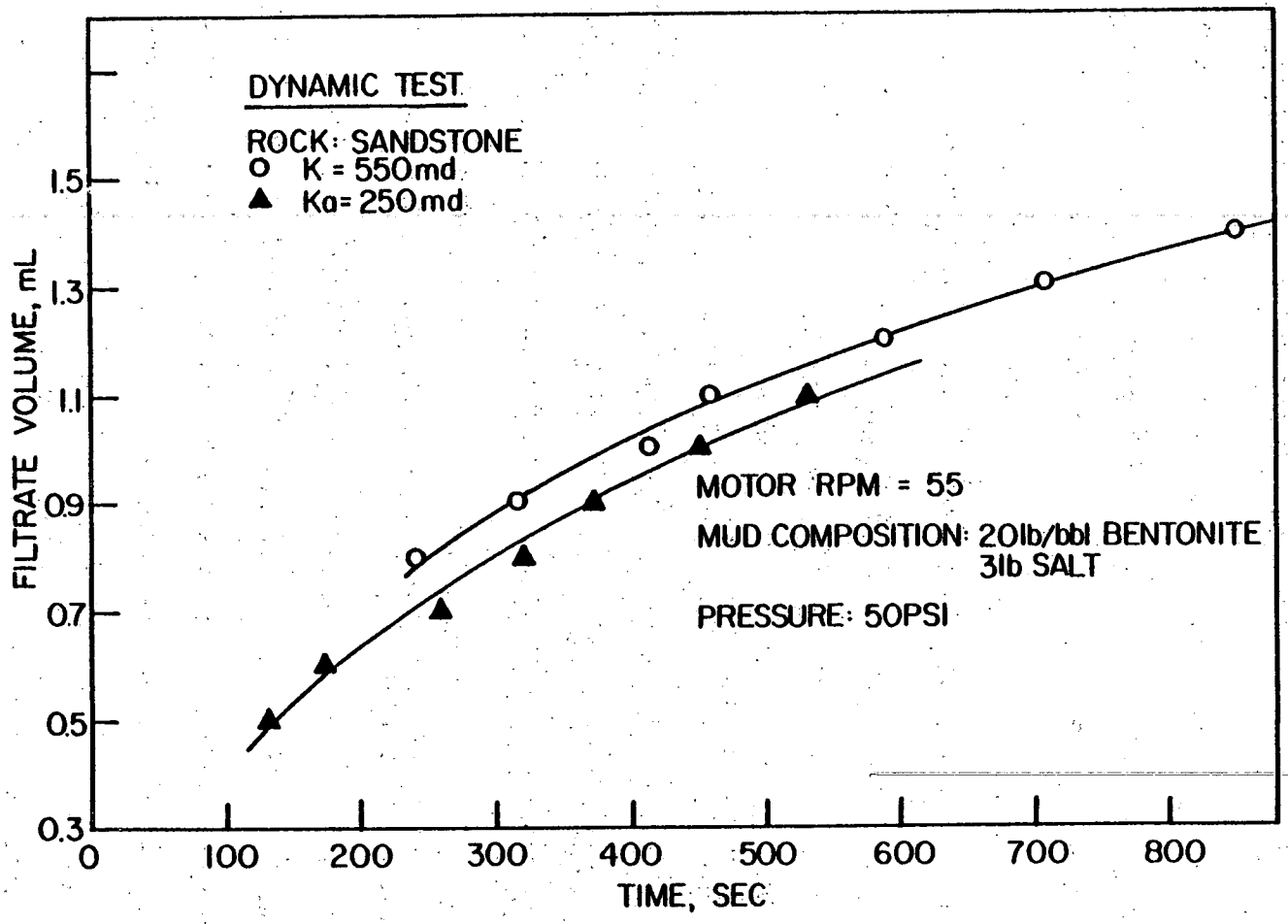

Fig. 4- Effect of Rock Permeability on Filtration Properties.

VISCOSITY OF GEOTHERMAL BRINES

Many theoretical studies published on reservoir and production characteristics of geothermal systems have used fluid properties representative of distilled water. Presence of dissolved ions in water may increase the viscosity by a factor of 1.018 to 1.7 for concentrations ranging from 1 to 22 wt.% at 25°C. This increase is also dependent upon temperature and pressure. The exact nature of viscosity change at elevated temperatures and as a function of dissolved solid concentrations must be included in all reservoir and production computations.

Data on temperature dependence of dynamic viscosity for NaCl solutions have been published by several authors. A very comprehensive literature review on this subject was published by Ozbek et al.[1] in 1977. They developed an empirical correlation to relate the dynamic viscosity of NaCl solutions with temperature and molal concentrations. Data used were mainly from Korosi and Fabuss, and Kestin. The correlation is valid to 150°C and cannot be extrapolated to higher temperatures. Numbere et al.[2] developed a correlation for viscosity of NaCl solution using the Fabuss and Korosi data. The correlation is based on the ratio of brine viscosity to water viscosity as a function of temperature and molal concentration. Potter used the concept of equivalent water temperature to relate the viscosity of NaCl solutions to water. He indicated that the correlation may be used for extrapolation purposes up to 325°C.

Potter and Haas[4] indicated that the NaCl solution may be used to model the properties of geothermal fluids. Studies conducted on the

dissolved ions in geothermal fluids indicate considerable variations from one area to the other. In general, geothermal brines are chlorine rich with the elements Na, K, and Ca the dominant species.

The purpose of this study was to measure dynamic viscosities of NaCl, KCl, and $CaCl_2$ and compare their behavior at elevated temperatures and at various levels of dissolved ion concentrations.

The study was prompted because of observations made earlier with respect to the electrical resistivities of geothermal brines. Reduction in electrical resistivity at elevated temperatures may be attributed to a decrease in solution viscosity. It was our expectation to observe a difference between the behavior of KCl or $CaCl_2$ solution and corresponding NaCl solutions. The level of and direction of difference was not clear.

Experimental Procedure

Viscosity measurements were conducted by using a high-temperature capillary tube method designed to operate up to a temperature of 315°C and 14 MPa. Figure 1 shows a schematic diagram of the experimental apparatus.

Flow in the capillary tube with a length of 30.48 cm was monitored by measuring the pressure differential across the capillary tube using a GOULD STATHAM differential pressure transducer (PD 2002-100-11).

The capillary tube was heated using flexible heating tapes. Therminol 66 heat transfer fluids was circulated around the capillary tube to equilibrate and maintain uniform temperature throughout the tube. Two J type thermocouples measured the inlet and the outlet temperatures.

Fluid flow measurements were conducted under steady state condition by using an accumulator at the upstream and back pressure regulator at the

downstream of the system. The hydraulic accumulator, rated at 21 MPa, had an internal volume of 1639 cc. Pressurization was accomplished by using nitrogen pressure.

The purpose of the back pressure regulator was to maintain a pressure very close to the upstream and to maintain the fluid in the system in the liquid phase. Fluid was cooled down by using a heat transfer coil immersed in water before entering the back pressure regulator.

Viscosity was measured using the Poiseuille's equation. The flow system was calibrated using distilled water.

Experimental Results

Viscosity of NaCl, KCl and $CaCl_2$ solutions were measured at concentrations ranging from 0.99 to 16.667 wt.% and at temperatures up to 275°C. Figure 2-4 show the combined effect of concentration and temperature on the dynamic viscosity of these solutions. As expected, for all concentrations viscosity drops rapidly in the temperature range of 25°C to 150°C. The rate of viscosity drop reduces at higher temperatures. The concentration effect lessens as higher temperatures are approached.

Comparing the viscosity data for KCl and $CaCl_2$ solution with NaCl solution, one notices significant differences over the temperature range studied here. For KCl solutions, viscosities are generally lower than corresponding NaCl solutions and the difference is temperature dependent. Above the 100°C, the deviation from NaCl values increases with temperature. For $CaCl_2$ solutions at temperatures below 100°C, the viscosity values are comparable to similar NaCl solutions. Above 100°C, however, the viscosity values are lower than the corresponding NaCl solutions and the difference increases with temperature.

Another way to demonstrate the difference between the KCl and $CaCl_2$ solutions is the use of multipliers. Figures 5 and 6 show the change in multipliers with temperature and as a function of concentration.

To test the application of the multipliers, two separate solution mixtures of the above compounds were prepared. Viscosity of these solutions were measured as a function of temperature. Through the use of multipliers, the mixture viscosities were predicted. A comparison of predicted and measured values are shown in Figures 7 and 8. The agreement is excellent. The use of NaCl data would have caused errors similar to ones shown below:

	100°C			250°C		
wt.%	Using NaCl data	Using Multipliers	% error	Using NaCl data	Using Multipliers	% error
9.091	0.435	0.415	4.59	0.11	0.09	18.18
13.044	0.470	0.46	2.13	0.14	0.115	17.85

The error increases with temperature. At high temperatures errors in the order of 1% to 20% would cause similar order of magnitude of errors in the estimation of production rates.

The relative change in viscosities as a function of concentration for two temperature levels 25°C and 100°C are shown in Figs. 7 and 8. These graphs conform to the observations reported by Ucok et al. on the behavior of resistivity data. Viscosities of $CaCl_2$ solutions at concentrations above 10 wt.% are generally higher than comparable NaCl and KCl solutions. As shown in Figs. 8 and 9 of reference 5 a similar effect is seen for the resistivity of $CaCl_2$ solution. Higher resistivities measured for $CaCl_2$ solution corresponds to higher viscosities which impede the ionic mobility.

CONCLUSION

From the experimental studies reported here, we have reached the following conclusions:

1. Viscosity data fro NaCl solution may not be adequate to represent viscosity of geothermal brines.
2. Behavior of brine resistivities at elevated temperature correlates well with the solution viscosities at such conditions.
3. Estimation of geothermal brine viscosities may be improved through the use of the multipliers shown in this paper.

REFERENCES

1. Ozbec, H., Fair, J.a., and Phillips, S.L. 1977, "Viscosity of Aqueous Sodium Chloride Solution form 0-150°C." Lawrence Berkeley Laboratory Report.

2. Numbere, D., Brigham, W.E., and Standing, M.B., "Correlation for Physical Properties of Petroleum Reservoir Brines." Stanford University Petroleum Research Institute, Nov. 1977.

3. Matthews, C.S. and Russell, D.G., "Pressure Buildup and Flow Test in Wells." Nomograph Vol. 1, Henry L. Doherty Series. Soc. of Pet. Eng., p. 158.

4. Potter, R.W. II, and Hass, J.R., Jr. "A Model for Calculation of the Bulk Thermodynamic Properties of Geothermal Fluids." GRC Trans. Vol. 1, 1977, p. 243-244.

5. Ucok, H., Ershaghi, I., Olhoeft, G., "Electrical Resistivity of Geothermal Brines." Journal of Pet. Tech., April 1980, p. 717-727.

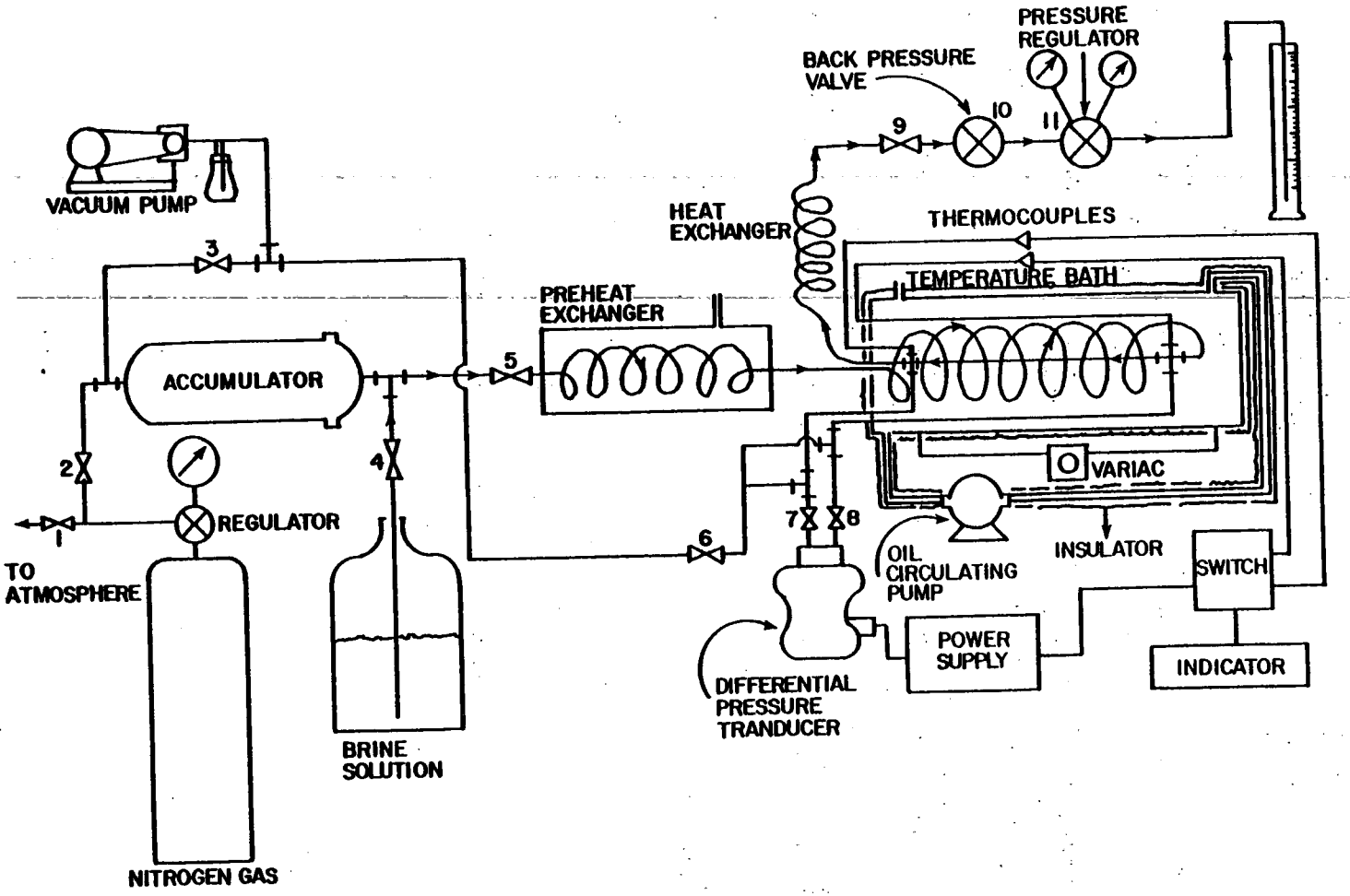

Fig. 1- Schematic Diagram of High Temperature Viscosities.

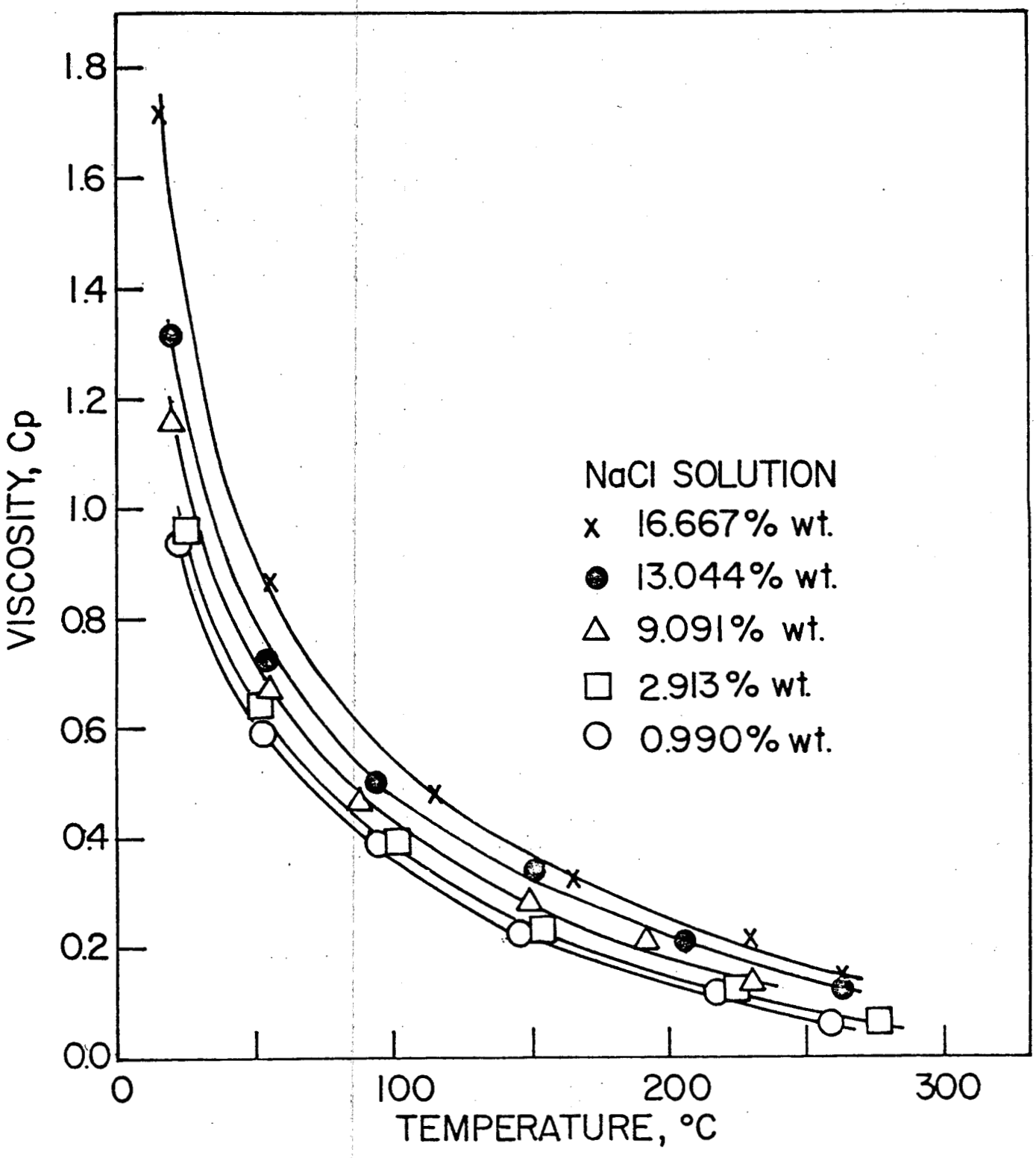

Fig. 2- Effect of Temperature on Viscosity of NaCl Solution.

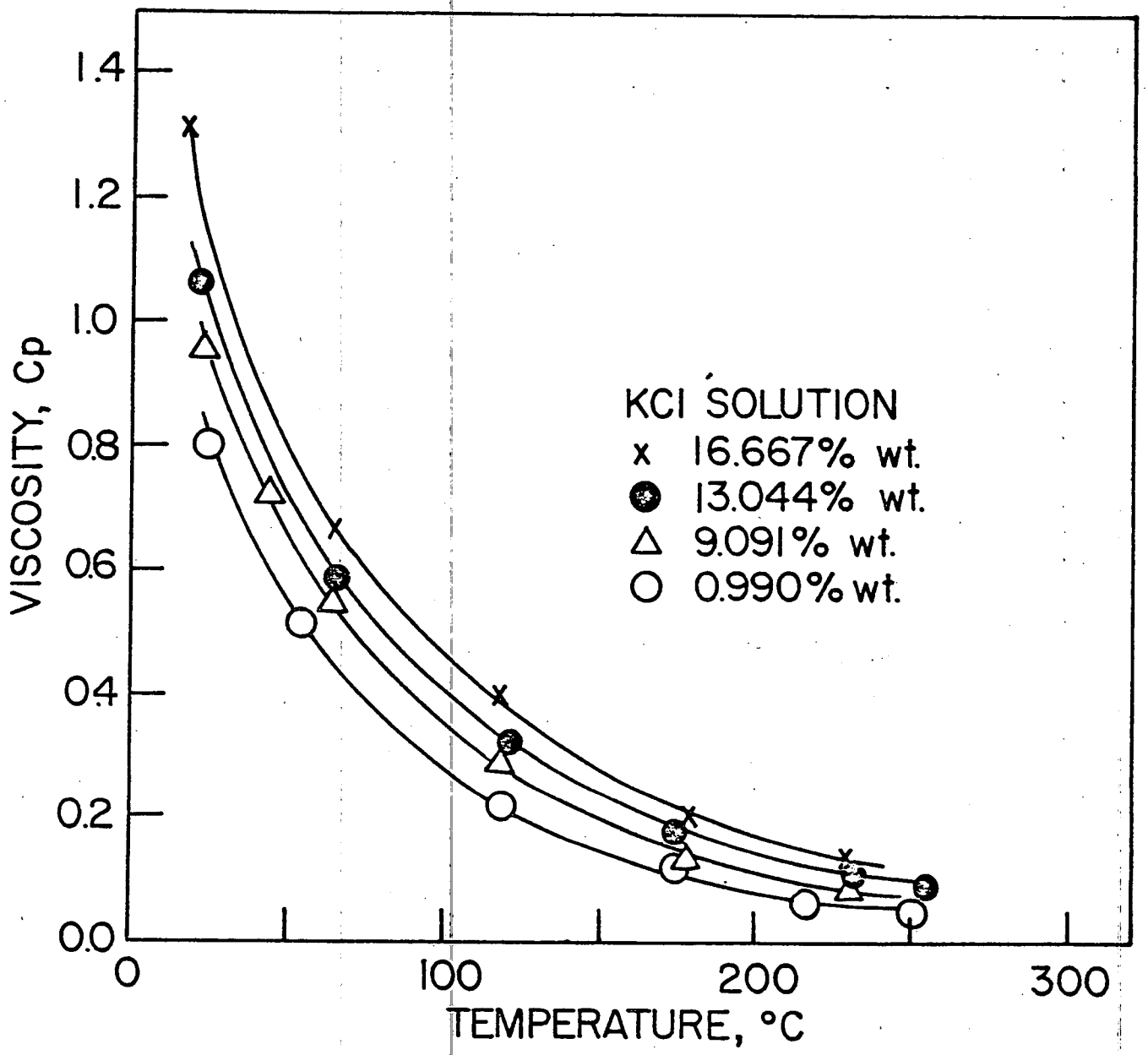

Fig. 3- Effect of Temperature on Viscosity of KCl Solution.

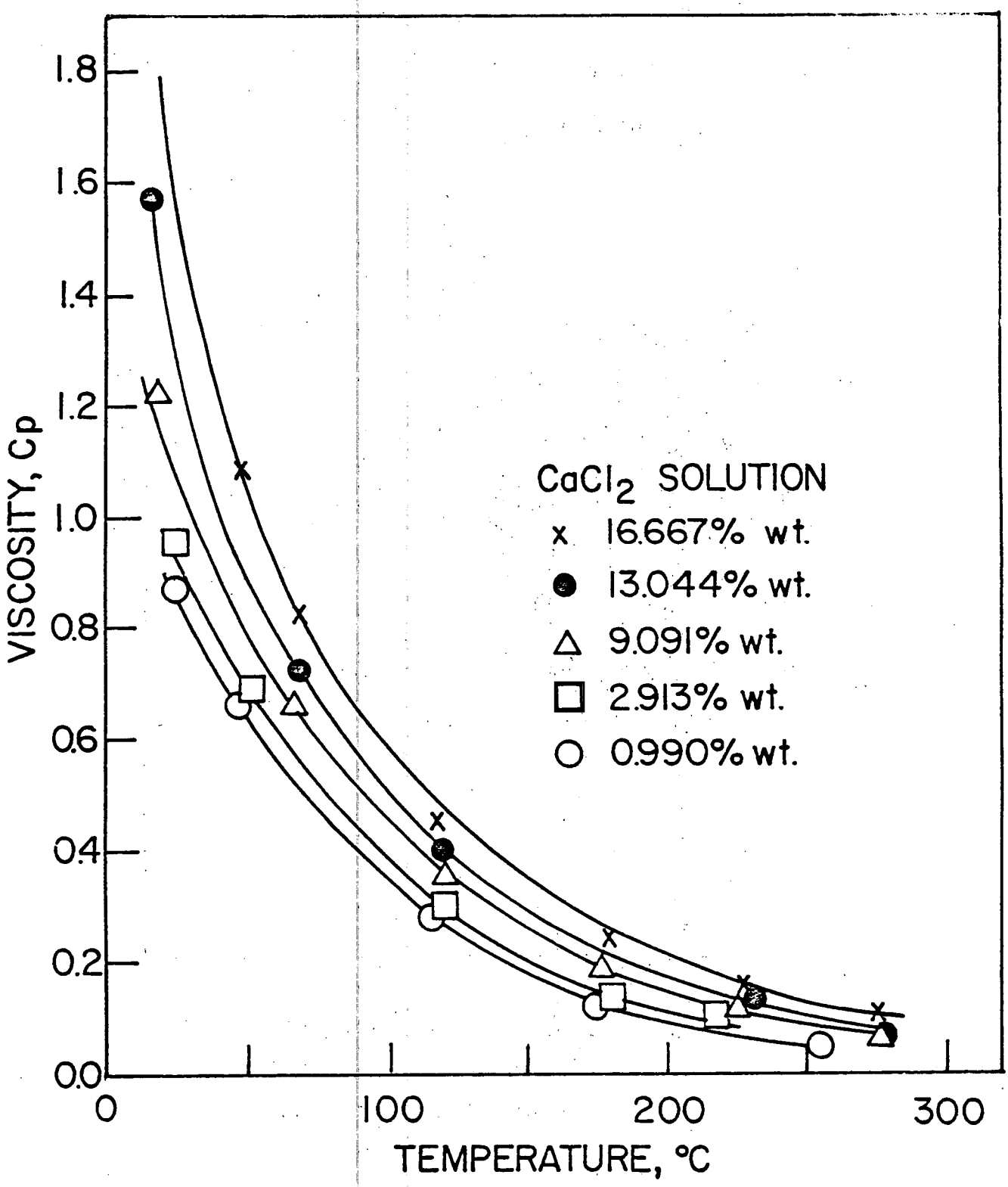

Fig. 4- Effect of Temperature on Viscosity of $CaCl_2$ Solution.

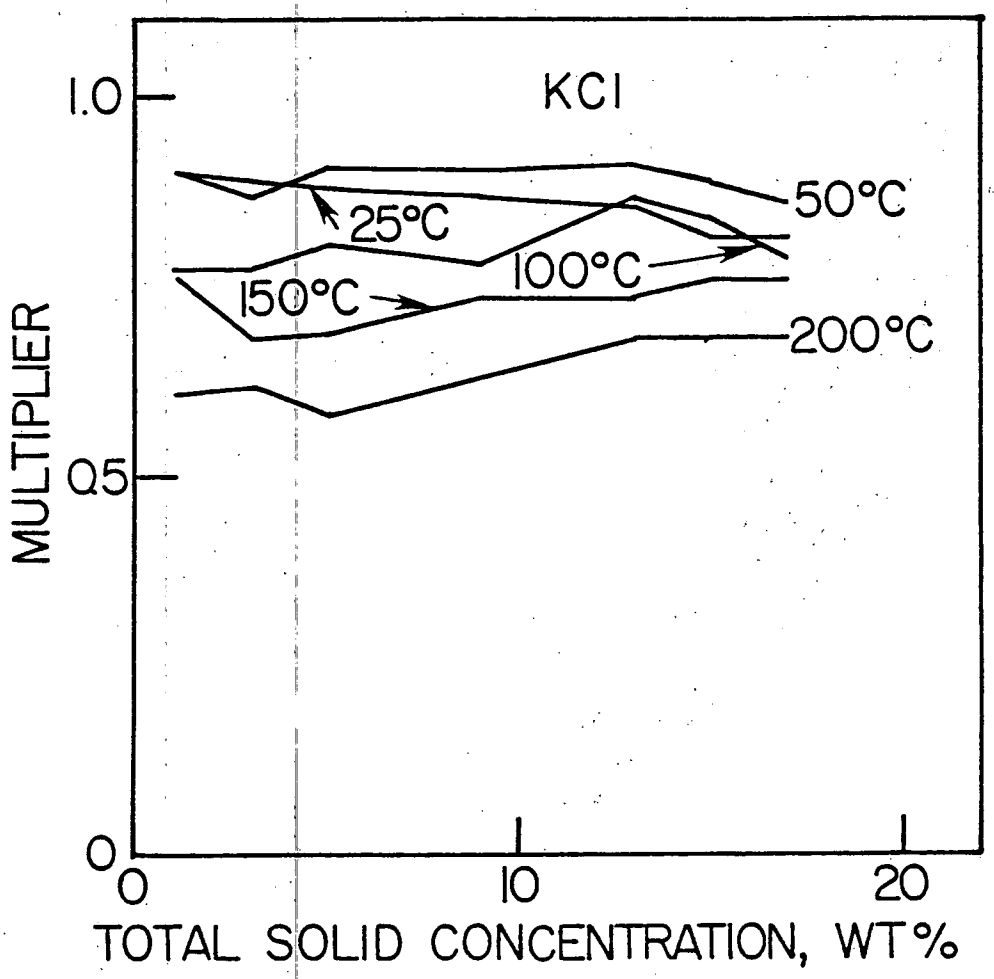

Fig. 5- Multipliers for KCl Solution.

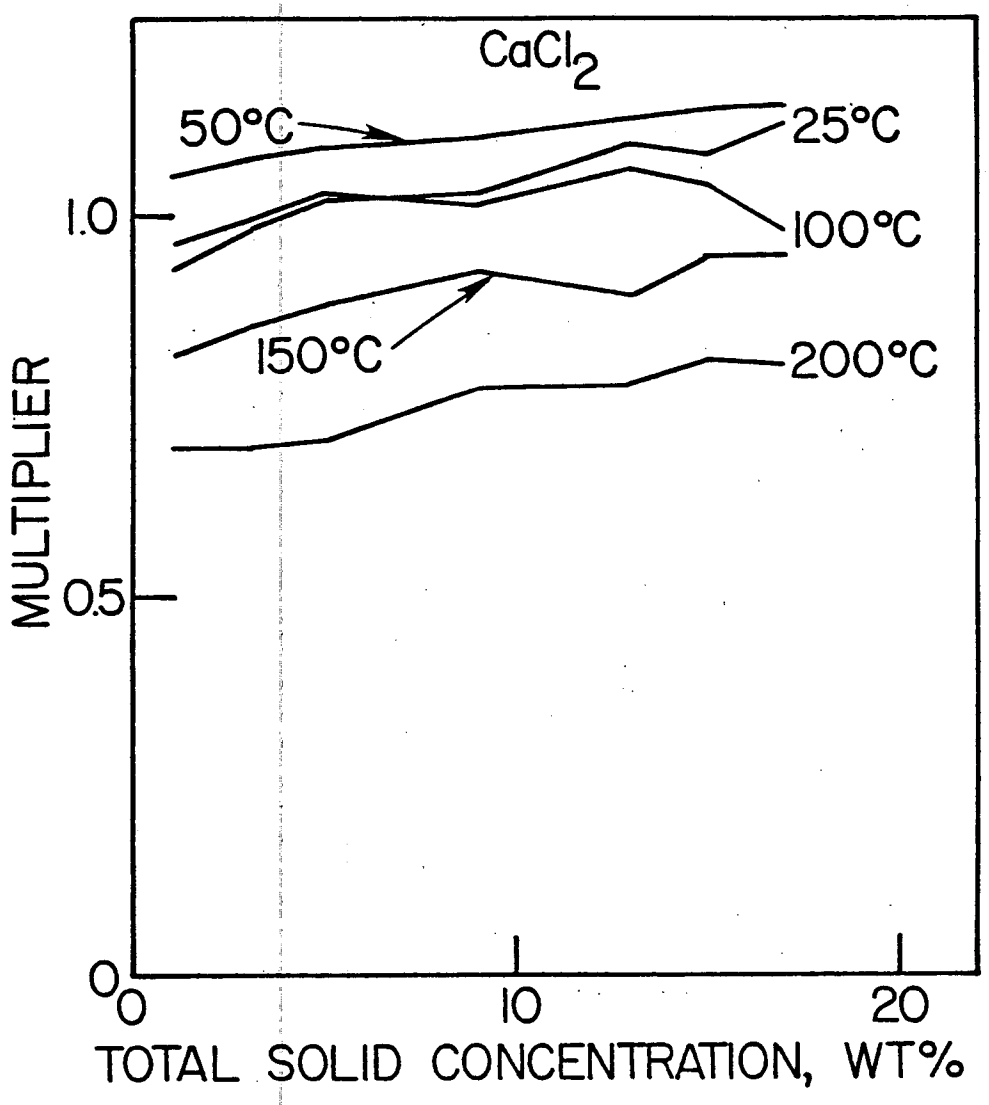

Fig. 6- Multipliers for $CaCl_2$ Solution.

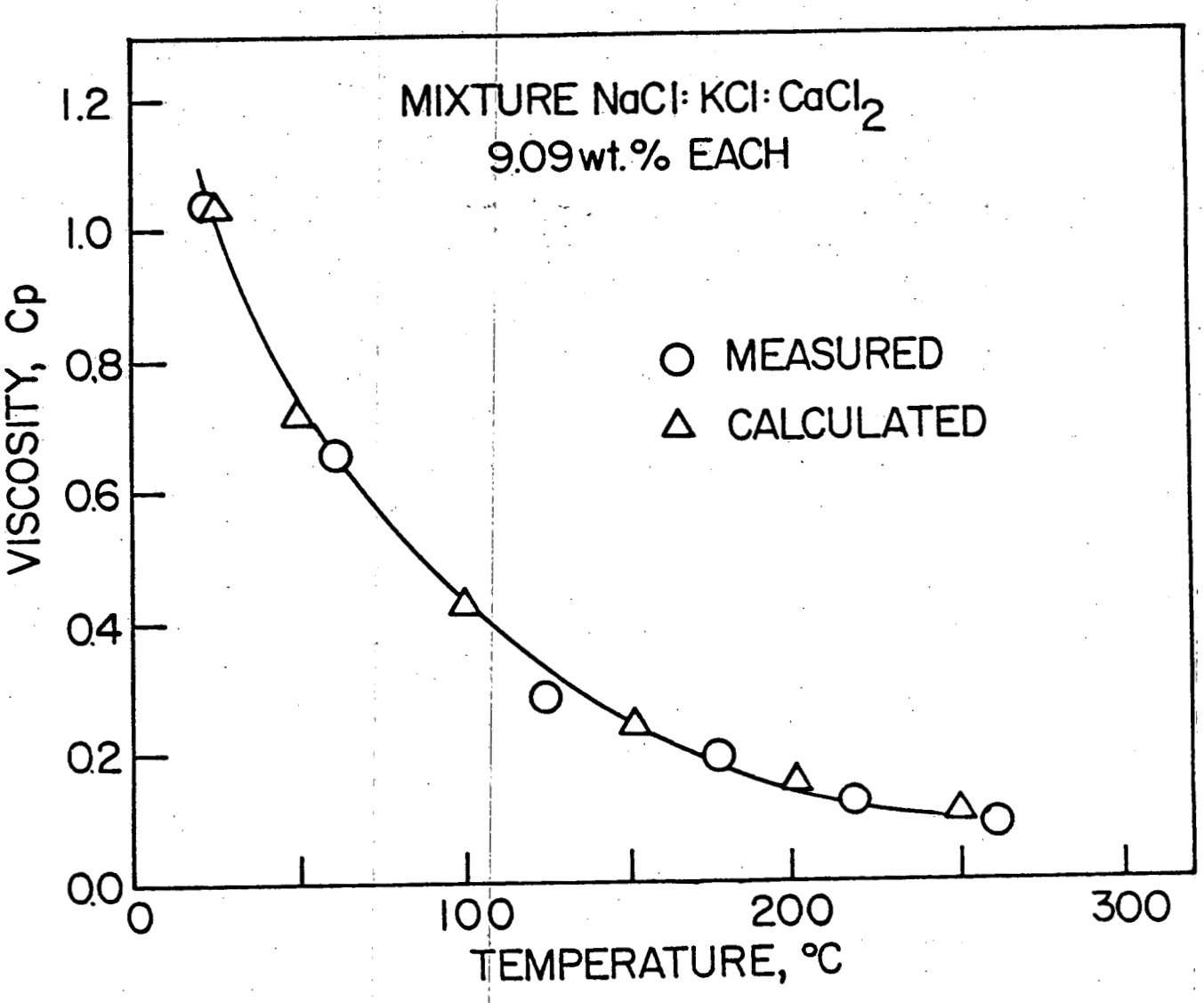

Fig. 7- Comparison of Measured versus Predicted Viscosity of the Mixed Brine (9.09%).

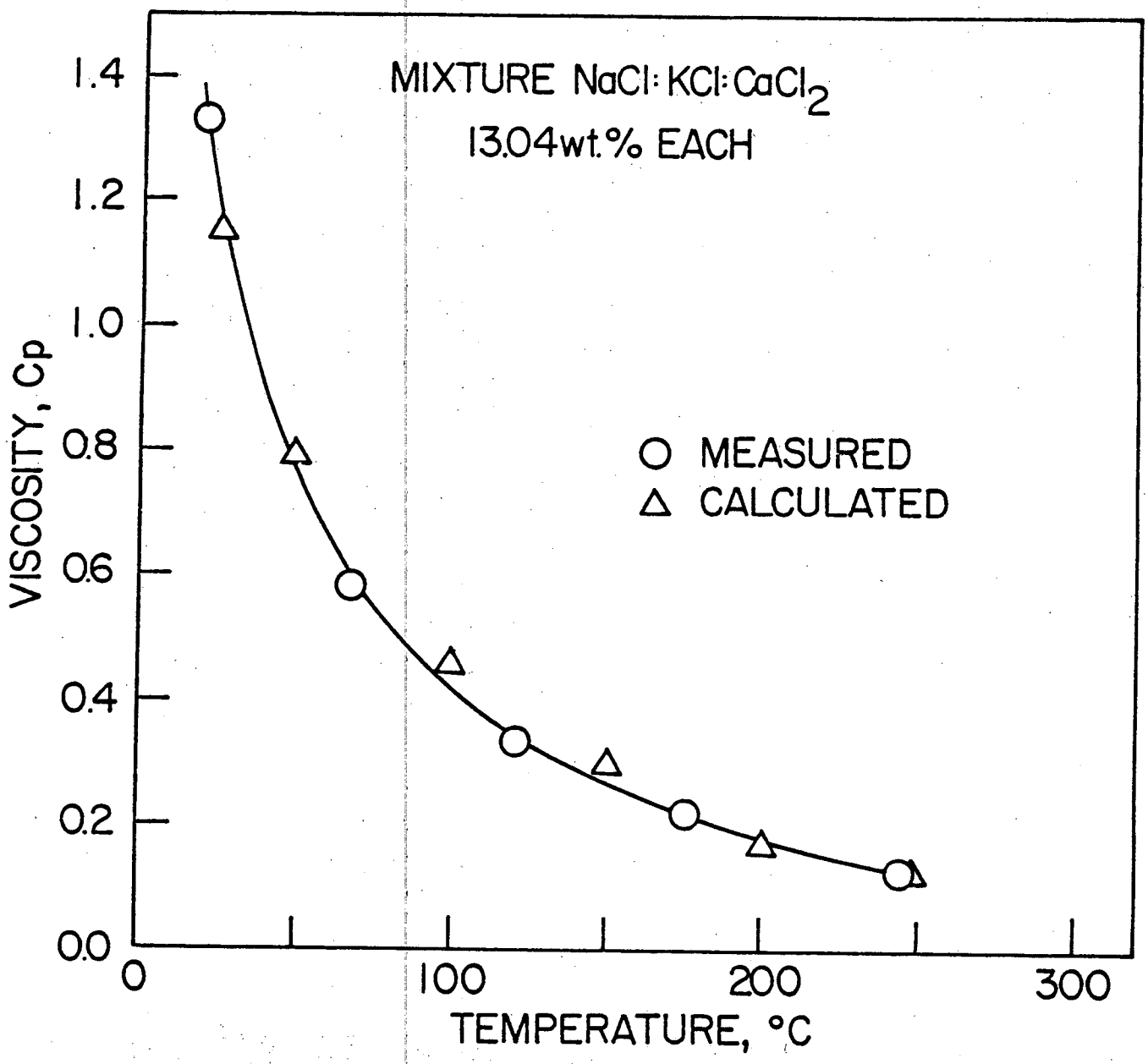

Fig. 8- Comparison of Measured versus Predicted Viscosity of the Mixed Brine (13.04%).

☆U.S. GOVERNMENT PRINTING OFFICE: 1981-740-145 2223